Giant Janus Liposomes: Preparation, Self-Assembly and Motion

by

Zening Liu

A dissertation submitted to the Graduate Faculty of
Auburn University
in partial fulfillment of the
requirements for the Degree of
Doctor of Philosophy of Science

Auburn, Alabama
August 8, 2020

Keywords: Janus Particle, Giant Liposome, Hydration Method, Self-assembly

Approved by

Wei Zhan, Chair, Associate Professor Department of Chemistry & Biochemistry
Christopher John Easley, Professor Department of Chemistry & Biochemistry
Steven Omid Mansoorabadi, Associate Professor Department of Chemistry & Biochemistry
Pengyu Chen, Assistant Professor Department of Mechanical Engineering
Monika Raj, Associate Professor Department of Chemistry & Biochemistry

ABSTRACT

Presented in this Dissertation are a series of studies on Janus liposomes, their formation, self-assembly and motion behaviors. Liposomes are closed, spherical lipid bilayer assemblies dispersed in water. Since their discovery in the 1960s, liposomes have become indispensable tools and ingredients not only in basic research but also in industry. Janus liposomes, on the other hand, are liposomes containing broken symmetry and surface heterogeneity in their structures. These less studied lipid structures are the focus of this Dissertation, specifically.

In Chapter 1, a literature survey is given on research topics mostly related to this work. Through the survey, the feasibility of preparing Janus liposomes is determined. In Chapter 2, I describe a high-yield procedure for preparing micro-sized (giant) Janus liposomes via gel-assisted lipid swelling. An optimized formation procedure is presented, which reproducibly yields large liposome populations dominated by a single domain configuration. In Chapter 3, by combining gel-assisted lipid hydration with membrane-based lipid extrusion, I demonstrate a general procedure for size-controlled preparation for giant unilamellar liposomes, including homogeneous and Janus liposomes. In Chapter 4, I describe a straightforward strategy to incorporate biotin-conjugated lipids into Janus liposomes' formation and clustering behavior of these liposomes directed by biotin-avidin affinity binding. In Chapter 5, I present the first report on dipolar Janus liposomes – liposomes that contain opposite surface charged decorating the two hemispheres of the same colloidal body. Using confocal fluorescence microscopy, the electrokinetic motion as well as electrostatic self-assembly of these new dipolar Janus particles are followed. Finally, in Chapter 6, I draw the main conclusion of my studies and offer an outlook of what might be accomplished in the near future along this direction.

ACKNOWLEDGMENTS

I would like to thank the following people, without whom I would not have been able to complete the research projects presented in this Dissertation, and without whom I would not have made it through my doctoral degree –

My sincerest thanks to my research group in the Department of Chemistry and Biochemistry at Auburn University, especially to my supervisor Dr. Wei Zhan, for his enthusiasm for the projects, for his support, encouragement and patience. Many thanks to my lab mates Dr. Mingming Wang, Mr. Chao Li, Shamim Iqbal, Jinyan Cui and Hui Jin for their support, assistant and encouragement.

My warmest thanks also extend to the following people: Dr. Michael E. Miller, for his support in confocal fluorescence microscopy measurement, Dr. Dongye Zhao, for his assistance in zeta potential measurement, Dr. Christopher J. Easley, for his permission in using fluorospectrometer; and to all the other students and faculty who gave me great technical support at Auburn University. I greatly appreciate many helps and advices I have received over the past five years from my committee members: Dr. Wei Zhan, Dr. Christopher John Easley, Dr. Steven Omid Mansoorabadi, Dr. Pengyu Chen, and Dr. Monika Raj.

Furthermore, I would also like to acknowledge the National Science Foundation (Award No. CHE-1808123) for supporting my projects; copyright permissions from American Chemical Society and Royal Society of Chemistry are also warmly acknowledged.

I would also like to thank my friends who helped me overcome the culture gap, and who supported and encouraged me to through everyday life challenges.

Finally, my special thanks to my family for their unconditional support and love across geographical distance during my study at Auburn University.

Table of Contents

List of Tables

List of Figures

List of Abbreviations

AC alternative current

AFM atomic force microscopy

BC Boerdijk-Coxetrer

Biotin-DOPE 1,2-dioleoyl-*sn*-glycero-3-phosphoethanolamine-*N*-(biotinyl) (sodium salt)

Bodipy-chol 23-(dipyrrometheneboron difluoride)-24-norcholesterol

DC direct current

DexPEG dextran poly (ethylene glycol)

DI deionized

DiPhyPG 1,2-diphytanoyl-*sn*-glycero-3-phosphoglycerol

DMPC 1,2-dimyristoyl-*sn*-glycerol-3-phosphocholine

DNA deoxyribonucleic acid

DOPC 1,2-dioleoyl-*sn*-glycero-3-phosphocholine

DOPE 1,2-dioleoyl-sn-glycerol-3-phosphoethanolamine

DOTAP 1,2-dioleoyl-3-trimethylammonium-propane (chloride salt)

DPhPC 1,2-diphytanoyl-*sn*-glycero-3-phosphocholine

DPPC 1,2-dipalmitoyl-*sn*-glycero-3-phosphochline

DPPE 1,2-dipalmitoyl-sn-glycerol-3-phosphoethanolamine

DPPG 1,2-dipalmitoyl-*sn*-glycero-3-phospho-(1′-*rac*-glycerol) (sodium salt)

DSPC 1,2-disteraroyl-*sn*-glycerol-3-phosphocholine

DSPE-PEG_{2000} 1,2-distearoyl-*sn*-glycerol-3-phosphoethanolamine-*N*-[amino(polyethylene glycol)-2000] (ammonium salt)

DSPG 1,2-disteraroyl-*sn*-glycerol-3-phospho-(1-rac-glycerol) (sodium salt)

EPR electron paramagnetic resonance

eSM egg sphingomyelin

FITC fluorescein isothiocyanate

FRAP fluorescence recovery after photo bleaching

FRET fluorescent resonance energy transfer

g gel phase

GJLs giant Janus liposomes

GUVs giant unilamellar vesicles

HSPC hydrogenated soy phosphatidylcholine

K_p partition coefficient

ld liquid-disordered

lo liquid-ordered

LUVs large unilamellar vesicles

MW molecular weight

NBD-PC 1-palmitoyl-2-[*N*-(7-nitro-2,1,3-benzoxadiazol-4-yl)amino-caproyl] phosphatidylcholine

NMR nuclear magnetic resonance

PB polybutadiene

PC polycarbonate

PDMS poly(dimethylsiloxane)

PE phosphoethanolamine

PEG polyethylene glycol

PMMA poly (methyl methacrylate)

PMTs photomultiplier tubes

PNIPAAm poly (N-isopropyl acrylamide)-based statistical terpolymer

POPC 1-palmitoyl-2-oleoyl-glycerro-3-phosphocholine

POPG 1-palmitoyl-2-oleoyl-*sn*-glycerol-3-phospho-(1'-*rac*-glycerol)(sodium salt)

PS polystyrene

PVA poly(vinyl alcohol)

rho-DOPE 1,2-*sn*-glycero-3-phosphoethanolamine-*N*-(Lissamine rhodamine B sulfonyl) (ammoniu salt)

SUVs small unilamellar vesicles

T_m melting temperature

*x*PMAA poly (methacrylic acid-*co*-ethylene glycol diacrylate)

CHAPTER 1. INTRODUCTION

This Dissertation presents a new, efficient procedure to prepare giant Janus liposomes (GJLs) via poly (vinyl alcohol) (PVA) gel-assisted lipid swelling. Based on this approach, another new procedure for size-controlled GJLs production is developed which combines gel-assisted hydration with membrane-based lipid extrusion. The versatility of these methods is shown by generating different types of giant liposomes and further demonstrated by the ability to afford straightforward incorporation of functional lipids (biotin-lipid and charged lipids) into the formation, which produce Janus liposomes with special domain-related characteristics.[1,2] The resulting features/behaviors of GJLs are carefully monitored and interpreted.

Prior to beginning the journey of preparing and investigating GJLs, it is necessary to answer several questions including (1) what is a giant Janus liposome; (2) how does this type of Janus particle form; (3) what features can be imparted; and (4) what are the benefits for this area of study.

1.1 Janus Particles

1.1.1 Overview of Janus Particle Field

In the prior several decades, significant attention has been given to a type of surface anisotropic material called patchy particles. Compared to the isotropic particle, this type of particle is advantageous in a wide range of applications that rely on the ability to combine multiple dissimilar properties into a single entity.[3-9] Additionally, the theoretical challenges rising from its symmetry-broken configuration have also triggered significant interest in the exploration of this type of material. The simplest and most special example of the patchy particle

is the Janus particle which contains two compartments with disparate physical-chemical (*e.g.*, electrical, magnetic, optical, *etc.*) properties.

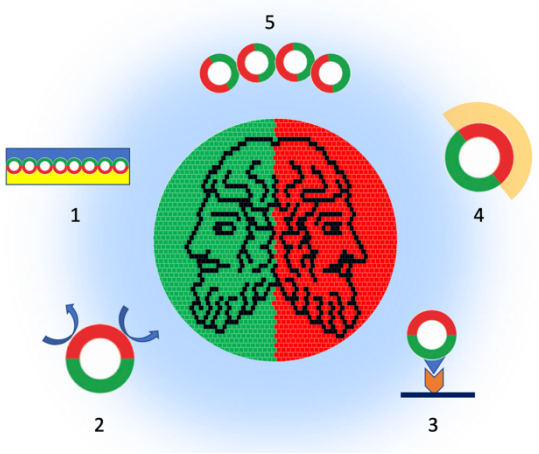

Figure 1-1. Schematic of Roman god Janus and Janus particle (middle). Five representative applications of Janus particles are arranged around it: 1- novel surface, 2- catalyst, 3- specific targeting, 4- imaging probe, and 5- self-assembly.

Janus is a god from Roman mythology who has two faces looking in opposite directions (see the central image in Figure 1-1) and whose name is borrowed to describe dual patch particles. The original research[10] on the Janus particle dates to the end of the 1980s when Casagrande and Veyssie created a new type of glass beads displaying two distinguishable hemispheres - one was hydrophobic and the other was hydrophilic. Then, in 1991, French physicist P. G. de Gennes did not only list representative soft materials, including polymers, surfactants, and liquid crystals in a Nobel lecture[11] but also the for first-time mentioned two types of "amusing" materials: one was ferro-smectic material, and the other was Janus grains. Henceforth, Janus particles were brought to worldwide attention and the concept of Janus particle is already far beyond the original spherical micro-sized amphiphilic beads at oil-water interface. These years, significant efforts have been devoted to studying and fabricating Janus

particles resulting in a broad variety of 1) morphology/dimensionality, 2) preparing strategies, 3) compositions, and 4) properties/behaviors as well as applications. In recent years, these developments have been well reviewed.[3-12]

With respect to the configuration of Janus particles, the fraction of the two opposite surfaces is not limited to a 50:50 division anymore. In addition, tunable patchy coverage (ratio of one compartment over another compartment on Janus particles) can be readily achieved by adjusting preparation parameters (*e.g.*, composition, apparatus parameter, interfacial chemical environment, *etc.*). Moreover, the altered Janus configuration is appealing in researches because they can offer essential information on configuration related properties as well as the opportunity to optimize these materials' properties/functions. For example, in the work of preparing bipolar charged Janus particles with various patchy coverages reported by Mani and co-workers,[15] the three phase contact angles (air/water/polystyrene (PS) microsphere) were modified by using a surfactant to reduce interfacial tension between air and water. In other words, the fraction of the PS particle undergoing thermochemical treatment was tuned through this strategy. The self-assembled structures composed by these particles were found to depend on patchy coverage. Alternatively, the patchy fraction of Janus particle prepared by using a microfluidic setup can be readily tuned through adjusting flow rate.[16] More straightforwardly, changing the composition of the chemicals constituting the Janus particles can control the Janus configuration as well (one example is described Chapter 2).

Janus particles can form through various mechanisms leading to diverse morphologies. Aside from spherical Janus particles, ellipsoidal, cylindrical, rod-like, dumbbell-like, snowman-like, disc-like, sheet-like, half-raspberry-like, and micelle/hairy Janus particles have been fabricated.[3-12] The size range of currently reported Janus particles extends from nanometer to

micrometer. The Janus particles prepared in this Dissertation is a kind of spherical micro-sized symmetry-broken material.

1.1.2 Janus particles preparation

Benefiting from the thriving progress of material engineering techniques, a great variety of approaches have been developed to fabricate Janus particles which can be briefly classified into two groups: surface modification and compartmentalization.[11] The reported methods have also been well summarized in excellent review papers from different viewpoints (e.g., materials, mechanisms, techniques).[3-12] In the following paragraphs I will introduce some commonly used techniques/strategies for preparing Janus particles.

(1) Modification

One of the most frequently employed procedure to fabricate Janus particle is masking. Homogeneous particle monolayer is immobilized in/on a substrate, and then the exposed segments are modified through either chemical reaction or physical deposition, followed by the releasing of Janus particles. This is the process by which the first reported Janus particle was fabricated.[13] Specifically, the hydrophilic glass bead was half embedded in plastic and the surface of the exposed half turned into hydrophobic through silanization. In another example, Granick and co-workers[17] prepared ammonium/carboxylic dipolar Janus particles also through this procedure. The PS microparticle monolayer was formed on glass substrate first after suspension liquid evaporated. Then a thin gold film was deposited on the accessible side by using the electron-beam deposition technique. Subsequently, through the procedure of thiol self-assembled monolayer formation, a positively charged hemisphere on this gold surface formed, whereas the unmodified hemisphere retained the negative charged feature. Similarly, Veleve and co-workers[18] selectively deposited magnetic active species on one hemisphere of PS particles in

which they used the metal evaporation technique to coat iron on the exposed side of a monolayer of pre-assembled PS microspheres and thus obtained a magnetic anisotropic material. However, the main challenge for the approach of masking is the large-scale production of Janus particles.[11]

Various mask-free methods have been developed to modify surfaces to produce Janus structures. One example is charged particle redistribution under an electric field. Reported by Li and Li,[19] positively charged aluminum oxide nanoparticles were uniformly adhered onto sessile oil droplet which posed opposite surface charges. However, the external electric field can drive the aluminum oxide nanoparticles to accumulate to the cathode-side facing hemisphere and the negative oil-water surface reappeared rendering dipolar Janus droplets. Mentioned by the authors, this type of dipolar particle was challenging for other approaches to fabricate. Furthermore, this type of material has been proven to be suitable for studying electroosmotic flow around dipolar Janus droplets.

The hybrid soft/hard Janus particles are frequently produced via strategy of selectively modifying an inorganic base with polymerizable moieties. One example of this is the dumbbell-like silica/PS Janus particle.[20] The pre-absorbed macromonomer (polyethylene glycol (PEG)) on a silica particle copolymerized with styrene monomers at the very first stage of the seeded emulsion polymerization. This was followed by styrene nucleation which then evolved into a PS particle on the silica.

(2) Phase separation

Unlike afore-described methods, phase separation of immiscible components offer opportunity to generate Janus particles through a strategy of compartmentalization, especially for preparing soft Janus particles which consist of polymers and organic molecules.[9,11] The chemical-physical dissimilarities among building blocks drive the formation of distinctive phases

and/or these molecules are ruled by interfacial tension (the attractive force between the molecules at the interface of two phases) for forming Janus structure, both of which aim at minimizing system free energy. Biphasic Janus particles are able to be fabricated by taking use of immiscible polymer blends which can be easily found in the example of popular composition: PS/poly (methyl methacrylate) (PMMA). Through either temperature control, molecular weight (MW) adjustment, or adding extra component, PS and PMMA would locate in different phases rendering Janus configurations.[9,21] For example, Okubo and co-workers[21] reported this kind of Janus particles through seeded emulsion polymerization. Emulsion droplets consisting of a PS/PMMA shell and a toluene core formed when the precursor polymer contained organic solution mixed with water, and then PS/PMMA particles formed followed by slow toluene evaporation. Such symmetry-broken particles were readily formed when the high MW polymers were used in this approach. In other words, because the interfacial tension between the polymer and the aqueous solution containing surfactant molecules was much higher than that between the separated phases (*e.g.*, the former is ~50 times larger than the latter), thus there was a Janus-like structure on the PS/PMMA particle at thermodynamic equilibrium. Interestingly, the morphology of these PS/PMMA Janus particles can be tuned by altering MW of the polymers as a result of interfacial tension balance. The procedure of generating Janus liposomes presented in this Dissertation also follows the strategy of immiscible components' phase separation (see Section 1.2 and 1.3).

The fast-growing microfluidic techniques in recent years offers another motivational force for the thriving development of Janus particles. One highly cited work is from Kumacheva and co-workers[22] in which amphiphilic Janus microspheres were synthesized by using a microfluidic flow-focusing device. Specifically, in the microfluidic channel Janus droplets

formed from a two-liquid thread with the assistance of shear stress imposed by the continuous water phase. This was followed by photoinitiated free-radical polymerization in which Janus droplets were exposed under UV light, and thus Janus particles were produced. Two key characteristics of these building materials contributed to the formation of such kind of particles: one was the positive interfacial tension between two components suggesting phase separation can occur, and the other was the fast polymerization providing a chance for the Janus structure in droplets to be trapped in the resulting solid state. Furthermore, in their work, both diameters and Janus configurations of thus-formed symmetry-broken microspheres were readily controlled by changing the ratio of flow rates of each phase. This example does not only demonstrate the usefulness of microfluidic techniques in fabricating Janus particles but also imply more precisely feature-controlled Janus particles (*e.g.*, size distribution, domain fraction, morphology) can be prepared through this procedure as compared with the phase-separation approaches mentioned before. In another example, Nisisaka and co-workers[23] prepared bicolored Janus particles in their microfluidic setup. The separated carbon black and titanium oxide dispersed acrylic monomers were introduced into the Y-junction to form a two-color stream. Janus droplets then formed due to a shear-rupturing mechanism and subsequently polymerized via thermal curing. In this case, when two segments shared the same viscosity, there was no convective transport across the two adjacent streams which rendered the Janus structure. The anisotropic optical characteristic of Janus-like materials is essential for being used as displays, such application can be found in the last example.[23]

Engineering progress always brings new technologies to serve for a variety of fields. In addition to the techniques described before for fabricating Janus particles, electrodynamic co-jetting has been employed in synthesizing this type of materials as well.[9,11,24,25] In this kind of

compartmentalization technique, when a high electric field is applied, the immiscible jetting solutions in dual capillaries overcome surface tension to form droplets and emit towards the ground substrate. Polymeric droplets containing dyes and other functional components (*e.g.*, Fe_3O_4, gold nanoparticles, etc.) subsequently underwent polymerization via either solvent evaporation or thermal curing and thus formed functional Janus particles. This method also demonstrates the capability to alter the morphologies of Janus particles by adjusting setup parameters (*e.g.*, flow rates, applied voltages) as well as polymers.

1.1.3 Janus particles application

The fast-growing development of synthesis routines and techniques in preparing Janus particles is highly beneficial for studying and utilizing Janus particles.[3-12] Over the past several decades, the behaviors and properties of Janus particles have been widely explored and their promised features as well as their appealing applications have been more and more reported. A variety of functions has been imparted to Janus particles. In addition to hydrophobic/hydrophilic features, other kinds of chemical, electrical, magnetic, and optical functionalities have been introduced into Janus particles. Indeed, recent studies on Janus particles have already uncovered several unique features, which their symmetrical counterparts do not possess. Some of these features and applications of Janus particles are summarized in Figure 1-1: 1- novel surface, 2- catalyst, 3- specific targeting, 4- imaging probe, and 5- self-assembly. It is important to be aware that the efficiency of Janus particles in certain applications is significantly dependent on their characteristics, including composition, morphology, configuration, and colloidal stability.

(1) Novel Surface

Similar to low-molecular-weight surfactants or block copolymers, amphiphilic Janus particles have served as stabilizers in emulsion polymerization which was envisioned by de

Gennes in his[9] Nobel lecture. Compared to homogenous particles in such application, the improved liquid/liquid interface adsorption energy from Janus structure has been predicted indicating better stabilization in the case when Janus particles are used.[9,12] Janus particles adsorbed on the interface of two phases, normally oil/water interface, are able to stabilize Pickering emulsions and to provide two distinctive interfacial chemical environments at the same time. One type of amphiphilic Janus sphere (PS/PMMA shell with polybutadiene (PB) core) was used in emulsion polymerization which was reported by Müller and co-workers.[26] It is worth mentioning that these particles formed from cross-linking the middle block PB in PS-PB-PMMA triblock copolymer self-assembled lamella sheets, which was followed by dissolution and hydrolysis. This is a common routine for preparing Janus particles through the self-assembly of ABC-type triblock copolymers,[9] in the example described here, middle block B is PB, mutually incompatible A and C blocks correspond to PS and PMMA. They took advantage of these Janus particles to stabilize emulsions containing either styrene or *n*-butyl acrylate monomer as well as to confine the formation of latex in the emulsions. In their work, they not only produced monodispersed PS latexes but they also demonstrated the ability to control latex diameters through altering the amount of stabilizer (Janus particle) used. As they suggested, these characteristics enable Janus particle use in fundamental research and future industrial applications.

Films composed with Janus particles can hold distinctive physical-chemical features on opposite sides. This is because 1) Janus particles have two surfaces with disparate characteristics, and 2) Janus particles are able to show selective orientation at the interface under certain conditions. Taking advantage of this fact, active interface bounded applications have been developed, such as fabricating optical active droplets, liquid marbles, displays, and catalysis.[12,23]

As noted, the bicolor Janus particles in section 1.1.2 are also dipolar charged colloidal particles.[23] This is because carbon black and titanium oxide (in white color) have disparate charging properties, the former is partially positive whereas the white compartment is partially negative. Thus, in the electrical actuation experiment, the monolayer of these Janus particles demonstrated an electric field regulated color switch (white/black) in a display panel. Similarly, symmetry-broken particles containing magnetically active species as well as anisotropic optical features are also suitable for use as displays.[12]

(2) Catalyst

In the field of catalytical application, anisotropic inorganic catalysts have demonstrated enhanced catalytical activity and, in addition, the Janus structure suggests other functions can be incorporated. Such an example can be found in bicompartmental gold/magnetite (Au/Fe_3O_4) Janus particles.[27] The nitrophenol reduction was catalyzed by Au nanoparticle, at the same time, the magnetic compartment imparted the ability for collecting and recycling this kind of catalyst by using an external magnetic field. Another impressive application, based on the symmetry-broken catalytical reaction on a single entity, is that Janus particles decorated with (bio)chemically reactive functionalities have been tested as micro- and nano-sized motors.[28-31] These colloidal particles can overcome Brownian motion in fluids in response to specific external stimuli. The motions of PS/platinum (PS/Pt) Janus nanoparticle is one good example of this type of application.[29] Reported by Howse and co-workers, PS was inert to hydrogen peroxide (H_2O_2) whereas Pt was able to catalyze H_2O_2 to decompose into water and oxygen, and thus the produced gas provided propulsion against self-diffusiophoresis and drove the particles autonomous swim. Three different enzymes, including catalase, urease, and glucose oxidase, were selectively linked on hollow mesoporous silica nanoparticles through glutaraldehyde.[28]

Thus, the biocatalytic reactions of the enzyme/fuel combinations were confined on one side of these Janus particles counteracting the effective self-propulsion force to power the active motion of the particles. As suggested by the reporters of this work, it may be highly beneficial to combine such biocompatible materials with electrically/magnetically active functionalities to serve in specific-targeting active drug delivery using field manipulation.

(3) Specific targeting

An alternate strategy for using Janus particles to directionally target certain types of cells is to decorate ligands on one side. The bicompartmental Janus particle (Au/Fe_3O_4), which combined characteristic surface plasmon resonance adsorption and magnetic property, has been synthesized by Sun and co-workers[32] through epitaxial growth of Fe_3O_4 on Au seeds. In a later contribution, Sun[33] selectively decorated a platin complex on the Au side by taking advantage of gold-thiol chemistry and linked a Her2-specific monoclonal antibody Herceptin to the Fe_3O_4 compartment through PEG and dopamine. The latter guaranteed target-specific platin delivery rendering enhanced toxicity to kill targeted tumor cells (Sk-Br3 cells used in their work) by platin. By contrast, there was no such specific binding ability to Her2-negative breast cancer cells in the control experiment. This research provides a good example for employing Janus particles as a platform to add other functionalities in building multifunctional material. In another representative work for realizing unidirectional association of Janus particles with cells, Lahann and co-workers[24] synthesized a novel type of bicolor bio-hybrid material through a three-step procedure. They first fabricated bicompartmental particles via electrodynamic co-jetting, then modified the particle surface with PEG, and subsequently selectively incorporated streptavidin on biotin-decorated hemisphere. The streptavidin modified compartment were able to specifically bind with human endothelial cells that were labeled with biotinylated antibody with

the assistance the PEG suppressed non-specific association. As suggested by the authors, this material may find applications in biology synthesis and medical imaging.

(4) Imaging probe

Optically anisotropic particles are suitable for use as imaging probes and Janus particles are advantageous in applications such as studying local biological environment rheology and cellular imaging. Another research from Sun's group[34] reported how to properly functionalize the Au/Fe_3O_4 Janus particle to serve as a probe for cell imaging. They modified the Fe_3O_4 side with the epidermal growth factor receptor enabling specific targeting A431 human epithelial carcinoma cells. Then they took advantage of characteristic reflectance originating from the Au compartment to visualize A431 cells with a confocal microscope. Additionally, the superparamagnetic characteristic of this Janus particle also offered the opportunity to probe A431 cells with a magnetic resonance imaging technique. Besides gold, other optically active species are useful in developing Janus imaging probes as well, such as fluorescent dyes, fluorescent quantum dots, photoluminescent ZnO, and others.[10]

(5) Self-assembly

It appears that the most intensively reported application of Janus particles is to serve as the building blocks in self-assembly. This capability originates from orientation-sensitive interactions among Janus particles which can be achieved through various specific interactions (*e.g.*, ligand-receptor specific binding,[1] electrostatic attraction,[2,15,17] van der Waals attraction,[35] depletion interaction,[36] *etc.*) or by the assistance of extra stimuli[18,37]. In following paragraphs, I will cover a few of the many examples of self-assembly of Janus particles driven by interactions or external fields.

Granick and co-workers[35] demonstrated self-assembly of Janus spheres with one hydrophobic hemisphere and one hydrophilic hemisphere. For the used amphiphilic Janus particles (50 : 50), there were at most six neighbors in a cluster which provided the chance for clusters to grow into larger assemblies. Under low electrolyte condition (typically 3.8 mM NaCl), amphiphilic Janus particles underwent dynamic interconversions. Multiple cluster structures containing at most seven particles were found as the products of step-by-step addition, fusion, and isomerization. When the NaCl concentration increased up to 5 mM, striking helical structures formed. Interestingly, these clusters were Boerdijk-Coxetrer (BC) helices which are less thermodynamically favored than other type of helix structure indicating that this structure was the product of kinetic selection. The six-member cluster (capped trigonal bipyramid), which was highly likely to form under low electrolyte content, could serve as the building segments for forming a BC helix. Thus, this type of helix was more quickly to form than other structures, and the consequence of this behavior was that the highly ordered BC helix was quite challenging to relax into a thermodynamic equilibrium product during which process a significant structure reorganization is required. The self-assembly behavior of amphiphilic Janus particles in the higher salt concentration in their work was different from the behavior of molecular amphiphiles (*e.g.*, surfactants, phospholipids) which undergo rapid shape equilibration.

Reported by Granick and co-workers,[17] unlike magnetic Janus particles or electric dipoles which tend to form lines and rings, the self-assembled structures of micro-sized dipolar charged Janus particles under a low electrolyte condition were in various shapes and sizes, which were well captured by the Monte Carlo simulation. Broad energy minimum, small contacting area, and relatively weak electrostatic attraction contributed to the polar axes of particles in the cluster could not be strictly in the same plane, thus the dipolar Janus particles tended to cluster together

forming ambiguous morphologies. However, the entire formed cluster featured a symmetry-broken surface charge in which one half was positive and the other half was negative. Thus, as they described, the oppositely charged sides from two clusters would attract each other resulting in facile assembly into larger aggregates.

Janus particles containing physically responsive functionalities can undergo regulated motion as well as arrangement when an external field (*e.g.*, electric or magnetic field) is applied. By using half gold deposited PS particles, Velvce[37] and Takei[38] systematically studied the response of electrical symmetry-broken Janus particles to AC electric fields which displayed either polarity-depended electrophoretic rotation under relatively low frequency electric field[37] or self-assemble into staggered chains, 2D crystals, or 3D bundles at higher frequency regions.[38] Similarly, chains of magnetic Janus particles have been observed by applying a magnetic field.[18] The particles in these two examples showed distinctive disassemble behavior. For the former, due to steric force and Brownian motions, the assembled Janus particle chains would fall apart when the electric field was switched off.[37] By contrast, the formed magnetic Janus particle assemblies have residual magnetization and would not disassemble until they were demagnetized.[18]

The shapes of self-assembled products vary among different Janus particle systems as the consequence of varied formation mechanisms which are influenced by orientation, size, surface physical-chemical characteristics (*e.g.*, roughness, charge, hydrophobicity, *etc.*), and other factors which contribute to local interactions. Nevertheless, the resultant supra-colloidal structures of Janus particles' self-assembly which are quite challenging or impossible for either isotropic particles or amphiphilic molecules. This is the primary driving force for the study of self-assembly using symmetry-broken particles. Therefore, 1) the emergence of new types of

materials based on the self-assembly of Janus particles, and 2) the building of complex structures through a "bottom-up" strategy by using Janus modules containing multiple species can be expected.

1.1.4 Janus particles composition

Briefly, according to the excellent Janus particle review paper from Pang and co-authors,[6] Janus particles can be classified into three categories: 1) hard Janus particles which consist of inorganic, metallic materials, for example, amphiphilic glass beads[13] and Au/Fe_3O_4[32-34]; 2) soft Janus particles which are made of polymeric, organic molecules, such as PS/PMMA[9,21] and ABC-type triblock copolymers-based Janus particles[26]; and 3) hybrid soft/hard Janus particles, for example, PS/Pt[29]. As described in the previous text, a broad variety of materials have been employed for fabricating Janus particles. In particular, polymers have been heavily used via either precise polymer synthesis or surface engineering.

By contrast, biomaterials are relatively less commonly used to prepare Janus particles. Nanosized Janus proteins have been built based on their intrinsic domain separation features or specific binding regulated masking.[8] Liposomes that are closed, spherical lipid bilayer assemblies dispersed in water and whose composition falls within dual-phase co-existence region, have the capability to form Janus particles over a wide size range (from nanometer to micrometer).[1,2,8,39] Compared with other commonly used materials, various benefits can be expected from the development of biomaterial-based Janus particles. This is largely based on the natural advantages of biomaterials in biological applications and fundamental researches, such as their biocompatibility, biodegradability, and biosimilarity which impart appealing features to newly developed materials as well as being suitable for mimicking biological structures.[40] Combining unique properties promised by Janus structures (especially the orientation-sensitivity)

with the benefits of using biomaterials, it is meaningful to devote efforts toward preparing biomaterial-based Janus particles and exploring their features.

Liposomes, like proteins, have significant values in biological researches/applications. There are extensive examples that show that liposomes are easier to prepare, manipulate, and observe as compared to proteins.[40] Hence, I decided to use this kind of material to prepare the all-lipid-based Janus particles for this Dissertation. Besides these experimental advantages over studying protein-based Janus particles, other reasons for choosing liposomes are listed below:

(1) Lipids are a kind of essential biomolecule, along with amino acids, nucleic acids and carbohydrates. For example, glycerophospholipids, which are the primary lipids employed in this work, are one of the main components in plasma membranes.[41,42] More than that, as an amphiphilic biocompatible molecule, lipids are one of the most appropriate materials to be used as pharmaceutical excipients.[43]

(2) Liposomes have found widespread use in a variety of application[40] ever since its discovery[44] in the 1960s.

(3) Currently, Janus liposomes have received relatively little attention. The soft, deformable, and flexible natural characteristics of liposomes can be used as a model system to offer the chance to test theories/predictions as well as to explore new properties/behaviors which are quite challenging for Janus materials with rigid surfaces.

The next step is to identify the possibility of preparing all-lipid versions of such heterogeneous particles from the biophysical principle of lipid phase separation. In the following sections, I will address this topic.

1.2 Lipids as molecular building blocks

1.2.1 Lipids

(1) Lipid species

Lipids are a group of macrobiomolecules that are soluble in non-polar or weak polar solvents (e.g., chloroform, methanol, octane, etc.) but insoluble in water. There are two main types of lipids are used in this Dissertation, one is cholesterol and the other is glycerophospholipid. Furthermore, synthetic cationic lipid 1,2-dioleoyl-3-trimethylammonium-propane (chloride salt) (DOTAP) (7 in Figure 1-2) whose trimethylammonium headgroup links with two oleoyl chains through glycerol without phosphate is also employed in preparing charged liposomes. The lipids molecular structures used are presented in Figure 1-2.

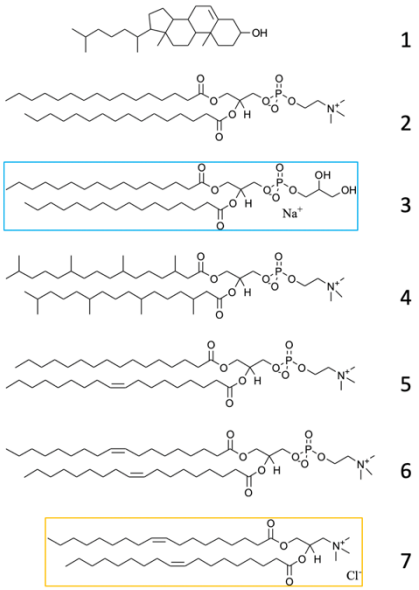

Figure 1-2. Main used lipids molecular structures. 1- cholesterol, 2- DPPC, 3- DPPG, 4-DPhPC, 5-POPC, 6- DOPC, 7- DOTAP. Anionic lipid is framed with blue and cationic lipid is framed with orange color.

Cholesterol (1 in Figure 1-2) is a kind of unique lipid and widely exists on bio-membranes where they have been extensively confirmed to play essential roles in biological functions.[41,42,45] With respect of their molecule structure, there is a small hydrophilic head –

hydroxyl group – in cholesterol, and a hydrophobic moiety consisting of a rigid, planar, fused ring, and a short hydrocarbon tail. Their molecular structure is quite different from phospholipids leading to their special roles in regulating lipids arrangement which will be discussed later.[42,46]

Depending on the alcohol links between hydrophilic headgroup and hydrophobic tails, phospholipids are divided into two types: one is glycerophospholipid which contains glycerol and which is used for preparing Janus liposomes in the presented research (2-6 in Figure 1-2) and the other is sphingomyelins which contains sphingosine. There are a few criteria used to further categorize glycerophospholipids. For the lipids used in this research, they can be categorized by: 1) According to the saturation of acyl chains: 1,2-dipalmitoyl-sn-glycero-3-phosphochline (DPPC) (di16:0) (Figure 1-2 2), 1,2-dipalmitoyl-sn-glycero-3-phospho-(1′-rac-glycerol) (sodium salt) (DPPG) (di16:0) (Figure 1-2 3), and 1,2-diphytanoyl-sn-glycero-3-phosphocholine (DPhPC) (Figure 1-2 4) (a kind of branched lipid containing diphytanoyl fatty acid chains) belong to saturated lipids, whereas for unsaturated phospholipids, there are double bonds in the tail of 1-palmitoyl-2-oleoyl-glycerro-3-phosphocholine (POPC) (16:0-18:1) (Figure 1-2 5), 1,2-dioleoyl-sn-glycero-3-phosphocholine (DOPC) (di18:1) (Figure 1-2 6), and DOTAP (di18:1) (Figure 1-2 7) (note that DOTAP is not glycerophospholipid). 2) Based on headgroup charges: zwitterionic lipids including DPPC, DOPC, and DPhPC whose net charge is 0 in pH 7, anionic lipid DPPG whose net charge is -1 in pH 7, and cationic lipid DOTAP which contains a positively charged trimethylammonium group on the polar moiety.

There is a long history of extracting lipids from animals and plants, for example egg yolk lecithin. However, high-degree purified and structure/configuration defined lipids are more appealing for fundamental researches and applications. Thanks to the development of purification techniques (*e.g.*, chromatography) and chemical synthesis, different kinds of lipids

and lipid derivatives have been commercialized, which greatly contribute to the thriving of lipids community in recent years.

(2) Applications of lipids

Phospholipids play many essential roles in biological structures and functions, and they have been widely employed in a variety of areas. One of the major applications of phospholipids involves developing drug delivery systems and is mainly due to their biocompatibility as well as amphiphilicity.[43] The latter confers their characteristics including self-assembly into liposomes, stabilize emulsions, and surface-active wetting which all are appropriate for pharmaceutical applications. In recent years, the U. S. Food and Drug Administration has approved a variety of phospholipid-related formulations, such as Ambisome® containing hydrogenated soy phosphatidylcholine (HSPC) and 1,2-disteraroyl-*sn*-glycerol-3-phospho-(1-rac-glycerol) (sodium salt) (DSPG), Doxil® containing HSPC and 1,2-distearoyl-*sn*-glycerol-3-phosphoethanolamine-N-[amino(polyethylene glycol)-2000] (ammonium salt) (DSPE-PEG_{2000}), and DaunoXome® containing 1,2-disteraroyl-*sn*-glycerol-3-phosphocholine (DSPC), to name but a few.[43]

For charged lipids, their crucial biological functions have been more and more reported in recent years. In nature, only negatively charged phospholipids (anionic lipids) have been discovered in the plasma membrane, and they mainly distribute at the inner leaflet of the membrane.[42,47] These lipids include phosphatidylglycerol (PG, net charge in pH 7 is -1), phosphatidic acid (net charge in pH 7 is -1), phosphatidylinositol (net charge in pH 7 is -1), phosphatidylserine (net charge in pH 7 is -1), and others.[43,47] Even though the charged lipids normally only account for a small fraction of biomembrane lipids, they play significant roles in regulating proteins. It has been reported that they are one of the factors in determining cell metabolisms, cell communications, and other biologically relevant processes. For example, one

of the most extensively studied charged lipids – PG – is rich in pulmonary surfactant (~11%), and it is an essential constituent for functions such as photosynthesis, RNA synthesis activation in mammal cells, and protein transport on bacteria membrane.[47] Conversely, commercial positively charged lipids (cationic lipids) are synthesized chemicals that have also been widely used. In particular, DOTAP is a star material in DNA-related pharmaceutical applications mainly because it can attach positive DNA chains efficiently.[48]

Lipid derivatives in which lipids link with other types of chemicals, such as PEG, DNA, biotin, and fluorophores, have also been employed in applications for modifying and functionalizing lipid membranes. Some of these modifications have been proven to alter the efficiency of lipid-based drug carriers. For example, there is extensive evidence that PEGylated liposomes can lengthen in vivo circulation because they can avoid being trapped by reticuloendothelial systems. The presence of hydrophilic PEG molecules on the surface of a lipid bilayer gives rise to depletion forces which can induce intramembrane interactions.[49] This characteristic makes the PEG-modified liposomes to more resemble cell membranes which is useful for fundamental studies. DNA hybridization has been employed in modifying interactions among lipid bilayer membranes.[39,50,51] Boxer and co-workers[50] synthesized DNA-lipid conjugates and introduced them into liposomes. They found that the presence of DNA on the surface could drive liposome fusion and the most efficient fusion occurred when the DNA on the reacting liposomes were complementary and in the opposite orientation.

(3) lipid bilayer membrane

In an aqueous environment, driven by attractive hydrophobic interactions from non-polar acyl chains and attractive hydrophilic interaction from polar headgroups, the lipids spontaneously assembly into lipid bilayer membranes to decrease the system's free energy (the

typical critical micelle concentration for lipid bilayer-forming is 10^{-10} M).[40,52] In the bilayer, the hydrophilic part faces the water while the hydrophobic part points toward the core of the membrane. Because the higher energy cost for water to stick with non-polar group as a consequence of hydrogen bond loss, therefore, hydrophobic moieties tend to minimize the exposed area to water. Under certain conditions (such as temperature, pressure, pH, ionic strength, composition), lipid bilayer membranes exhibit different characteristics, including mobility, rigidity, thickness, as well as others.[42,45,46,53] We refer to these lipid bilayer membranes with differing characteristics as being in different phases.

1.2.2 Lipid phases

Under specific temperature and pressure (low temperature and/or high pressure), lipids are tightly, orderly packed on a membrane in which the hydrocarbon chains of lipids are parallel with each other. However, the orientation of the lipids' axes is not parallel with the membrane normal and this is referred to as tilt of fatty acid tails. In such a case, the lipid bilayer membrane is in a crystalline solid state with a low fluidity and permeability, designated as a solid phase (g). When the temperature increases, the acyl chains' configuration will undergo conversion and the associated interfacial area per lipid increases leading to a less packed lipid arrangement on the membrane. When the temperature is over a critical point, namely, melting temperature (T_m), the g phase turns into a fluidic state termed as liquid disordered phase (ld) (also referred to as the Lα phase in some published work[54,55]). The less ordered lipid organization results in structure parameter changes: for example, for DPPC, the average interfacial area/lipid is 47.9 Å in g phase (20 ^{o}C) and increases up to 64 Å in ld phase (50 ^{o}C), while the thickness of the hydrocarbon chain decreases from 34.4 Å to 28.5Å, corresponding to g and ld phase. This is the consequence of the increased number of gauche "kinks".[56,57] During this endothermic transition, an

intermediate phase – ripple phase – has been identified.[54] In very general, lipids containing two long, straight, and saturated acyl chains have much higher T_m than unsaturated ones. This is because the inherent kinks arising from double bonds weaken van der Waals interactions among hydrocarbon chains of unsaturated lipids, thus less energy is required for disrupting the ordered packing than for saturated lipids whose acyl chains are in a nearly all-trans configuration.[57] For highly branched phospholipid DPhPC, there is no observed g phase over a wide range of temperature (-120 ~ 120 ^oC) due to the methyl branching which causes the reduced lipid condensation and formation of kinks.[58,59] The melting temperatures of lipids used in this Dissertation are listed in Table 1-1.

Table 1-1. Melting temperature (T_m) of lipids used in Dissertation

High-Melting Lipid		Low-Melting Lipid		
Saturated Lipid		Unsaturated Lipid		Branched Lipid
DPPC	41 ^oC [a]	DOPC	–17 ^oC [a]	DPhPC
DPPG	41 ^oC [a]	POPC	–2 ^oC [a]	–120 ~ 120 ^oC in
		DOTAP	< 5 ^oC [b]	liquid phase [a]

[a]: data from Avanti Polar Lipids Inc. (Alabaster, AL)[60]

[b]: ref48

Besides raising the temperature to induce phase transition from g to ld phase, introducing cholesterol can also lead to new phases formation. Cholesterol plays essential roles in regulating the structures of lipid bilayer membranes. For binary mixtures containing cholesterol and phospholipid, there are various phases that have been identified. For example, in de Meyer and Smit's research, they displayed five different phases of the DMPC/cholesterol bilayer showing varied structural features (*e.g.*, the order and tilted extend of acyl tails).[54] In the research for this

Dissertation, I focused on the following three phases: g phase, ld phase, and a newly formed liquid ordered phase (lo). When the cholesterol is introduced into a fluidic bilayer membrane (ld phase) consisting of pure phospholipids, it can cause the area per lipid to significantly decrease and is associated with an increase in the thickness of the lipid bilayer. This effect has been widely identified and called the condensation effect.[54] One consequence of this condensation is membrane fluidity reduction. Above a certain temperature and certain cholesterol content, a new phase is formed, namely the lo phase. In another case, when a certain amount of cholesterol is added into a lipid bilayer membrane consisting only with saturated lipids in g phase, it can inhibit the tilt of lipid tails as well as increase membrane mobility resulting in conversion into lo phase.[61] In such a phase, the lipid bilayer membrane displays characteristics of low fluidity as the g phase with a high disordered packing as the ld phase. Therefore, the characteristics in this phase are between the g and ld phase, for example, the fluidity g < lo < ld, and rigidity g > lo > ld.[61] The question is why cholesterol can cause the condensation effect and new phase formation. Stepping back to look at the molecular structure of cholesterol (1 in Figure 1-2), as compared with phospholipid, there is a much smaller hydrophilic headgroup but a bulky ring structure in hydrophobic moiety. Therefore, based on the umbrella model, the hydrophobic part cannot be efficiently shielded by the hydrophilic head. In other words, in order to minimize the increased hydrophobic zone in the plane of the lipid membrane, caused by the presence of cholesterol, being exposed to water, the lipids organization undergoes adjustment rendering lipid bilayer membrane characteristic changes. This hypothesis has been confirmed by Smit and co-worker,[54] in which they took use of a mesoscopic water-lipid-cholesterol model to study the effect of cholesterol on phases. They modified cholesterol molecules 1) with a shorter hydrocarbon tail length, 2) with an additional hydrophilic group, and 3) by replacing the planar, fused ring with a

linear chain. They found that in both the cases of 2) and 3), the condensation effect was dismissed thus confirming the contribution to this effect came from the small hydrophilic moiety as well as the ring structure.

1.2.3 Phase separation

The interactions and mutual preferences between lipids vary significantly in different systems. They can be influenced by many factors, for example, the conformational entropy of the acyl chains, hydrogen bonds, hydrophobic interaction, electrostatic interactions, etc.[62] It is challenging to give a solid and universal conclusion about how these factors affect the lipid organizations in lipid bilayers. However, the general trend is, if the interactions among two types of lipids are repulsive, then the lipids will demix. When this repulsion is sufficiently great, the components will completely separate.[55,62] Gibbs free energy of interaction between unlike lipids can provide a thermodynamic view to understand lipids mutual preferences. Note that the unlike lipids can be different lipid species or the same kind of lipid in different phases. Defined in Almeida's review paper, unlike nearest-neighbor interaction, ω_{AB}, is the Gibbs free energy change when two pairs of like lipids (AA and BB) undergo an exchange reaction to produce two pairs of unlike lipids (AB). If $\omega_{AB} \leq 0$, A and B will ideally mix with each other, whereas, if $\omega_{AB} > 0$, these unlike lipids will demix, also called nonideal mixing. In the latter case, the more positive ω_{AB}, the more complete the separation. For example, for the lipid pair DSPC (di18:0) and DOPC (di18:1) in ld phase at 60 ºC, the ω_{AB} is +110 cal/mol, indicating that these two lipids try to avoid mixing with each other randomly.[62] This positive number can be explained by hydrophobic mismatch originating from the varied saturation degree in the hydrocarbon tails. One general trend is when two types of phospholipids share sufficient acyl chain similarities, they tend to mix ideally, whereas, the dissimilar acyl chains can result in immiscibility because

of the considerable energy cost for placing them together.[55,63] In addition to saturation degree differences contributing to hydrophobic mismatch, acyl chain length is another factor that can cause hydrophobic mismatch. For example, ω_{AB} is +80 cal/mol for the lipid pair of 1,2-dimyristoyl-*sn*-glycerol-3-phosphocholine (DMPC) (di14:0) and DSPC (di18:0) in ld phase.[62] Another trend worth mentioning is that the interactions between anionic lipids and zwitterionic lipids at pH 7 in either g phase or fluid phase are normally favorable ($\omega_{AB} < 0$). This is because the electrostatic repulsion from like charged lipids drives them to mix with the zwitterionic ones.[62]

The non-ideal mixing between lipids leads to the formation of lipid rafts and lipid phase coexistence.[42,45] In the case of a lipid bilayer membrane containing multiple kinds of lipids, there are interaction differences among different kinds of lipids. Thus, lipids with low ω_{AB} tend to mix with each other to form lipid clusters resulting in separation from lipids with large, positive ω_{AB}. These lipid clusters show different lipid organization characteristics as compare to neighboring lipids. Once these lipids cluster sufficiently to form nanosized domains, they are termed lipid rafts (domains). Note there is no widely accepted criteria to define over what size a lipid cluster is referred to as a lipid raft (domain) and the terms of lipid raft and lipid domain are sometimes used interchangeably. In this Dissertation, I refer to lipid clusters whose size is smaller than the visible light wavelength (~200 nm) as lipid rafts, whereas, those above this size (> ~200 nm), are referred to as lipid domains. The latter can be identified by commonly used confocal fluorescence microscope.

The lipid-lipid interaction energies have been introduced into Monto Carlo computer simulations to examine lipid distributions which offers the opportunity to understand lipid rafts and their dynamics.[42,62,64] If the lipid interactions are moderate, these rafts have short lifetime

and are very fluctuated. If the lipid interactions are sufficiently great, phase separation occurs where there is a clear phase boundary on the interface of the lipid rafts and the neighboring environment. In very general, for the lipid bilayer membranes that only contain phospholipids, there are g, ld single phases and solid/solid or fluid/solid phase coexistences.[46]

When cholesterol is present in the lipid bilayer, there are two consequences 1) lo phase formation, and 2) ideal/nonideal mixing with phospholipids.[46,54,64] Thus, it can be expected that phase behaviors become more complex and more coexistence phase regions appear as compared with phospholipids only systems. First, for cholesterol inclusive binary mixtures, there are g, ld, and lo single phase regions as well as g-lo and lo-ld coexistence phase regions.[46] The fluid-phase immiscibility of this type of system was first observed by McConnell and co-worker[65] in 1986 in which they used fluorescence microscopy to visualize 1-palmitoyl-2-[*N*-(7-nitro-2,1,3-benzoxadiazol-4-yl)amino-caproyl]phosphatidylcholine (NBD-PC) (fluorescent probe for DMPC-enrich phase) contained DMPC/cholesterol monolayer spread at an air-water interface and observed fluorescent domains surrounded by a continuous dark environment. Thompson and co-worker[46] employed electron paramagnetic resonance (EPR) to identify cholesterol induced liquid-liquid immiscibility in the binary lipid mixture bilayer (DPPC/cholesterol). They incorporated a phosphatidylcholine biradical spin labeled at the 16th position in both the *sn*-1 and *sn*-2 chains (di-16-doxyl-PC) into the DPPC/cholesterol mixture for the ESR tests. Characteristic peaks for both the lo and ld phases were determined in this system over a wide range of cholesterol content. They detected different time-average distributions of cholesterol in the lipid membrane within the two liquid phases which was used to account for the observed cholesterol-induced liquid-liquid immiscibility. They also found similar lo-ld coexistence phase

behaviors in a mixture of cholesterol with sphingomyelin and in mixtures of cholesterol with glycerophospholipids containing different headgroups and acyl chains.

Interestingly, there is significant evidence that cholesterol demonstrates clear interaction preferences between saturated and unsaturated phospholipids. Summarized ω_{AB} data from Almeida's review[62] show this trend. For the lipid pair of DPPC and cholesterol (60/40 in mol %) in the lo phase at 45 ^{o}C, the ω_{AB} is -190 cal/mol,[62] suggesting cholesterol interacts favorably with the saturated DPPC. Contrary to saturated phospholipids which preferentially mix with cholesterol, placing a cholesterol molecule next to an unsaturated phospholipid requires a large entropic penalty mainly due to their highly flexible hydrocarbon chains. In other words, cholesterol has a preference to interact with saturated lipids rather than unsaturated lipids. For example, ω_{AB} is +200 cal/mol for the lipid pair of POPC and cholesterol in ld phase at 25 ^{o}C.[62] This preference, together with the fact that cholesterol can regulate lipid packing features (g to lo or ld to lo phase transfer) in bilayer membranes, suggests that the occurrence of liquid-liquid immiscibility enables the formation of lipid rafts in cholesterol-contained lipid mixtures.[45,65]

In biological membranes, the concept of lipid rafts has been widely accepted. They are nanosized lipid clusters in lo phase which are rich in cholesterol, saturated lipids (e.g., high melting temperature glycerophospholipids, sphingolipids), and proteins.[64,66] An estimate of the number of lipid rafts in a cell plasma membrane would be on the order of 10^5 to 10^6,[45] which plays essential roles in biological processes, such as signaling, membrane traffic, and fusion.[45,67,68]

A variety of techniques have been employed for examining lipid phases and lipid rafts (domains), including mass spectrometry, atomic force microscopy (AFM), nuclear magnetic resonance (NMR), EPR, and optical techniques, to list a few.[46,69] Each technique has its own

advantages and bears some limitations as well. Here I would like to mention three techniques for characterizing lipid rafts (domains). AFM is a powerful tool to analyze the three-dimensional topography and to examine lipid organizations of lipid bilayer membrane absorbed onto solid substrates. The lo and ld phases are readily distinguishable by this technique because of their inherent thickness difference. For example, the sphingomyelin (SM)- and cholesterol-enriched lo phase is about 0.8 nm higher than the DOPC-enriched ld phase in the mica-supported lipid bilayers reported by Chiantia and co-workers.[70] Other advantages of using AFM is in enabling the ability to determine the mechanical properties of lipid bilayer membranes. Takechi-Haraya and co-workers[61] carefully pressed the cantilever against a liposome (a structure of closed-up lipid membrane) which lead to a small deformation of the liposome, and in such condition, the force-deformation curves could well fit shell-deformation theory. Based on the theory, they obtained bending modulus of nanosized liposomes. They declared that the thermodynamic phase state dominated the bending modulus which decreased in the order of g > lo > lg. NMR has been widely used to characterize lipid phases as well. In deuterium (^{2}H) NMR, quadrupole splittings are used to distinguish different phases. Introducing DPPC-d_{62} into lipid mixture enabled Veatch, Davis and their co-workers[66,71] to study phase dynamics in which the lo phase showed wider splittings as compared to the ld phase which showed a series of narrow and well resolved splittings, and quite differently, larger and poorly resolved quadrupolar splittings were produced from the g phase.

Currently, the fluorescence microscope is the most popular technique in studying lipid rafts (domains) because it is highly sensitive, is non-destructive, allows in-situ study, is available for both model membranes and living cells, and can offer local environment information, to list some of the advantages.[69,72] Epifluorescence, confocal and two-photon fluorescence microscopes

are classic instruments in this kind of technique. Laser-scanning confocal microscope (Nikon A1+/MP) is the main instrument employed in this Dissertation. It is suitable for investigating thin specimens mainly because out-of-focus light gets rejected from the image with the assistance of a pinhole aperture in this type of microscope which ensures acquiring images on a focal plane.[72] By incrementally stepping through a sample, images at different focal planes (Z stacks) are acquired to render and visualize the entire sample volume. Fast speed response photomultiplier tubes (PMTs) are the detector in confocal microscope which guarantees the sensitivity of this technique. In the Nikon A1+/MP confocal microscope, the detector device, InGaAsP PMTs, has a higher sensitivity and quantum efficiency as compared to normal PMTs. Another advantage is that there are multiple excitation lasers (excitation wavelength of used confocal microscope in this work include 405.8, 488.0, 561.5, 637.9 nm) in confocal microscopes that allow for simultaneous imaging of multiple indicators which is critical for observing lo and ld phases at the same time. The rapid development of fluorescent dyes and advanced fluorescence techniques (*e.g.*, single molecule fluorescence microscope, fluorescence correlation spectroscope, *etc.*) offers more options for systematically studying lipid organizations.[69]

Up to now, plenty of fluorescent molecules have been extensively employed in the research of membrane phases. These can be categorized into three main classes[69]: 1) Lipid-recognizing probes, which can bind to lipids and are usually proteins. 2) Environment-sensitive probes. They show altered spectroscopic properties in different environments, and the most frequently used one is Laurdan. 3) Partition-selective probes, which locate preferentially in either lo or ld phase. The probe in this group acts as a lipid because the fluorescent moiety is labeled on a lipid. This kind of molecule offers the most straightforward approach to study lipid phases.

Both 1,2-*sn*-glycero-3-phosphoethanolamine-*N*-(Lissamine rhodamine B sulfonyl) (ammonium salt) (rho-DOPE) (max absorbance at ~560 nm, max emission at ~583 nm) and 23-(dipyrromethene boron difluoride)-24-norcholesterol (Bodipy-chol) (max absorbance at ~495 nm, max emission at ~507 nm) used in this work belong to this group of probes. As shown in Figure 2-6, a large fluorescent moiety (Lissamine Rhodamine B) bond on the headgroup of unsaturated lipid (DOPE) gives rise to rho-DOPE very high ld phase partition (> 90%).[69] While Bodipy-chol shows a preference to bind to the lo phase (> 75%).[69] This feature is because cholesterol selectively mixes with saturated lipids in the lo phase, and Bodipy is a low polarity fluorophore which likely provides a minor disturbance to the interaction preference of cholesterol. These fluorescent phase probes are very powerful for investigating lipid domains when using fluorescence microscopes.

Due to the size issue and complexity of components, lipid rafts in biological membranes have proven rather elusive. A more efficient and direct strategy to study lipid rafts is to examine lo-ld phase behaviors in model membranes of defined compositions.[64] Currently, the most frequently employed model system is a ternary lipid mixture which contains one low-melting lipid, one high-melting lipid, and cholesterol.[55,64] There are several advantages for choosing this system in biophysical membrane researches: 1) precise control compositions, 2) various phase regions (single phase, biphasic coexistence, and triphasic coexistence regions); 3) large lo-ld coexistence regions over a wide range of temperatures in several widely used ternary lipid systems; 4) well-established phase diagrams are available.

To help better understand the phase behaviors of lipid mixtures, phase diagrams have been introduced and offer important information. Currently both NMR and fluorescence microscopes are the most popular characterization tools for mapping phase diagrams.[66] In

addition, these years, several well-established binary, ternary lipid mixture phase diagrams (*e.g.*, DPPC/DOPC/cholesterol, DPPC/DPhPC/cholesterol, POPC/PSM/cholesterol, *etc.*) have been constructed,[64] and Figure 1-3 is a general triangular compositional phase diagram. Note that the specific phase regions vary with certain ternary systems and environmental parameters, such as temperature and pressure.

The lo-ld phase coexistence in these three-component systems is the result of hydrophobic mismatch as well as cholesterol-induced liquid-liquid immiscibility. Mixing lipids into dissimilar lipid domains would greatly disrupt the preferred lipid packing and motion therein and thus skyrocket the potential energy of the system. This energy penalty, for example, amounts to about $2k_BT$ per lipid[66] for DOPC mixed with DPPC and cholesterol at room temperature, which the system elects to avoid by undergoing phase separation. As mentioned before, lipid rafts form when lipids undergo non-ideal mixing, and the properties mismatch between lo and ld phase give rise to a tension on the interface where two phases meet which is termed as line tension. Because the line tension scales linearly with the boundary, thus, to reduce the global energy of the system, the dispersed small lipid rafts (domains) tend to merge into a big one.[73] The resultant domain shows a smooth, round boundary.

So far, it is clear that lipid rafts (domains) may occur when there are repulsive lipid interactions in lipid bilayer membranes containing multiple kinds of lipids, and phase separation will appear when these interactions are sufficiently strong. The excellent and most widely employed model system for examining phase behaviors is the afore-mentioned three-component lipid mixture with the composition of one high-melting lipid, one low-melting lipid, and cholesterol. Various techniques, especially fluorescence microscopes, have been used to study these model systems and some of their phase diagrams have been well constructed. Currently,

both supported lipid bilayers and liposomes (lipid vesicles) are heavily used in studying lipid phases and lipid rafts (domains). Considering the goal of this Dissertation is to prepare Janus particles, liposomes has been chosen and they are covered in the following section.

1.3 Giant unilamellar liposomes

In an aqueous solution, structures containing an exposed hydrophobic part are energetically unstable and, therefore, the lipid bilayer membrane with exposed ends tends to curl and close up spontaneously forming a vesical called a liposome.[40] The history of liposomes can trace back to 1960s when Bangham and co-worker[44] observed ring-like structures by electron microscope when they placed a drop of negative stain (saponin containing sodium phosphotungstate aqueous solution) onto dry phospholipids (lecithin, cholesterol) on carbon-coasted cellulose grids. Since then, liposomes have drawn great attention and significant amounts of effort have been devoted to preparing (see Chapter 2), examining, and utilizing liposomes. This type of vesicle, especially symmetrical liposomes bearing homogeneous surface composition, has found widespread use in fundamental research[74-76] (*e.g.*, cell biology, biophysics, and biotechnology) as well as in industry[77-79] (*e.g.*, food, drug delivery, and cosmetics).

There are different criteria used to categorize liposomes. One is based on lamellarity numbers, like unilamellar, oligolamellar, and multilamellar liposomes. Another is based on liposomes' diameter: there are small (size < 100 nm), large (100 nm ~ 1 μm), and giant (≥ 1 μm) liposomes. In fundamental researches which focus on lipid domains, phase behaviors, and liposome shapes, giant unilamellar vesicles (GUVs) are heavily employed, mainly due to the following reasons:

(1) Observation/Characterization. The most obvious advantage of using GUVs is that it can be directly observed by regular optical microscopes which are quite unsuitable for small sized liposomes.[40] In addition to the phase-contrast microscope, different kinds of fluorescence microscopes have been extensively employed to study giant liposomes. This highly sensitive and selective method, together with the drastic development of fluorescent methods as well as fluorescent molecules in recent years, gives many possibilities to fully investigate GUVs.[69] Moreover, this advantage provides convenience for monitoring and analyzing a large number of samples, which is impractical for other time/money-consuming characterization instruments (e.g., NMR, cryogenic electron microscope, etc.). The fluorescent technique is also useful to provide information on lamellarity. Cross-section fluorescence intensity profiles enable the straightforward ability to distinguish GUVs and multilamellar liposomes.[80,81] There are two sharp maxima at the rim of vesicle together with a flat baseline region in the middle of the GUVs, whereas there are multiple distinguishable peaks in the multilamellar liposomes' profiles (see Chapter 3 Figure 3-7). Another more reliable and accurate method is to use the pore-forming toxin α-hemolysin which 1) can only make a pore in a unilamellar membrane because the comparable length of the transmembrane pore formed by α-hemolysin (~5.2 nm) to the thickness of the lipid bilayer membrane (~4 nm), 2) only small molecules can go through because of the pore size of α-hemolysin (~2.8 nm).[82] Chiba and co-workers[82] measured the cross-section fluorescence intensity profile of the prepared liposomes firstly, and then employed this toxin to further identify the lamellarity of giant liposomes produced from the inverted emulsion method. They added a high salt buffer containing α-hemolysin into the liposomes solution in which the liposomes encapsulated actin monomers, and then the actin polymerization reaction occurred as the consequence of the buffer exchange between the inside and outside of the vesicle. This

identified polymerization indicated that the liposomes prepared through their procedure were GUVs. Technically, any characterization technique being used to test lipid organization can be applied to analyze GUVs. Therefore, the complementary experiment results are available for comparing and better understanding of GUVs-based properties/behaviors. For example, Keller's group used both NMR and fluorescence microscopes to study phase behaviors of liposomes which contributed detailed phase dynamic information to the liposome community.[66]

(2) Manipulation. GUVs can be directly manipulated under an optical microscope using cytological techniques (e.g., holding pipettes and injection needles). For example, in Menger and co-worker's work,[83] they used homemade holding pipettes to capture negatively charged GUVs (POPC/cholesterol imparted with anionic lipids (*e.g.*, 1-palmitoyl-2-oleoyl-*sn*-glycerol-3-phospho-(1'-*rac*-glycerol)(sodium salt) (POPG) used in their work)) which allowed them to study interactions between negatively and positively charged GUVs (POPC/dimethyldioctadecylammonium (bromide salt) (DDAB)/cholesterol). The study of adhesion between oppositely charged liposomes were observed and recorded by a phase-contrast microscope. Furthermore, real-time monitoring and recording are beneficial for exploring detailed functions/processes. Another manipulation advantage in GUVs research is the ability to readily control the compositions of liposomes.

(3) Soft material. Labeled as a deformable biomaterial, GUVs are advantageous in studying intra-vesicle interactions. Compared with other kinds of soft materials, such as oil-in-water emulsion droplets and lipid-coated particles, GUVs are more deformable.[84] Thus, the shape adjustment is more profound and sensitive to physical/chemical perturbations than other soft materials. Particularly, when it is modified with functional chemicals (*e.g.*, charged lipids, DNA, proteins, *etc.*), the relatively simple interfaces offer an opportunity to clarify the

mechanisms behind membrane-involved biological processes as well as to develop new applications. Parolini and co-workers[84] prepared DNA functionalized fluorescent homogeneous GUVs through incubating preassembled DNA constructs (cholesterol-a long double-stranded spacer- an unpaired single-stranded DNA sequence) with DOPC GUVs where cholesterol inserted into the hydrophobic core of the lipid bilayer. Attractive forces, arising from the process of complementary DNA strands forming inter-vesicle bridges, drove adhesion of GUVs resulting in the deformation of liposomes and the appearance of a quasi-flat adhesion patch. They found that the brightness and the area of this patch together with the distance between the centers of a typical pair of DNA-GUVs depended on temperature. Similarly, the GUVs also clearly showed deformation when oppositely charged liposomes underwent adhesion, hemifusion, and fusion.[83] In another application, based on the deformable nature of GUVs, researchers were able to track the deformation that were induced by physical/chemical stimulus.[130] The observations in such experiments can help to test/correct/complete theories or models.

(4) Model system. 1) The size range of GUVs covers most types of cells (especially animal and plant cells); 2) they have similar curvatures to cells; and 3) most importantly, their bilayer membrane contains similar biomolecules and shares a similar structure to cell membranes. All of these characteristics make GUVs to be the most suitable model system for biomembrane-related researches.[40] Apart from the fascinating artificial cell fabrication, the powerfulness of GUVs is found in studying phase behaviors, domains, line tensions, and others. As mentioned in the last section, GUVs consisting of a high-melting lipid, a low-melting lipid, and cholesterol have been developed into a model platform for these purposes.[55,64] As we know, structural mismatch between lo and ld phases gives rise to line tension along the phase boundary which is a characteristic for heterogeneous liposomes. By taking advantage of heterogeneous

large unilamellar vesicles (LUVs) and GUVs composed of ternary lipid systems (e.g., DPPC/DOPC/cholesterol, DSPC/DOPC/cholesterol used in their work), Yang and co-workers[85] found that line tension contributed tens of k_BT energy to drive HIV gp41-fusion peptide-mediated fusion. Another contribution from this example is to offer a strategy for altering line tension by adjusting lipid compositions. Other than this, there are a number of examples for using these three-component-based GUVs to directly observe lipid domains by using fluorescence microscopes. Therefore, this unique platform for studying phase separation on lipid bilayer membranes has been employed in my Dissertation to build giant Janus liposomes (GJLs).

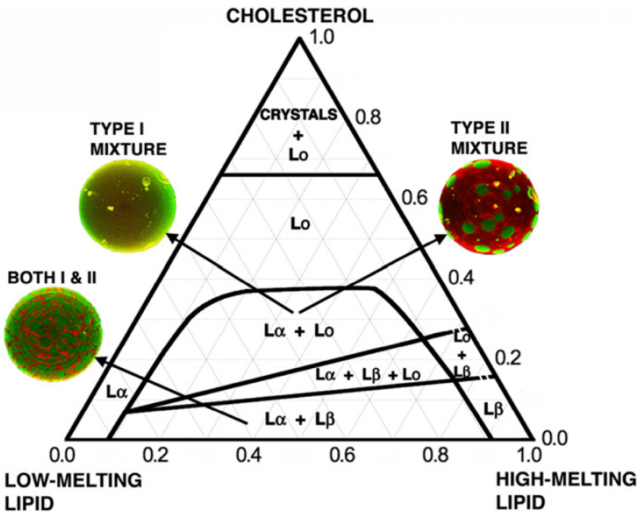

Figure 1-3. Compositional phase diagrams of ternary lipid system consisting of cholesterol, high-melting and low-melting lipids. In the diagram, Lo, Lα, Lβ refers to liquid-ordered, liquid disordered, and solid phase, respectively. Type I, Type II mixture indicates that the giant unilamellar liposome contains nanoscopic domains and micron domains, respectively. Reprinted with permission from ref. 55. Copyright 2009 Elsevier.

In these ternary lipid systems, normally there are large lo-ld coexistence regions. Based on the lipid rafts (domains) size formed in this region, Feigenson divided ternary lipid systems

into two groups (Figure 1-3): nanoscopic lipid rafts (domains) in Type I lipid mixtures and macroscopic lipid domains in Type II lipid mixtures.

Nanoscopic domains cannot be identified by commonly used fluorescent microscopes because their sizes are smaller than the wavelength of visible light. These lipid rafts have been confirmed by either NMR or the fluorescent resonance energy transfer (FRET) technique of which the latter is inherently sensitive to distance in the size range up to ~50 nm. For example, Frazier and co-workers[86] identified nano-sized lipid domains in SM/POPC/cholesterol lipid mixtures by combining FRET and Monte Carlo simulations. In their work, an excellent Förster energy transfer pair (donor MB-POPE and acceptor NBD-POPE) was incorporated in a lipid bilayer membrane to resemble POPC behaviors. By increasing the POPC content in the lipid system the Förster energy transfer efficiency increased to a maximum (~30 mol% of POPC) and then decreased, suggesting non-ideal mixing behavior. This is the consequence of weakly repulsive SM/POPC and POPC/cholesterol interactions but favorable SM/cholesterol interactions. Lipid rafts (domains) with sizes from tens to hundreds of nm were able to form and were further confirmed by lipid distribution snapshots which were produced from Monte Carlo simulations. Other researches also proved the existence of nanoscopic lipid rafts by FRET even though the lipid bilayer membrane displayed uniform fluorescence.[87] Compared to macroscopic domains, these nanosized lipid rafts are entropic unfavorable. They may be the products of the kinetic trap due to membrane viscosity or interdomain repulsion, or as Feigenson mentioned, there plausibly exists a low line tension system.[55] Note that line tension varies in different lipid compositions. For example, Yang and co-workers[85] compared the domain size of GUVs which were made up of DOPC, cholesterol, and saturated lipids with various acyl chain lengths. They found that the size of the lo domain in DSPC contained GUVs was larger than those in DPPC

contained GUVs, and they attributed this domain size difference to line tension variation. However, some researchers think nano-sized lipid rafts are the results of compositional fluctuation and should not be recognized as lipid domains.[71]

Macroscopic domains are thermodynamic favorable products and fluorescence microscopes are suitable for observing them. Both DPPC/DOPC/cholesterol and DPPC/DPhPC/cholesterol have been confirmed to be Type II lipid mixtures.[73,88] In addition, their phase diagrams have been established by using fluorescence microscopes to trace their phase behaviors. Veatch and co-worker[73] reported domain kinetics in the DPPC/DOPC/ cholesterol GUVs which was incorporated with the ld phase probe (Texas Red dipalmitoyl-phosphatidyletheanolamnie). For GUVs with the composition of DPPC/DOPC/cholesterol = 37.5/37.5/25 mol %, the small domains formed when the temperature was lowered into a lo-ld phase coexistence region, and then underwent merging, and finally liposomes completely phase separated into a single dark region and a single bright region. Three things can be learned from this observation: 1) Temperature dependent liquid-liquid immiscibility. For a specific lipid composition, lo-ld phase coexistence occur in a certain temperature range. When the temperature increases, the order of the lipid acyl chain decreases and the repulsive lipids interactions are not strong enough for supporting phase separation, rendering the whole lipid bilayer membrane in the single ld phase. When the temperature passes the miscibility transition temperature, cholesterol regulates the packing of saturated DPPC causing it to turn into the lo phase, whereas most unsaturated DOPC lipids maintain in the ld phase, thus liquid-liquid immiscibility occurs. When the temperature is too low, the lipid bilayer is in g phase. Note that this transition temperature is different from the melting temperature of lipids described in section 1.2. Through systematically varying the lipid mixing ratios and monitoring the miscibility transition

temperature in DPPC/DOPC/cholesterol system, they found this parameter was significantly influenced by membrane composition.[73] Additionally, compared to another model ternary mixture DPPC/DPhPC/cholesterol studied by the same research group,[88] domains can form even at 50 ^{o}C suggesting that altering the lipid species with disparate melting temperatures enables the ability to adjust the temperature range for lo-ld phase coexistence region. 2) Domains ripening. Line tension drives small domains to collide and coalesce with each other to form larger sized domains for lowering system energy. 3) Janus structure formation. In thermodynamic equilibrium state, there are two distinctive compartments in one entity featuring with different physical-chemical properties, such as fluidity, rigidity, and lipid compositions. Half-half Janus liposomes were observed in both DPPC/DOPC/cholesterol and DPPC/DPhPC/cholesterol-based GUVs. This fact reflects the feasibility to obtain giant Janus liposomes for this research.

GUVs featuring two distinctive macroscopic liquid domains have been widely mentioned, however, to my knowledge, there are few published works that have systematically studied this kind of heterogeneous liposomes. Taking advantage of the Janus-like structure originating from hydrophobic mismatch and cholesterol-induced liquid-liquid immiscibility, Beales, Nam, and Vanderlick carried out the first systematic study on giant Janus liposomes electroformed from DPPC/DOPC/cholesterol in 2011.[39] Electroformation is the most frequently employed approach for producing GUVs in which the liposomes form from dried lipid stacks in a hydration solution with the assistance of an electric field. The big drawbacks of this method include wide size distribution, lipid damage, and bias towards charged lipids. Using lipid-phase separation to guide DNA anchoring on these liposomes, furthermore, they successfully rendered these Janus liposomes asymmetrical binding ability, which preferentially occurs via lo domains. Mixing such Janus liposomes carrying complementary DNA strands then led to the formation of

various size-limited liposome clusters, a unique behavior not displayed by homogeneous single-domain liposomes. This work clearly demonstrated the possibility to prepare Janus particles using lipids and moreover, unique features of liposomes as a colloidal material, *e.g.*, their deformable surface. In addition, this work also demonstrated a widely used strategy to modify liposomes, that is, to add lipid derivatives into a lipid matrix. More importantly, lipid interaction preference enables the ability to sort these lipid derivatives into a certain phase, rendering phase-specific functions. In the example of DNA functionalized Janus liposomes, DNA tethered cholesterol preferentially join in the cholesterol-enriched lo phase. Moreover, the DNA-conjugated lipid (lipid moiety containing two octadecyl chains which is similar to acyl chains in DPPC) selectively partitioned into the DPPC-enriched lo phase. They also found this partition preference could be enhanced by incorporating highly unsaturated lipids (*e.g.*, bovine heart cardiolipin showed the strongest effect). This was the result of lateral packing stresses created in the ld domain, thus if cholesterol- or lipid-DNA was inserted into ld domain containing highly unsaturated lipids, it would cause the free energy cost increase.[39]

Based on these findings from DNA functionalized giant Janus liposomes, combining the novel properties/behaviors promised by Janus particles with the biochemical values as well as practical manipulation of GUVs, I decided to systematically study giant Janus liposomes. Prior to developing fascinating applications that rely on GJLs, first it is essential to search for a more robust procedure for preparing GJLs as compared with electroformation, and then to interpret the corresponding behaviors in a relatively simple system for offering valuable information for further use.

1.4 Goals and main topic of this Dissertation

There are three main goals throughout this Dissertation:

(1) Employ a relatively novel but promising procedure – PVA gel-assisted hydration – to prepare GJLs consisting of ternary lipid system who has a lo-ld coexistence region;

(2) Prepare GJLs containing physically response or (bio)chemically reactive functionalities and examine their properties;

(3) Detect behaviors of the functionalized GJLs, mainly focusing on two parts: self-assembly and motion.

In the following four Chapters, these goals will be addressed.

In Chapter 2, DPPC/DOPC/cholesterol will be first used for preparing GJLs via PVA gel-assisted lipid swelling procedure. The versatility of this method will be further demonstrated by generating DPPC/DOPC/cholesterol GJLs with tunable Janus configurations as well as preparing DPPC/DPhPC/cholesterol GJLs.

In Chapter 3, a new procedure – membrane-gated and gel-assisted hydration – will be developed for obtaining size-controlled giant liposomes, including homogeneous and GJLs. The other two procedures, membrane-free gel-assisted hydration and extrusion, will be introduced to evaluate the performance of the new method.

In Chapter 4, biotin-DOPE decorated GJLs will be prepared first, and then the location of biotin-DOPE will be detected. Finally, the domain-specific cluster/aggregate formation of these GJLs will be carefully monitored and interpreted.

In Chapter 5, charged lipids will be added into DPPC/DOPC/cholesterol system to prepare charged GJLs. Properties, such as charge placement and zeta potential, will be determined. Both electrokinetic motions under direct current and electrostatic self-assembly of GJLs will be carefully monitored and interpreted.

CHAPTER 2. PREPARATION OF GIANT JANUS LIPOSOMES: A GENERAL ROUTE VIA GEL-ASSISTED LIPID HYDRATION

2.1 Introduction

2.1.1 Preparation of Giant Liposomes: An Overview

Ever since the discovery of liposomes in the late 1960s, researchers have been interested in developing facile and efficient methods for the preparation of high-quality giant liposomes. Thanks to their efforts, several general strategies have been established over the past decades, which mainly fall into three categories according to the liposome formation mechanisms: (1) lipid hydration, (2) emulsion, and (3) lipid membrane rearrangement.

(1) Lipid hydration

Lipid hydration generally refers to the processes by which the dried lipid films are rehydrated in aqueous solutions. Hydration based methods are probably the most extensively used strategy for producing giant liposomes because they are simple to operate, low-cost, and can be generally applied to a wide range of lipids under physiological conditions.[40,74,89] For achieving dried lipid stacks, lipids are dissolved in organic solvents (*e.g.*, chloroform) first, then they are deposited onto a substrate, and finally they are exposed under a nitrogen stream or vacuum to drive the solvents away. During the hydration, generally, mechanical agitation (*e.g.*, shaking, swirling, vortexing) leads to a high percentage of multilamellar vesicles being produced. In contrast, high yields of unilamellar liposomes are formed with the assistance of gentle physical disturbing (*e.g.*, electric filed oscillation, cushion gels swelling). It is necessary to mention that, for preparing GUVs consisting of the ternary lipid system, the hydration temperature is required to be higher than the T_m of the high-melting lipid. The commonly accepted mechanism for the formation of giant liposomes in this category is: 1) amphiphilic

lipids self-assemble into bilayers in an aqueous environment; 2) the upward vertical forces originating from water transfer, which exert normal to the formed lipid lamellae, cause the lipid bilayers to separate and swell, to bulge/bud, and to then form lipid vesicles which are entangled on the lipid stacks; 3) giant liposomes eventually form as a consequence of the fusion of adjacent lipid vesicles.[40,90] It has been reported that the separation and swelling of lipid lamellae can be altered by applying additional mechanical forces, which is the case in electroformation (also called electroswelling) and gel-assisted hydration (the procedure used in this work). It is necessary to mention that, for preparing GUVs composed of the ternary-lipid system, the hydration temperature is required to be higher than the high-melting component's T_m. For example, the hydration temperature for preparing DPPC/DOPC/cholesterol GJLs in this Chapter was 45 ^oC, which was higher than the T_m of DPPC (T_m ~41 ^oC).

Gentle hydration (or natural swelling) is the most straightforward approach for liposome production, but high yield multilamellar giant liposomes produced from this method are very problematic for further applications.[40,89,91] Electroformation is a much more common method used in giant liposome formation. In this method, lipid layers are initially coated onto the conductive indium tin oxide (ITO) glass or Pt wire and then experience enhanced swelling in an aqueous solution when an electric field is applied. Two of the main issues for electroformation are the limitation of lipid species and hydration solution options, both of which have been tackled recently by modifying the hydration parameters (*e.g.*, electric field frequency, voltages, or temperature).[40,89] However, disadvantages, such as the high risk of lipid oxidation, low encapsulation efficiency, and the requirement of special equipment (*e.g.*, power supply, special designed liposome producing and harvesting apparatus), are still significant concerns when choosing this procedure. [40] In recent years, the emerging gel-assisted hydration procedure (see

2.1.2) has already opened a new window to improve the issues encountered in gentle hydration and electroformation.[1,2,90,92-94]

(2) Emulsion-based methods

For this strategy, lipid-dispersed water-in-oil-in-water (W/O/W) emulsion droplets are first produced, often through multiphase laminar flows. Subsequent removal of the oil phase from the emulsion then causes the outer lipid monolayer to collapse onto the inner one, producing liposomes with size comparable to the water core.[40,91,95-98]

The development of microfluidic techniques is also beneficial to the preparation of giant liposomes through the emulsion-based strategy. One representative example which employs microfluidic devices to efficiently prepare monodispersed GUVs was reported by Deshpande and co-workers.[97] Similar with other published microfluidic setups, a double-emulsion droplet was formed by pinching off the lipid-carrying organic phase with outer fluid streams in the special-designed six-way-junctional microfluidic device. One remarkable finding from this work is that 1-octanol exhibited the best performance for producing giant liposomes via this approach as compared with other solvents used for the lipid-carrying organic phase (*e.g.*, oleic acid, propanol, *etc.*). More than that, by contrast with the slow solvent-extraction process that commonly exist when using other organic solvents, a spontaneous and fast budding-off process was observed by using 1-octanol. This is mainly because there is a big interfacial tension gap between 1-octanol/water and lipid membrane/water (mN m^{-1} *vs.* μN m^{-1}) as well as hydrophobic mismatch among 1-octanol and the used lipids (8 carbon atoms *vs.* 18 carbon atoms). Thus, the double-emulsion droplet underwent the phase segregation between the lipid bilayer and 1-octanol molecules followed by 1-octanol pocket separation, which resulted in the formation of GUVs. One significant advantage of microfluidic techniques in giant liposome formation is that the size

distribution and lipid components can be well controlled by regulating the flow rates of different phases and channel dimensions. For example, tunable homogenously size-distributed GUVs were produced, as in the work previously described, through adjusting the technical parameters of their microfluidic device.[97] Even though there was no noticeable 1-octanol in the formed GUVs and the fact that 1-octanol has low water miscibility, they could not completely eliminated the possibility of potential contamination. The residual organic solvents in the lipid bilayer membrane may introduce artificial effects during further utilization. Nevertheless, this method has several advantages such as a high encapsulation efficiency, controllable liposomes sizes, and the feasibility of preparing asymmetric leaflet bilayer liposomes, which are beneficial for several applications.[40,91]

(3) Lipid membrane rearrangement

Normally the formed liposomes are stable in an aqueous environment, however, when extra physical-chemical stimulus are applied, the lipid bilayer may experience rearrangement resulting in liposomes' size change. One classic example is extrusion.[40,74,99] When the extra pressure is applied to drive pre-produced giant liposomes to pass a thin and porous polymer membrane with feature pore size, liposomes which are smaller than and/or around the size of the defined pores can go through the membrane because of their flexible nature. However, the over-sized liposomes (larger than pore size) will burst and the resulting lipid bilayer membrane will assemble into liposomes with smaller diameters. Similarly, small sized liposomes can be obtained through powerful sonication. Normally, the strategy of liposome break-down is extensively used for preparing small unilamellar vesicles (SUVs) and LUVs from GUVs. The reverse process to produce big liposomes from small liposomes can also be realized through fusing SUVs or LUVs. Typically, divalent cations (especially Ca^{2+}), PEG, or fusogenic peptides

are added to help the liposomes overcome the energy barrier to fuse.[40] The challenges for this method include poor size and lamellarity control, low encapsulation efficiency, and limited lipids selection.

So far, there is no versatile procedure for giant liposome preparation after more than a half-century of development. Different methods exhibit their limitations in experimental and practical aspects, such as contamination, low encapsulation, and time costing, to list few.[40] The microfluidic assisted approach holds the primary benefit of controlling liposome formation, which is problematic in the hydration method. However, liposomes from this method bear issues, such as low stability and potential cytotoxicity, stemming from the residual organic solvent's presence. To my knowledge, solvent-free hydration is still the most popular method in many labs, especially electroformation. Although gel-assisted swelling is still a relatively new method, several advantages using this procedure have been reported and some pressing issues in the gentle and electro-swelling procedures have been overcome. [89] The advantages include a gentle hydration environment, time-saving (~30 minutes compared to electroformation 2-4 h, or gentle hydration > 24 h), high encapsulation efficiency, and no need for special equipment. More importantly, vesicles composed of a wide range of amphiphilic molecules (lipids, polymers) can form under various conditions. These benefits cause this method to draw significant interest since the first publication in 2009.[90] Therefore, in the following part, I will focus on introducing gel-assisted hydration.

2.1.2 Gel-Assisted Hydration

Traditionally, for the solvent-free hydration method, lipids are deposited onto a bare glass before the hydration step. The lack of agitation and the strong interactions between lipid stacks during natural hydration can cause the formation of multilamellar vesicles, poor efficiency for

specific lipid composites, and other issues which have been widely complained. While introducing a gel cousin between the glass substrate and lipid films has been proven to be a practical approach for improving the ability of gentle hydration, which was first reported by Horger and co-workers[90] in 2009 by employing agarose hydrogel. Unlike gentle hydration and electroformation, the gel-assisted hydration method has shown the capability for both zwitterionic and charged lipids to prepare high-yield GUVs under either deionized water or buffer solutions. [89]

Thus far, the mechanism of gel-assisted hydration hasn't been completely understood and has been a topic of exploration in this community. One hypothesis is that the presence of the extra main water access pathway arising from hydrogel swelling exerts a new upwards force normal to the deposited lipid stacks, which can enhance the bulging and separation of the lipid bilayer and the growth of vesicles.[92] At the same time, the other two main water access modes in gentle hydration are still available: 1) direct water transport from bulk solution into the lipid membranes, and 2) interlamellar water penetration. Additionally, some works assumed that the gel surface corrugation and stretching during swelling is another critical reason for the fusion of adjacent liposomes as well as the water penetration enhancement arising from the increased chemical potential gap between the bulk solution and the dried gel.[90,92] One more thing that needs to be mentioned is that the hydrogel film's physical-chemical properties (e.g., roughness, thickness, surface chemistry of hydrogel) potentially affect liposome growth. For example, Movsesian and co-workers[94] controlled two characteristics, morphology and thickness, of cross-linked poly (methacrylic acid-*co*-ethylene glycol diacrylate) (*x*PMAA) porous hydrogel substrate through a chemical vapor deposition method. They found these two characteristics could influence the formation of liposomes. Specifically, thinner and more structured porous hydrogels

favored yielding giant liposomes which was plausibly attributed to an optimal number of nucleation sites in these hydrogels in order for the lipid films to grow into vesicles. From the same work, they compared the formation efficiency of zwitterionic and charged giant liposomes through their procedure. The cationic liposomes composing of DOTAP demonstrated a significant yield decrease, mainly due to the electrostatic attraction among the positively charged lipid stacks and the negatively charged hydrogel surface.

Up to this point, different kinds hydrogels, such as agarose,[90,100] starch,[101] PVA,[1,2,92,102] and crosslinked polymers[94,103-105] have been employed in gel-assisted hydration method. Agarose is a kind of polysaccharide and is highly porous in the gel-state. The enhanced contact between agarose gel and lipids as well as the hydrogel swelling process, contribute to the growth of giant liposomes.[100] However, contamination happens during this process, primarily due to the lipids highly permeated into the hydrogel and the highly likely dissolving nature of agarose gel. The existence of agarose in lipid membranes and inside liposomes has been confirmed. The consequence of contamination is the alteration of physical-chemical properties (especially mechanical properties, like membrane fluidity, bending, *etc.*) of the liposomes, which hints at the artifacts in liposome research and the potential influence on their application in drug delivery or others. Lira and co-worker[100] systematically tested the response of GUVs contaminated by dissolved agarose to electric pulses (electroporation experiment) to determine the presence of this polysaccharide in/on liposomes could influence the liposomes' mechanical properties. For example, after applying electroporating pulses, liposomes underwent deformation and membrane poration, followed by membrane resealing. However, they found agarose contained GUVs significantly slowed the last step (~10 ms for agarose-free GUVs *vs*. ~20 ms for agarose-contained GUVs). This observation could be explained by the fact that agarose which was

trapped across the lipid membrane could lower the membrane edge tension and thus prevent the process of normal membrane resealing.

A more robust hydrogel material, PVA, was first introduced by Weinberger and co-workers in 2013.[92] In their work they substituted agarose with PVA, which is less dissolvable than other physical hydrophilic gels at room temperature, and carried out PVA gel-assisted hydration for preparing GUVs. The high molecular weight PVA gel-assisted hydration method not only suppresses gel contamination but also maintains all other advantages of the gel-assisted hydration method mentioned previously. For example, 1) they observed numerous unilamellar vesicles within 2 min of hydration, 2) no traces of fluorescent PVA was found in/on the DOPC GUVs which were formed at room temperature, 3) liposomes consisting of various compositions (*e.g.*, DOPG, DOTAP, *etc.*) as well as polymersomes ($PDMS_{10}$-$PMOXA_{87}$-$PDMS_{10}$) were obtained by using either PBS buffer or sucrose as the hydration solution, and 4) actin filaments could be readily encapsulated in the interior of the GUV, which could further form actin bundles when streptavidin was available in the vesicle. However, one should be aware of PVA gel integrity loss under high temperature. As mentioned in the pioneering work described above, high MW (145 kDa) fluorescent PVAs dissolved from the hydrogel when exposed > 50 ^{o}C for longer than 30 min, and low MW (~16 kDa) partially dissolved even at room temperature.[92] Dao and co-workers[102] thoroughly evaluated the mechanical properties, including stretching elasticity, membrane fluidity, and local membrane packing, of GUVs produced from either electroformation or PVA gel-assisted hydration by using different techniques, including the micropipette aspiration technique, fluorescence recovery after photo bleaching (FRAP), and Laurdan generalized polarization. FRAP is a powerful technique for evaluating liposome membrane fluidity by determining lateral diffusion coefficients for which a smaller number

means lower membrane fluidity. They found that the diffusion coefficient of fluorescein isothiocyanate (FITC) on POPC GUVs, which were produced from PVA (145 kDa) gel-assisted hydration under the condition of room temperature using sucrose hydration solution, decreased by a factor of 2.7 as compared to PVA-free POPC GUVs. This membrane fluidity deviation indicated the presence of PVA chains in the lipid bilayer membrane as well as in the suspending medium.

A few kinds of cross-linked polymers, including xPMAA,[94] dextran poly (ethylene glycol) (DexPEG),[103,104] and poly (N-isopropyl acrylamide)-based statistical terpolymer (PNIPAAm),[105] have also been employed for preparing GUVs through the gel-assisted hydration procedure as well. Schultze and coworkers[105] incorporated PNIPAAm with a micropatterning hydration approach to produce mono size dispersed giant unilamellar anchored vesicles. They took advantage of a photolithography technique as well as UV light exposure dose controlled PNIPAAm cross-linking density to develop a new type of substrate with featured patterns, and then deposited lipid stacks on the polymer film for further forming GUVs through the gel-assisted hydration approach. Interestingly, GUVs were only formed on the weakly cross-linked and strongly swollen pillars with the predefined diameter. Another two highlights of their method are 1) the size of the formed GUVs was well defined by the pillars' diameter mainly due to the inhibited further fusion with adjacent vesicles; 2) the formed GUVs were anchored on the substrate as the consequence of lipids partially penetrated into the polymer network. This gel micropatterning method provided a new direction for using the gel-assisted lipid swelling procedure, that is, to combine gel-assisted hydration with other techniques that have been employed in liposome production. However, so far, limited hydrogel materials from a big family of this type of material have been reported to serve as a swelling-cousin in the gel-assisted

hydration approach. Considering the significant benefits obtained from using hydrogels in GUVs' preparation, I am expecting that more swelling-capable materials will be used in the future to boost the application of the gel-assisted hydration method.

After comparing the advantages and disadvantages of different giant liposome preparation methods, I decided to make use of the PVA gel-assisted hydration method to fabricate giant Janus liposomes (GJLs). The reasons for selecting PVA in my work are: 1) PVA is more robust than agarose, 2) an easy-to-follow procedure to prepare PVA hydrogel on a substrate as compared to cross-linked polymers, and 3) PVA is biocompatible and commercially available. As a relatively novel method, the current gel-assisted hydration researches mainly focus on the capability of giant liposomes preparation and the efficiency of encapsulation. However, these reported works barely focused on phase-separated liposome formation or the phase behaviors of prepared liposomes, which are crucial for giant liposome research. In addition, the gel-assisted hydration approach had not been employed to prepare Janus particles before my research. Therefore, the following text will explore how PVA gel-assisted hydration works on phase-separated giant liposome formation, which has been widely investigated by using other methods.

2.2 Experimental Section

(1) Reagents

All lipids, including DPPC, DOPC, rho-DOPE and Bodipy-chol were products of Avanti Polar Lipids (Alabaster, AL). Other chemicals, including PVA (MW: 89 000− 98 000 and 145 000), cholesterol, were obtained from Sigma-Aldrich. Deionized (DI) water of 18.2 MΩ × cm (Millipore) was used throughout this work.

(2) Liposome preparation

Giant Janus liposomes of desired compositions were prepared by following the gel-assisted lipid swelling method reported by Marques and co-workers[92] with minor modifications. In the sequence of operation, specifically, the procedure can be broken down into four steps.

1. Material/substrate preparation, which included PVA solution, glass substrates, and lipid precursor solutions. The PVA aqueous solution used in this procedure contained 5 wt % polymer, which was dissolved by continuously stirring the polymer in DI water maintained at 80 °C, whereas the glass slides (VWR, 1 × 1 in, 1 mm thickness) were cleaned by sonication in acetone, DI water, dilute detergent aqueous solutions, and DI water again and then blow-dried by a nitrogen stream. All lipid precursors used in this work were prepared in chloroform with total lipid concentration of 5 mM, and their compositions are specified in the main text.

2. PVA gel preparation, which was done by first evenly spreading 100 μL of the PVA solution on a precleaned glass slide at room temperature and then drying it on a hot plate at 50 °C for 0.5 h.

3. Lipid deposition on PVA gel. To achieve this, a 5 μL lipid precursor was first cast on the PVA gel film prepared above using a microsyringe. This quickly produced a lipid thin film upon solvent evaporation, which was further dried under vacuum overnight in the dark at room temperature.

4. Liposome production, which was carried out by hydrating the lipid films deposited on PVA gel with 1 mL of DI water at 45 °C for either 1 h or 2.5 h. After a brief shake of the hydration cell housing the lipid deposits/gel/glass substrate, thus-produced liposomes were harvested with a pipette and stored at room temperature.

The freshly prepared liposomes predominantly showed patchy structure which contained several dispersed micro-sized domains. Therefore, all thus-formed liposomes were subsequently

given 5−7 days to reach complete coalescence of their lipid domains before further use. Overall, PVA gels prepared from the two molecular weights were found to yield comparable liposome products.

(3) Fluorescence Microscopy

Fluorescence images of giant liposomes were acquired on a Nikon A1+/MP confocal scanning laser microscope (Nikon Instruments, Inc., Melville, NY) using 10× objective and excitation laser lines at 488 and 561 nm. The corresponding green and red emission signals were filtered at 525 ± 25 and 595 ± 25 nm. For each measurement, a 10−15 μL liposome solution was first pipetted into a home-prepared poly(dimethylsiloxane) (PDMS, Sylgard 184, Dow Corning) microwell (diameter: 3 mm; depth: 2 mm) reversibly sealed to a precleaned microscope cover slide (Corning No. 1, 22 × 22 mm, Corning, NY) and then given 1 h to settle under 100% humidity. Images of on-gel liposomes were obtained from an epifluorescence microscope (Nikon TE-2000 U, Japan) using 10× objective; filters used: excitation, 475 ± 20 nm, and emission, 561 nm long pass.

2.3 Results and Discussion

2.3.1 Giant Liposome Formation

I chose DPPC/DOPC/cholesterol ternary system for this investigation mainly because its liquid-ordered (lo) and liquid- disordered (ld) phase coexistence has been quantitatively mapped out and can be stably maintained at room temperature.[66,71,106,107] To form liposomes of this system, I have adopted a protocol based on gel-assisted lipid swelling developed by Marques and co-workers[92] in 2013. Compared to passive supports, such as glass, the gel can provide active assistance to the hydration process in that its water-pulling gel matrix constantly drives water penetration along the direction perpendicular to the lipid stacks.[92] This greatly improves the

liposome formation and detachment. As described in Experimental Section and illustrated in Figure 2-6, this procedure mainly features a hydration step, in which lipid stacks deposited on a dried PVA gel layer are soaked in water at 45 °C, which was above the phase-transition temperature of both DOPC and DPPC. Also included in the lipid precursors were 0.2 mol % Bodipy-chol and rho-DOPE, which are known to preferentially partition into the liquid-ordered[69,108] (lo) and liquid-disordered[69,109] (ld) phases, respectively, and served as fluorescent lipid-phase indicators.

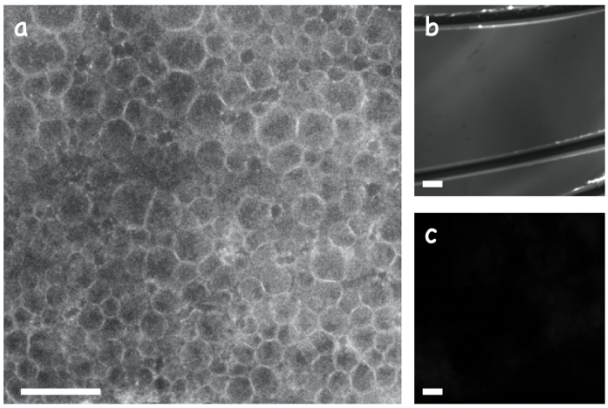

Figure 2-1. Fluorescence images of the PVA gel-assisted DPPC/DOPC/cholesterol (35/35/30 mol %) liposome (colored by 0.2 mol % rho-DOPE and 0.2 mol % Bodipy-chol) production process. (a) Fluorescence micrograph of giant liposomes as they emerged from the PVA gel upon 1 h hydration. (b) Fluorescence micrograph of lipid stacks deposited on the PVA gel before hydration. The lipid/gel film was intentionally scratched by microtweezers to give contrast to the image. (c) Fluorescence micrograph of the same sample took after hydration and liposome harvesting. The scale bar is 100 μm.

Fluorescence imaging of the hydration process revealed fast production of high-quality liposomes, which formed densely on the PVA gel and were largely free of other irregular lipid structures (Figure 2-1, a). A significant portion of liposomes tended to remain associated with

each other and with the gel at the end of 1 h hydration, which could be easily suspended by briefly shaking the hydration cell. Only a low residual fluorescence could be observed from the gel layer after this process (Figure 2-1 c), which suggested a nearly complete removal of lipid deposits. Such high-yield liposome production has enabled me to routinely harvest these liposomes for subsequent uses. On the other hand, size analysis of >200 such liposomes from multiple batches showed a relatively wide distribution from a few to ~40 μm (Figure 2-3 left).

2.3.2 Janus liposome formation

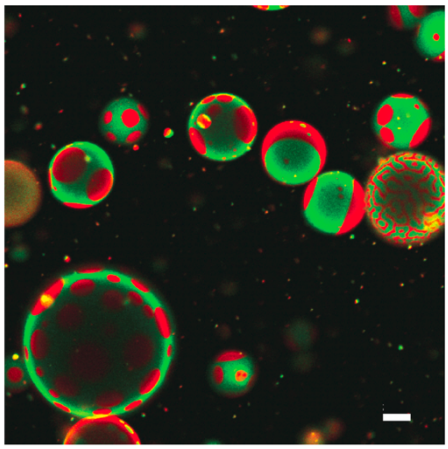

Figure 2-2. Confocal fluorescence micrograph of precursor Janus liposomes images 1 day after preparation. Liposomes composition was the same as in Figure 2-1. The lo and ld domains were marked by Bodipy-chol (green fluorescence) and rho-DOPE (red fluorescence), respectively. The scale bar is 20 μm.

Confocal fluorescence microscopy further revealed that freshly prepared liposome samples only contained a small portion of liposomes with desired Janus geometry, that was, with their lo/ld phases separated completely into two hemispheres. By contrast, the majority of the liposomes initially displayed partial phase separation of some degree. Here, the predominant morphology featured small circular ld domains dispersed in a single, globally continuous lo

domain, while a small number of liposomes with stripe-shaped ld/lo domains were also observed (Figure 2-2). Such polymorphism reflected the kinetic mismatch between fast liposome formation and much slower domain coalescence within individual liposomes[55,86], allowing the latter process to be on full display while in transition. With respect to the energy landscape of lipid organization within individual liposomes, these morphologies correspond to the local energy minima.

Complete coalescence of small lipid domains (Figure 2-3 right), which represents the global energy minimum of these liposomes,[55,73] typically took several days when stored at room temperature. Compared to this slow aging procedure, attempts to speed up the domain coalescence, for example, by overnight incubation of the harvested liposomes at 45 °C, only led to products of inconsistent quality. All DPPC/DOPC/cholesterol-based liposomes presented in this Chapter and Chapter 4, therefore, had been first given 5−7 days to reach the intended Janus structure before further use, and the resultant Janus liposomes remained stable for at least several months.

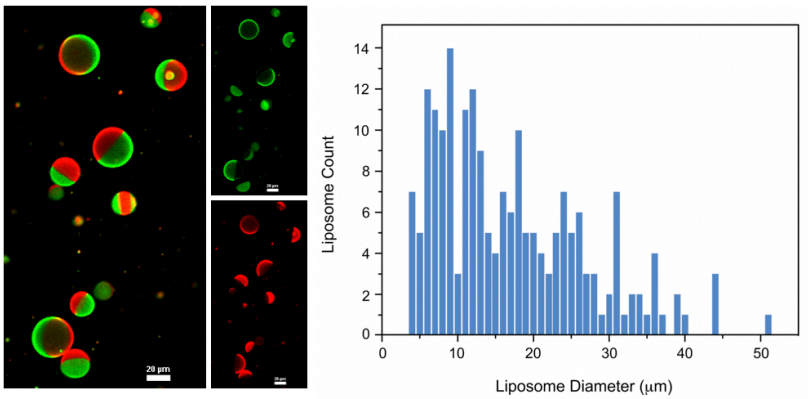

Figure 2-3. Even-split GJLs (DPPC/DOPC/cholesterol/rho-DOPE/Bodipy-chol = 35/35/30/0.2/0.2 mol %). (left) Typical confocal fluorescence micrograph of even-split GJLs: dual (image on the left) and single (two images on the right) channel excitation. Scale bars are 20

μm. (right) Janus liposomes size distribution: 200 liposomes from different batches were analyzed to construct this histogram. The diameter of liposomes is presented in the x-axis in 1-μm increments, y-axis is the total number of liposomes corresponding to each liposome size.

2.3.3 Janu Liposomes with controlled Janus configurations

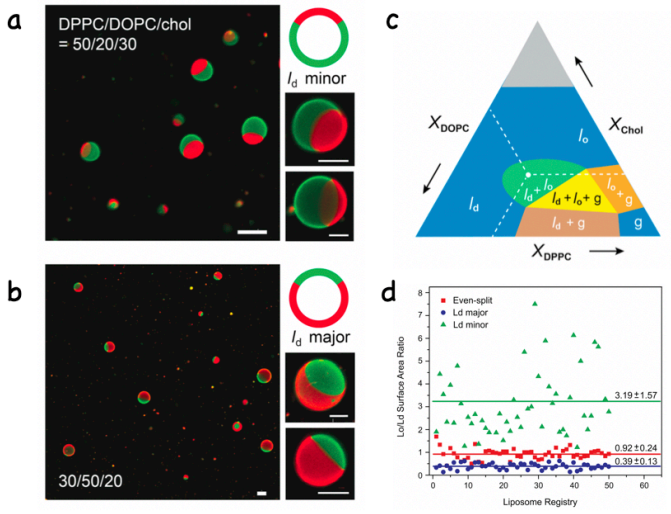

Figure 2-4. DPPC/DOPC/cholesterol GJLs with controlled domain configurations. (a) and (b) are confocal fluorescence micrographs of ld minor and ld major GJLs, respectively, in each case, one large-area (scale bar: 20 μm) and two close-up (scale bar: 5 μm) images and cartoon drawings are presented. (c) A general triangle phase diagram of DPPC/DOPC/cholesterol system at room temperature. Different phases are color-coded, in which lo-ld coexistence region is shown in green. (d) Janus ratios of three types of GJLs. In each domain configuration, a total of 50 liposomes were analyzed to produce the mean (indicated by solid lines) and standard deviation reported in the d.

Subsequent fluorescence measurements of these Janus liposomes in addition revealed that the majority of Janus liposomes formed within the same batch carried comparable lo-to-ld domain ratios. Such uniformity manifested another strength of this gel-assisted formation method

and, moreover, presented an opportunity to engineer the domain configuration in these liposomes through control of lipid composition. To test this possibility, three liposome samples were prepared, containing the following DPPC/DOPC/cholesterol mixing ratios (mol %): 50/20/30, 35/35/30, and 30/50/20. All three compositions fell within the lo/ld-coexistence region in the phase diagram (area marked in green in Figure 2-4 c) and were therefore expected to yield Janus liposomes with minimized line tension across phase boundaries. Images shown in Figure 2-3 (left), Figure 2-4 a and b clearly confirmed this projection and in addition identified a trend of transition in the relative domain size of these liposomes, going from ld-minor (50/20/30) to roughly even-split (35/35/30) and then ld-major (30/50/20) domain configurations. This trend was more quantitatively revealed by the Janus ratio, *i.e.*, areal ratio of lo to ld domains, associated with these liposomes: ld-minor (3.19 ± 1.57), even-split (0.92 ± 0.24), and ld-major (0.39 ± 0.13) (Figure 2-4 d).

2.3.4 DPPC/DPhPC/cholesterol Janus liposomes

The versatility of the PVA gel-assisted method was further demonstrated by its ability to prepare Janus liposomes consisting of DPPC/DPhPC/cholesterol. Diphytanoyl lipid is a widely employed highly branched saturated zwitterionic phospholipid featuring a super low melting temperature (~-120 ^{o}C).[59] It is heavily used in electrophysiological researches (particularly in ion-channel related experiments) mainly because of the high electrical resistance across the DPhPC lipid membrane.[59] The branched fatty acid chains on DPhPC significantly disrupt the lipid arrangement in the lipid bilayer membrane leading to a less packed lipid organization. Thus, DPhPC lipids behave more like unsaturated lipids and preferentially distribute into ld phase. However, the hydrocarbon chains of DPhPC is less flexible than those in unsaturated lipids.[110] Similar to the DPPC/DOPC/cholesterol system, a big lo-ld coexistence region has been identified

in the DPPC/DPhPC/cholesterol ternary system over a wide range of temperature by detecting the liposomes obtained from electroformation.[88] Therefore, it is reasonable to expect to be able to prepare DPPC/DPhPC/cholesterol GJLs through a similar procedure that was used for producing DPPC/DOPC/cholesterol GJLs.

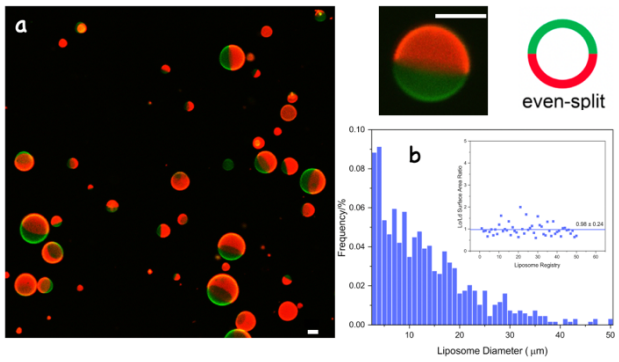

Figure 2-5. Even-split GJLs (DPPC/DPhPC/cholesterol/rho-DOPE/Bodipy-chol = 40/40/20/0.2/0.2 mol %). (a) Typical confocal fluorescence micrograph of even-split GJLs. One close-up image and cartoon drawing is presented on top right. Scale bar: 10 μm. (b) Janus liposomes size distribution: 200 liposomes from different batches were analyzed to construct this histogram. The diameter of liposomes is presented in the x-axis in 1 μm increments, y-axis is the frequency of liposomes corresponding to each liposome size. Janus ratio (inserted) resulted from 50 liposomes analysis.

As shown in Figure 2-5, high-yield and high-quality Janus liposomes were obtained by following the afore-described procedure (note: the optimal hydration condition was at 45 ^{o}C, 2.5 h). For the liposomes with same content of high-melting and low-melting phospholipids, even-split Janus liposomes were observed, whose area ratio of lo to ld domains was 0.98 ± 0.24. They displayed a wide size distribution (Figure 2-5 b), similar to Janus liposomes in Figure 2-3. It is worth mentioning that, unlike DPPC/DOPC/cholesterol, the thus-formed

DPPC/DPhPC/cholesterol GUVs already displayed Janus structures and no further ageing was required.

In this Dissertation, all of the other Janus liposomes were prepared in Chapter 3, 4 and 5 by following the similar procedure as described in this Chapter with minor modifications (*e.g.*, deposited lipids content, hydration time and hydration temperature).

2.4 Conclusion

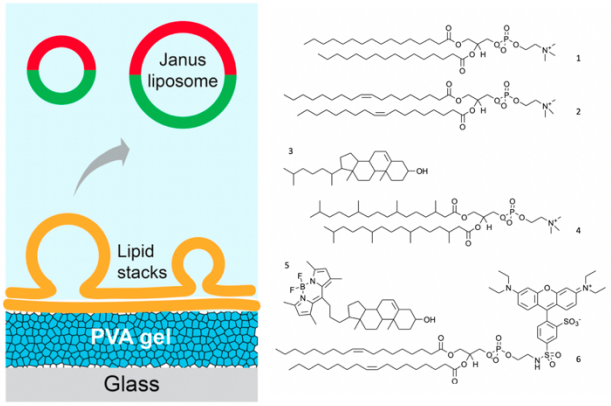

Figure 2-6. Formation of GJLs via PVA gel-assisted lipid swelling. (left) Schematic of the gel-assisted liposome formation process. (right) Lipids employed in this Chapter (1-6): DPPC, DOPC, cholesterol, DPhPC, Bodipy-chol, rho-DOPE.

In this Chapter, I have demonstrated a high-yield procedure for preparing micro-sized Janus liposomes via a PVA gel-assisted lipid swelling procedure. As shown in Figure 2-6, the swelling/budding process of deposited lipid stacks gets enhanced by the swollen PVA cousin, which resulted in the formation of high-density and high-quality DPPC/DOPC/cholesterol GUVs associated on the PVA gel film after 1 h hydration. With the assistance of fluorescent lipid phase probes, by characterizing with a confocal fluorescence microscope, the detached GUVs displayed polymorphism domains which could be understood as kinetic favorable products. These GUVs underwent several days of aging to complete domains coalescence for achieving

the thermodynamic equilibrium state. Liposomes consisting of two macrodomains in distinctive fluid phase (lo and ld phases) formed eventually, named as giant Janus liposomes (GJLs).

Since this method exploits general lipid-organizing principles to form the liposome, it is expected to be applicable to other types of phase-separating lipid systems, for example, the DPPC/DPhPC/cholesterol GJLs prepared in this Chapter. In addition, this method is also precise, enabling Janus liposomes of specific domain configurations to be reliably produced through adjusting lipid compositions which fell within the lo-ld coexistence region of DPPC/DOPC/cholesterol ternary systems at room temperature, which, to my knowledge, have not been previously demonstrated.

CHAPTER 3. SIZE-CONTROLLED PRODUCTION OF GIANT UNILAMELLAR LIPOSOMES: MEMBRANE-GATED, GEL-ASSISTED LIPID HYDRATION

3.1 Introduction

The amphiphilicity of lipids, and hence their intrinsic tendency to self-assemble in water, almost always guarantee some liposome formation, more challenging is the precise control of lamellarity and size of the final products. Like in the last Chapter, a wide-size distributed Janus liposome are found in both DPPC/DOPC/cholesterol and DPPC/DPhPC/cholesterol systems. To this end, much recent work has been directed toward size-controlled preparation[78,95-97,99,105,111-114] of giant liposomes.

One proven approach to liposome size control is through apportioning the amount of lipids that assemble into individual liposomes. By limiting and homogenizing the quantity of the constituents, this approach removes a major contributor to liposome size variation, i.e., random lipid uptake from a large continuous lipid supply, from the vesiculation process. Depending on how exactly the lipid apportionment is realized, most of the existing work can be fitted into three categories: 1) Microcontact printing,[111,115,116] in which minute amounts of lipids are microarrayed onto a planar substrate via a positive-featured stamp. 2) Lipid backfilling.[105,112-114] In this case, the location of lipids on the substrate is defined by a support structure containing, *e.g.*, lithographically-defined recesses and then lipid islands undergo liposome formation via either hydration or electroformation. 3) Double emulsion (see section 2.1).

In this Chapter, a new approach to size-controlled giant liposome production by combining gel-assisted lipid hydration with membrane-based lipid extrusion has been developed. In this method, the deposited lipid stacks are additionally covered atop with a polycarbonate

(PC) membrane featuring a defined pore size. Upon hydration, the underlying lipids can only go through pores of the PC membrane into the main aqueous solution resulting in upper-limit size controlled giant liposomes. Both homogeneous and heterogeneous liposomes are prepared from this new approach and their characteristics, including size distribution, yield, and lamellarity are further determined by fluorescent techniques. This procedure thus offers a simple and fast alternative route to size-controlled giant unilamellar liposomes.

3.2 Experimental Section

(1) Regents and Materials

All lipids, including DPPC, DOPC, POPC, rho-DOPE, and Bodipy-chol, were products of Avanti Polar Lipids (Alabaster, AL). Other chemicals, including PVA (MW: 145,000), cholesterol, chloroform, were obtained from Sigma-Aldrich. DI water of 18.2 MΩ × cm (Millipore) was used throughout this work.

Track-etched polycarbonate (PC) filter membranes employed in this work were either Whatman Nuclepore™ (GE Healthcare; thickness: 7-22 μm) or Isopore™ (Millipore Sigma, thickness: 21-27 μm) membranes with pore sizes of 3, 5, 8 and 10 μm and nominal thickness of 0.25 mm.

(2) Liposome Preparation Procedures

Preparations of giant liposomes via three routes were tested and compared in this Chapter: 1) gel-assisted lipid hydration, 2) membrane-gated, gel-assisted lipid hydration and 3) gel-assisted lipid hydration followed by liposome extrusion.

1) Gel-assisted lipid hydration. This was done by following the gel-assisted hydration method[92] by Marques et al. with minor modifications. Briefly, dry PVA films were prepared by first spreading a 5 wt% PVA aqueous solution on precleaned glass slides, followed by drying at

50 °C for 0.5 h. On each of these dry PVA films, a 5-μL drop of a lipid stock solution (1 mM total lipid dissolved in chloroform) was then cast, and subsequently dried under vacuum for overnight at room temperature. Composition wise, these lipid stock solutions contain either a single component (DPPC, DOPC and POPC), or their binary mixtures with cholesterol at 7:3 mol mixing ratio, or 35/35/30 (mol%) DPPC/DOPC/Chol in the case of Janus liposomes. In the final step, such dried lipid films were hydrated in DI water to yield liposomes. Depending on the lipid composition, the hydration temperature/duration vary: 40 °C for 1 h for low-melting DOPC and POPC (with/without cholesterol), 55 °C for 1 h for DPPC and 60 °C for 2 h for Janus liposomes. At the end of the hydration process, liposomes were harvested with pipettes and stored at 4 °C.

2) Membrane-gated, gel-assisted lipid hydration. In this procedure, PC membranes with specific pore sizes were conformally placed on top of the lipid deposits prior to hydration. To achieve so, the PC membrane was first wetted with DI water briefly and while it was still moist, gently pressed onto the dry lipid stacks similarly formed on PVA gel as before. The glass slide carrying the PC membrane/lipid/PVA assembly was then fitted face-down to a precleaned polypropylene cell (Qorpak® polypropylene screw cap, 22-400, unlined). The cap was pre-filled with DI water to a level a few mm below its rim, so that the latter was not in direct contact with the lipid stacks upon sealing. To ensure a good seal, the cell is further secured with a low-tension spring clip clamp; to start the lipid hydration, the assembled cell was simply turned upside down. The hydration temperature/duration conditions were identical to those specified in Method 1). Thus-produced liposomes are similarly harvested and stored.

3) Gel-assisted lipid hydration followed by liposome extrusion. In this case, the liposomes were produced from a two-step procedure, in which 1 mL POPC, or

POPC/cholesterol, or Janus liposome samples obtained by lipid hydration (Method 1) were further extruded through PC membranes with 10-μm pores using a plunger-based lipid extruder (Mini-Extruder, Avanti Polar Lipids). The final products were collected after passing the liposome solutions through membranes for 10 rounds.

(3) Confocal Fluorescence Microscopy

Fluorescence images of giant liposomes were acquired on a Nikon A1+/MP confocal scanning laser microscope (Nikon Instruments, Melville, NY) using 10× objective and excitation laser lines at 488 and 561 nm. The corresponding green and red emission signals were filtered at 525 ± 25 and 595 ± 25 nm, respectively. The confocal pinhole was typically set at 50 μm. As imaging cells, home-prepared PDMS microwells (diameter: 3 mm; depth: 2 mm) fixed on glass slides were employed. All liposome samples were given 1 h to settle in the PDMS cells under ~100% humidity before imaging.

Z-stacked fluorescence images of liposomes as they were forming during hydration (~16 min) were acquired with the same fluorescence microscope by taking xy-plane slices along the z-axis in 1-μm increment for 50 steps. As samples, lipid stacks of POPC doped with 0.2 mol % rho-DOPE, either deposited on PVA gel or further covered by PC membranes (pore diameter: 10 μm), were hydrated in DI water at room temperature in PDMS chambers (diameter: ~1 cm, depth: 1 cm). Three-dimensional (3D) rendering of these images was performed with Nikon NIS-Elements AR software package.

Fluorescence imaging of liposomes used for lamellarity analysis was similarly acquired with the same confocal microscope, except with a lower dye loading (0.05 mol % rho-DOPE and/or Bodipy-chol) in the samples. For each sample, ~200 liposomes were analyzed to obtain the reported lamellarity.

(4) Quantification of Liposome Yields

The relative yields of liposomes prepared from all three methods were determined by fluorescence measurements using a NanoDrop 3300 fluorospectrometer (Thermo Fisher Scientific). To do so, liposome samples, containing either POPC or POPC/chol (70/30 mol %) doped with 1 mol % rho-DOPE, were first prepared using methods 1 and 2 from comparable amounts of lipid precursors; parts of liposome products obtained from method 1 were further extruded to yield samples of method 3 as described above. All samples were then diluted by a common dilution factor so as to be within the linear fluorescence response window of the spectrometer. The fluorescence emission of these diluted samples was then compared at 590 nm following an identical white-light excitation (460-650 nm). For each sample, typically eight replicates were conducted.

(5) Estimation of Liposome Size

The size of liposomes was determined from representative fluorescence micrographs of liposome samples prepared from multiple batches, which typically involves counting a few thousand liposomes from a dozen micrographs per sample. In the case of homogenous liposomes, their cross-section area of (A) was first obtained using the 'Particle Analysis' function in ImageJ (version: 2.0.0-rc-69/1.52p). The corresponding liposome diameter (d) was then estimated following the formula $d = 2(A/\pi)^{1/2}$. The size of Janus liposomes was measured using NIS-Elements AR software. Finally, the size distribution of these liposomes was analyzed using Origin data processing software (OriginLab Corp.).

3.3 Results and Discussion

3.3.1 Experimental Design

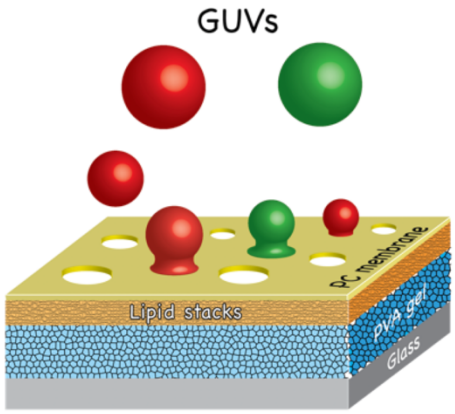

Figure 3-1. Schematic of the experimental design employed in this work. For clarity, the water layer atop of the assembly is omitted from the drawing.

As shown in Figure 3-1, the experimental setup features planar lipid stacks sandwiched between a porous PC membrane and a PVA gel layer fixed on glass. The latter structure forms the basis of the gel-assisted giant liposome preparation method[92] developed by Marques and coworkers, which we found to be quite reliable for making phase-separated Janus liposomes[1,2] as well (see Chapter 2). PC membranes, on the other hand, are a standard component in lipid extrusion, a technique broadly employed to produce small (nanosized) unilamellar liposomes.[74,117] To make these disparate methods(/setups) work together, there are two issues that need to be satisfactorily addressed: 1) Conformal, gap-free lamination of the PC membrane atop of the lipid stacks; and 2) A mechanical driving force strong enough to push the lipid bilayers through the membrane pores, *i.e.*, lipid extrusion.

As detailed in the Experimental Section, the first issue could be resolved simply by pre-wetting the PC membrane, whose moist surface tended to cling to the dry lipid stacks by capillarity upon contact with the latter. During the hydration, moreover, water absorption not only drove the swelling of dry lipid/gel layers but also a water influx moving in the opposite direction, further reinforcing the position of the PC membrane sandwiched in between. As to the

other issue, I hypothesized that the interior of the membrane pores, hydrophilic and ~20 μm across, poses only a partial and surmountable physical barrier for lipid vesiculation. The opposite scenario, *i.e.*, membranes with micro-sized, water-accessible openings shut off lipid hydration completely when placed atop, would be inconsistent with recent results, for example, on liposome array formation via lipid backfilling.[113,114]

3.3.2 Confocal fluorescence characterization of membrane-gated liposome formation

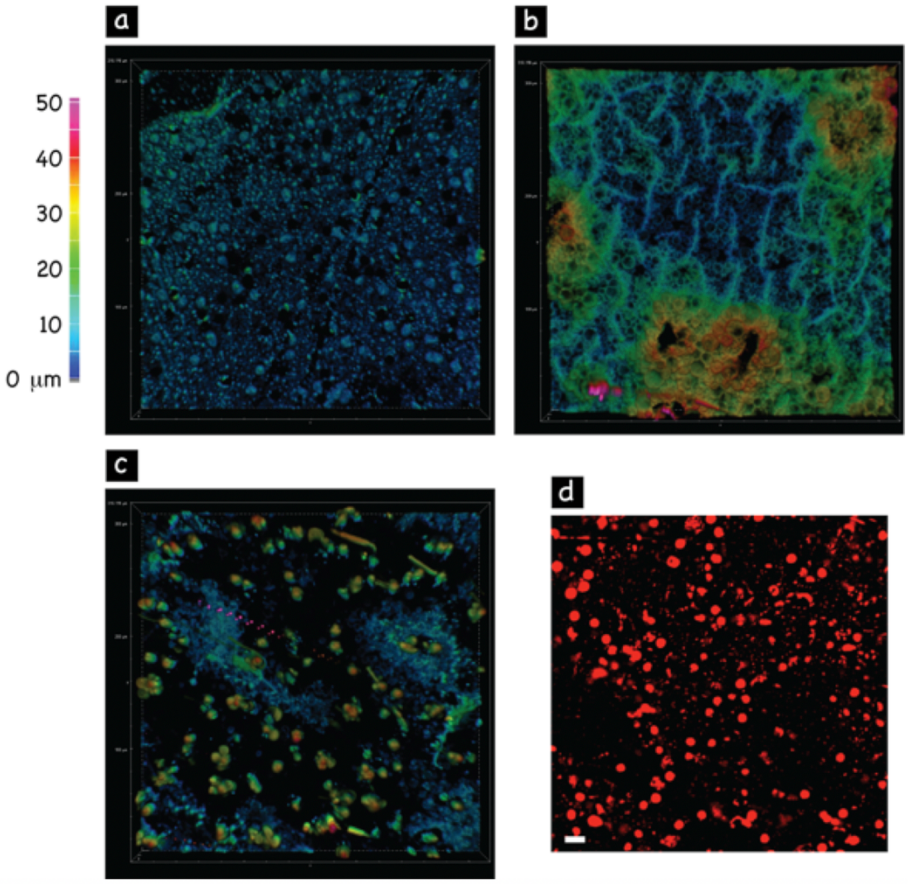

Figure 3-2. Confocal fluorescence monitoring of liposome formation during gel-assisted hydration (~16 min). Images (a) to (c) are z-stacked fluorescence micrographs with dimensions of (x, y, z) 318 × 318 × 50 μm; the scanned depth in the z-axis is indicated by the color-coded scale bar. (a) Dry lipid deposits on PVA gel before hydration; (b) Liposome formation on PVA gel alone; (c) Liposome formation on PVA gel further covered with a PC membrane (pore

diameter: 10 μm). (d) Fluorescence micrograph of a PC membrane (pore diameter: 10 μm) after being used in size-controlled liposome production; scale bar: 20 μm. In all cases, the lipid sample contained POPC doped with 0.2 mol % rho-DOPE.

Using confocal fluorescence microscopy, I first examined 1) Whether liposomes can be produced by this membrane-installed setup and if yes, 2) How the membrane impacts the liposome products (Figure 3-2). Prior to hydration, the lipid stacks were relatively evenly deposited on the PVA gel surface, taking the latter's contour with an average roughness of a few microns (Figure 3-2 a). Minutes into hydration, densely packed liposomes that crowded into several layers could be observed at the gel surface (Figure 3-2 b). With swelling, the gel layer now appeared highly corrugated, as previously observed by Marques and coworkers.[92]

When the lipid deposits were in addition covered atop with a PC membrane, strikingly, the predominant objects in view were particles of roughly comparable size protruding from the gel surface (Figure 3-2 c). The size and distribution of these objects, furthermore, matched with that of the membrane pores; the latter could be visualized and identified readily from the residual rho-DOPE on the membrane after hydration (Figure 3-2 d). Thus, it is evident that the particulate feature resulted from lipid stacks swelling through the pores, likely yielding liposomes on the other side.

3.3.3 Size Distribution of Liposome Products

To further characterize these extruded lipid particles, I next prepared such samples using several types of lipids on PC membranes with different pore sizes. Similar to the membrane-free liposome production, these samples were collected in the aqueous phase and examined by confocal fluorescence microscopy afterwards. As shown in Figure 3-3, good quality liposomes

were produced in every tested series and moreover, there existed a clear dependence of liposome size on the diameter of the membrane pores.

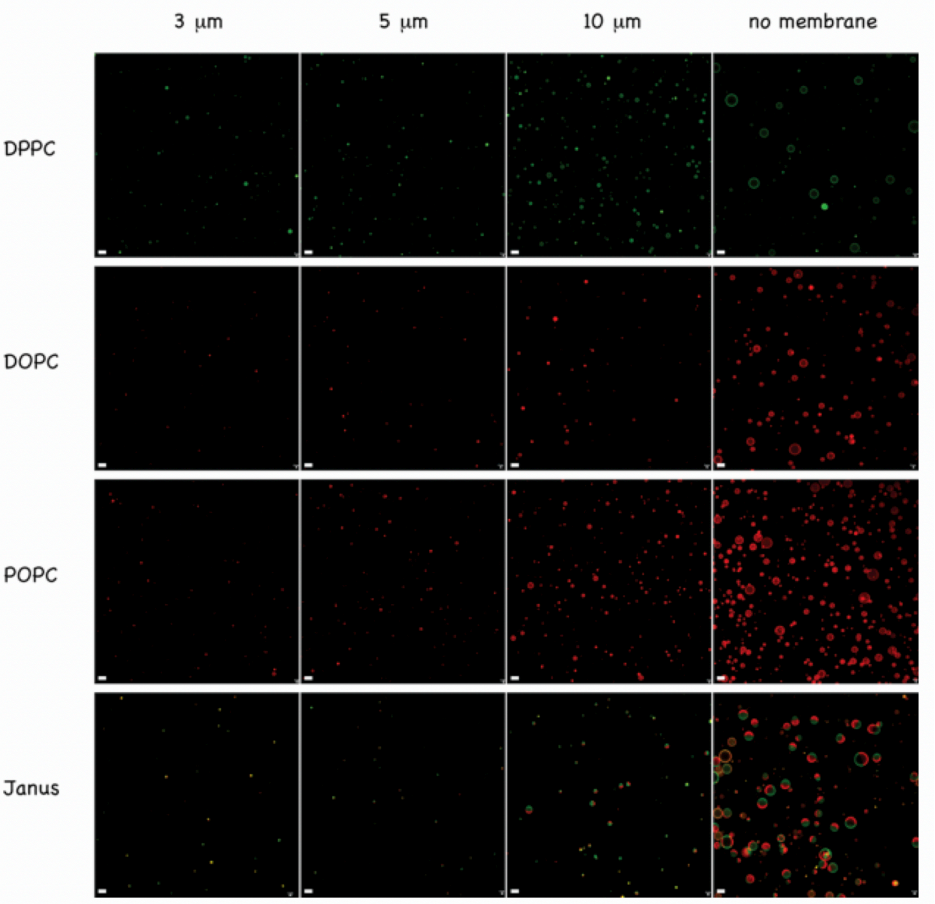

Figure 3-3. Fluorescence micrographs of four types of liposomes (DPPC, DOPC, POPC and Janus) produced either with or without PC membranes. Nominal pore size of PC membranes: 3, 5 and 10 μm; scale bar: 20 μm. See the Experimental Section for more details.

This size dependence was further confirmed by the detailed size distribution analysis (Figure 3-4), and a close inspection of these histograms in addition revealed the following trends.

1) Relatively broad liposome size distribution from (membrane-free) gel-assisted lipid hydration, with diameter ranging from 1 μm (the lower limit of our liposome counting) up to 30-40 μm.

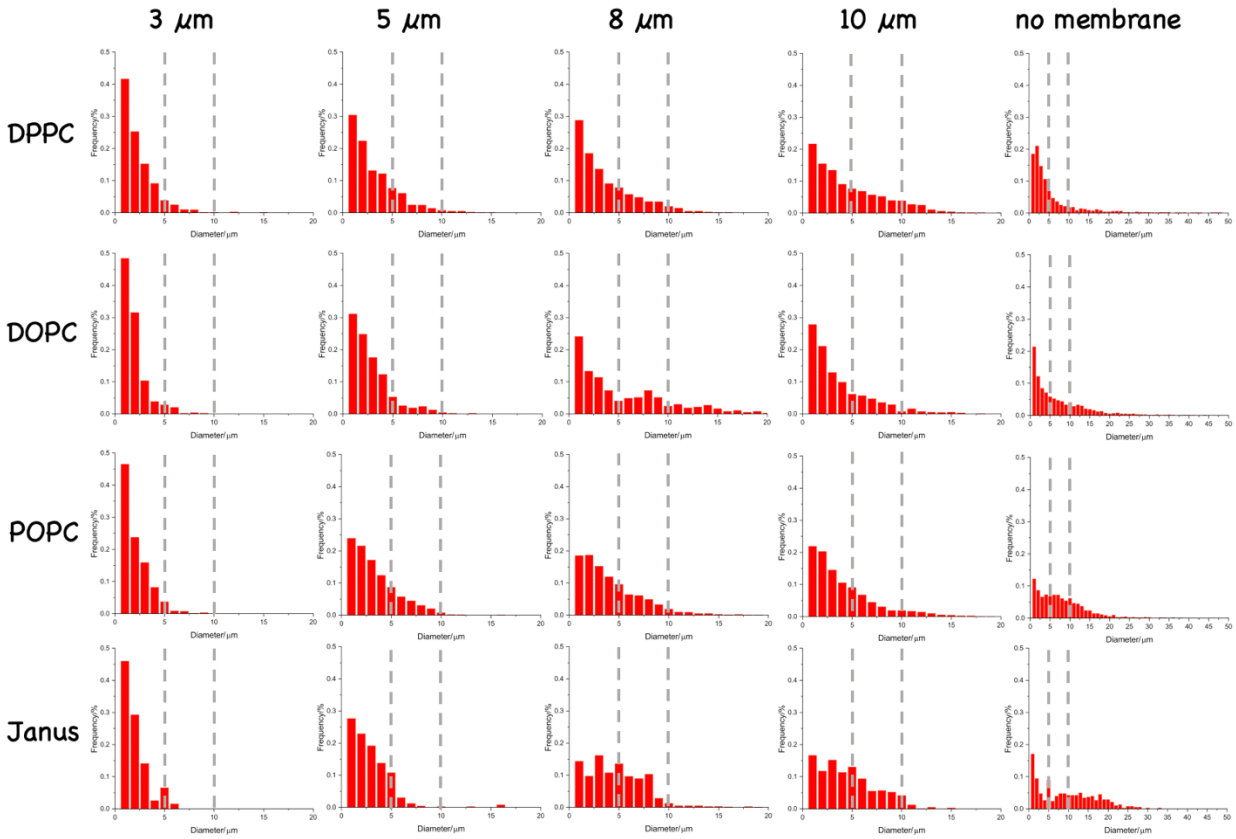

Figure 3-4. Histograms of liposome size distribution of four types of liposomes (DPPC, DOPC, POPC and Janus) produced either with or without PC membranes. The PC membranes employed have nominal pore sizes of 3, 5, 8 and 10 μm. In each plot, the red bars represent relative populations of liposomes of certain size in a sample with 1-μm increment, whereas the dashed lines represent the 5-μm and 10-μm marks. In each series, the relative abundance (y-axis) of liposomes is maintained and comparable across difference pore sizes.

2) Plausible liposome size dependence on lipid type. For the Janus liposome group, specifically, 40% of the population had a diameter larger than 10 μm, giving an overall wider size distribution compared to the other lipid groups. Of the three single-component products, the majority of the liposomes fell within the 10-μm size mark. For DPPC and DOPC, moreover, the

relative abundance of liposomes decreased exponentially as their size became larger. This trend should be read with caution, however, considering possible complications due to liposome preparation and finite sampling.

3) Effective upper-limit size control by membrane. With the 10-μm-pore membrane installed, for example, the portion of Janus liposomes with diameter >10 μm went down from 40% to 2%. As a result, ~30% of liposomes now fell within the size range of 6-10 μm, nearly a doubling from the membrane-free counterpart. When the 5-μm-pore membrane was used instead, <5% liposomes were found to occupy the same size window. And still smaller pores led to even narrower liposome size distribution. While the membrane-based size control was generally observed in all cases, it was also evident that the membranes do not completely shut off the formation of larger liposomes. Such "leaky" size control was not unexpected, since the continuous, elastic lipid-bilayer sheets could easily squeeze past the pores during the swelling process – in a way similar to lipid vesicles formed by micro-pipet aspiration.[118,119] Another plausible contributor was the interfusion of liposomes as they came out of adjacent membrane pores at the same time (Figure 3-2 c).

4) Unhindered small-sized liposome production. Not surprisingly, liposomes with size smaller than the membrane pores, which were being produced even when no membrane was used, still formed and could pass the pores freely.

As a separate control, giant liposomes prepared by the conventional extrusion procedure were also tested, which was carried out by passing gel-assisted hydration liposome products through PC membranes using an extruder. Here, while narrower size distribution was generally observed, the population of liposomes with targeted size was always low and sometimes missing entirely (Figure 3-5). Take the extruded POPC liposomes, for example, the majority of the

liposomes were just a couple of microns in size, largely independent of the membrane used. The predominance of small-sized products likely resulted from the lipid pickup by PC membranes as liposomes passed the pores repeatedly during extrusion, which will be further confirmed in the next section. Similar size discrepancy was also observed previously in preparation of nanosized lipid vesicles,[120,121] where extrusion through >100-nm pores yielded smaller products.

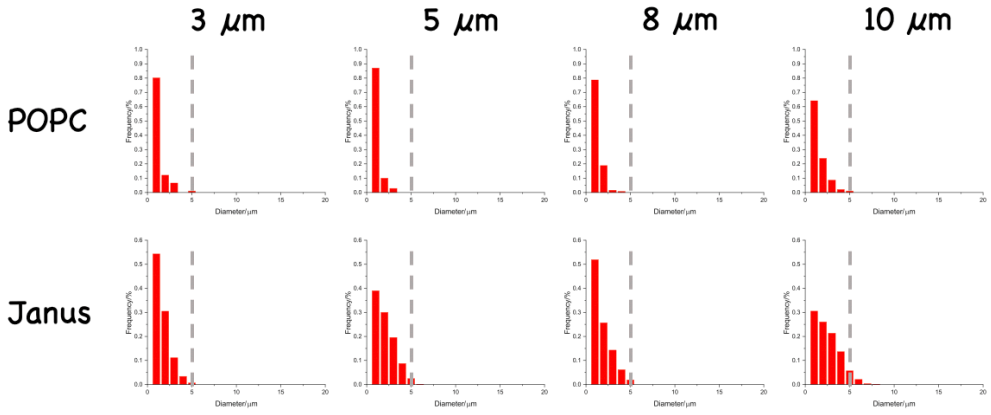

Figure 3-5. Histograms of liposome size distribution of POPC and Janus liposomes produced by gel-assisted lipid hydration followed by extrusion. The PC membranes employed have nominal pore sizes of 3, 5, 8 and 10 μm. In each plot, the red bars represent relative populations of liposomes of certain size in a sample with 1-μm increment, whereas the dashed lines represent the 5-μm mark.

3.3.4 Liposome Yields and Lamellarity

Next, the yield of these membrane-gated liposome products prepared from 10-μm-sized membranes were determined. As shown in Figure 3-6, using the gel-assisted hydration (Method 1) samples as the baseline, the findings were 1) relative yields of 69% for the membrane-gated (Method 2) and 55% for the hydration/extrusion (Method 3) POPC liposomes, respectively, and 2) relative yields of 75% for the membrane-gated (Method 2) and 55% for the

hydration/extrusion (Method 3) POPC/cholesterol liposomes, respectively. Clearly, the hydrophilic surface and pores of PC membranes were suitable sites for lipid deposition, even under significant shear conditions. Many microporous materials,[122-125] including PC membranes, have been employed previously as solid supports to afford stable formation of lipid bilayers. On the other hand, it is interesting to note that, with its <10% porosity (estimated from fluorescence analysis of Figure 3-2 d), the 10-μm-pore membrane laminated atop of the lipid stacks only causes a moderate, ~30%, decrease in liposome yield. This result highlights the dynamic and continuous nature of the lipid hydration/swelling process, by which the bulk of the lipid deposits can move about and exit successfully from the membrane openings that account for <10% of the total area.

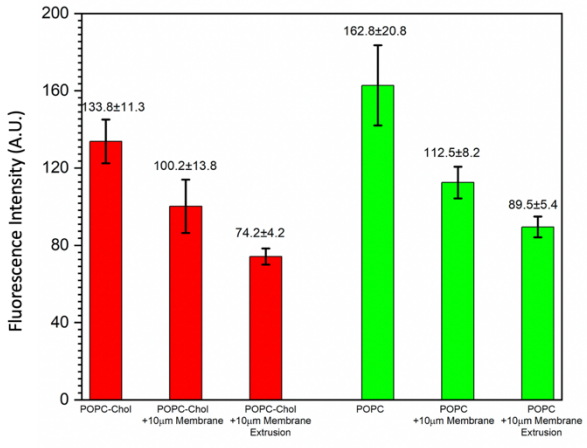

Figure 3-6. Relative yields of liposomes from different methods, which were indicated by relative fluorescence intensity of rho-DOPE in liposomes (n = 8) (1 mol % of rho-DOPE was added in either POPC or POPC/cholesterol (70/30 mol %) liposomes).

In addition, with respect to the domain size of the phase-separated DPPC/DOPC/cholesterol liposomes, as shown in Figure 3-3, there were two micro-sized domains on giant liposomes prepared from the membrane-gated, gel-assisted lipid hydration

procedure featuring two distinctive fluid phases. This suggested that the newly developed method was able to preserve the Janus structures of liposomes. By a marked contrast, liposomes displaying macroscopic domains, which were in comparable size as liposomes produced from Method 2, were barely found after extruding the GJLs prepared from membrane-free gel-assisted hydration (Method 3).

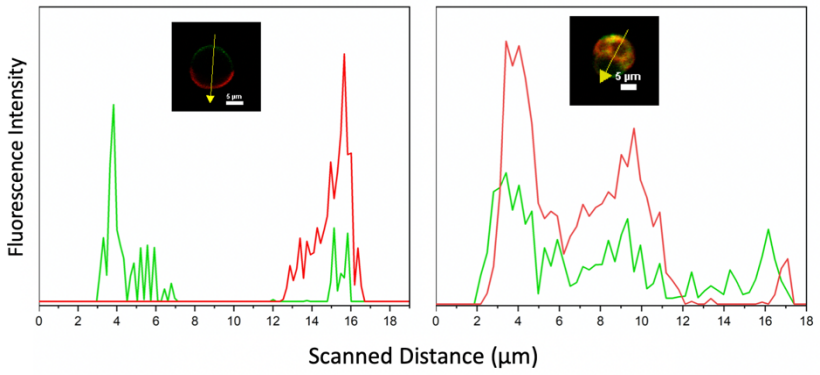

Figure 3-7. Fluorescence microscopic characterization of liposome lamellarity. Lipid composition: DPPC/DOPC/chol 35/35/30 (mol%), all additionally containing 0.05 mol % rho-DOPE. Insets: fluorescence images of the liposomes analyzed; the arrowed lines indicate the position/direction of the fluorescence intensity scan. Scale bar: 5 μm.

Finally, the lamellarity of membrane-gated liposome products was assessed based on their cross-section fluorescence intensity profiles. As demonstrated by other workers previously,[80-82] fluorescence intensity scan across the equator of lightly labeled, homogeneous giant unilamellar liposomes typically yields a symmetrical profile featuring two sharp maxima at the boundary together with a flat baseline region in the middle, which correspond respectively to the rim and the lumen of liposomes. One of such cases is shown in Figure 3-7 (left), whose profiles could be easily differentiated from multi-compartment (Figure 3-7 right) liposomes. Using this method and based on counting ~200 particles (size > 4 μm) in each case, I found the

following relative yields of unilamellar liposomes: 78% for POPC and 89% for Janus liposomes. These yields were quite comparable to those obtained from Method 1 (64% for POPC and 92% for Janus liposomes), suggesting that the placement of microporous hydrophilic membrane on top of the lipid/gel layers did not significantly alter the hydration/swelling process.

3.4 Conclusion

Above, I have demonstrated a new procedure for size-controlled giant liposome production combining gel-assisted lipid hydration with membrane-based lipid extrusion. Featured in this procedure were planar lipid stacks deposited on PVA gel, which were further laminated atop with PC membranes. Control of liposome size was thus realized through the uniform-sized pored of the PC membranes, which provided the only access for the underlying lipids to enter the main aqueous phase upon hydration. Production of both single-phased and biphasic (Janus) liposomes using several commonly employed model lipids, including DPPC, DOPC, POPC, and cholesterol, was presented. The size distribution as well as lamellarity of these liposome products have been characterized and analyzed in detail by a confocal fluorescence microscope and the yields of produced liposomes have been determined by fluorospectrometer. The procedure of membrane-gated, gel-assisted lipid hydration enjoyed many of the same benefits of gel-assisted lipid hydration technique, such as generality, flexibility and speed, and adds size control to the membrane-based lipid extrusion with a moderate decrease in liposome yield. More importantly, the upper-limit size controlled GJLs could also be readily obtained from this novel method, however this was quite challenging for either the membrane-free lipid hydration or the hydration/extrusion method. While the level of size control achieved here was not on par with some other recently reported approaches, it produced freestanding,

largely unilamellar liposomes in one straightforward hydration step with no extra preparation or setup, *e.g.*, micropatterning or microfluidics.

CHAPTER 4. BIOAFFINITY GIANT JANUS LIPOSOMES

4.1 Introduction

One significant development in lipid phase research is the quantitative description of model lipid system,[55,62,66,73,106] such as DPPC/DOPC/cholesterol as described in Chapter 2. This not only provides an essential window to look into the baseline protein-free biomembrane thermodynamics and associated critical phenomena, but also offers opportunities for development of new lipid-based biomaterials.

Described in Chapter 1 section 1.3, Beals and co-workers[39] for the first time, systematically studied GJLs and imparted asymmetrical reactivity on those liposomes using DNA hybridization through complementary DNA strands which were tethered with either cholesterol or lipid. This work clearly demonstrated the possibility to prepare Janus particles using lipids and moreover, unique features of liposomes as a colloidal material, *e.g.*, their deformable surface.[39,68] Besides directly taking advantage of the DNA hybridization, DNA can also be further linked with other functionalities to impart new functions of liposomes. Reported by Amjad and co-workers,[126] cholesterol-anchored double-stranded DNA constructs, which were tipped by a biotin molecule at the DNA end, were inserted into the hydrophobic core of the lipid bilayer of both GUVs and supported lipid bilayers (SLBs) consisting of DOPC. The former was produced by electroformation, and the latter was produced by preparing SUVs firstly, and then the SUVs ruptured on a hydrophilic glass coverslip which subsequently formed a lipid bilayer film. The biotinylated GUVs and SLBs, which incorporated biochemically reactive functionality, allowed them to study intermembrane interactions. In their system, the GUV adhered on the SLBs through bridging by multivalent streptavidin resulting in a truncated spherical GUV.

Moreover, they found the degree of the GUVs' deformation depended on the concentration of streptavidin, indicating the potential to develop a biosensing system.

DNA has been frequently employed to bridge inter-surfaces, other than that, another important biological molecule – biotin – has also been reported to be directly used for modifying liposomes through inserting lipid tethered biotin into a hydrophobic core of a lipid bilayer membrane. The reason to produce biotin-decorated liposomes is that the biotin-avidin affinity binding enables the ability to couple proteins and other ligands to lipid bilayer membranes. Momin and co-workers[63] synthesized biotin-conjugated lipid molecules (named as DP-EGn-biotin in their paper) starting from 1,2-dipalmityl-glycero-3-triethylene glycol and compared the phase partition preference of these designed biotin-lipids with commercialized biotin-phospholipids (note there were two types of these products used in their work: one was biotin directly linked on phospholipid (DPPE-biotin and DOPE-biotin), and there was a hydrophobic spacer between biotin and phospholipid in the other type (DPPE-cap-biotin and DOPE-cap-biotin)). In their work, they used fluorescent FITC-labeled streptavidin to detect the partitioning behavior and determined the partition coefficient ($K_{p\ lo/ld}$) based on average pixel green fluorescence intensity along the lo and ld domains of a DPPC/DPhPC/cholesterol GUV. Similar to Sarmento and co-workers' result,[127] they found DOPE-biotin, DPPE-cap-biotin, DOPE-cap-biotin showed predominant partitioning to ld phase for which the K_p were < 1 while the DPPE-biotin exhibited a weak lo phase partition preference (K_p = 1.1). These results suggested 1) with respected to spacer-free biotin-phospholipids, the saturation of acyl chains could influence the location of biotin on the lipid membrane; 2) the presence of the hydrophobic spacer unfavored the partitioning to lo phase. By contrast, by substituting the hydrophobic spacer with a hydrophilic one (PEG), the lo phase partition was significantly increased (K_p of up to 7.3).[63]

These findings identified the possibility to sort biotin-functionalized lipids in a specific phase, which enables the ability to selectively modify the GJLs prepared in Chapter 2.

Following the routine used in Chapter 2 to prepare giant Janus liposomes, this Chapter presents a straightforward strategy to impart asymmetrical reactivity on these liposomes using biotin-avidin affinity binding. Similar as DNA hybridization, the robust ligand-receptor pair – biotin-avidin – are also able to induce intramembrane adhesion.[126,127]

4.2 Experimental Section

(1) Reagents

All lipids, including DPPC, DOPC, biotin-DOPE, rho-DOPE, and Bodipy-chol were products of Avanti Polar Lipids (Alabaster, AL). Other chemicals, including PVA (MW: 145 000), cholesterol, NeutrAvidin biotin-binding protein, and Alexa Fluor 488-conjugated avidin, were obtained from Sigma-Aldrich. DI water of 18.2 MΩ × cm (Millipore) was used throughout this work.

(2) Liposome Preparation

Janus as well as symmetrical giant liposomes of desired compositions were prepared by following the gel-assisted lipid swelling method reported by Marques and co-workers[2-9] with minor modifications. The procedure in this Chapter was same as described in Chapter 2, the only two differences were: 1 mol % biotin-DOPE was added into lipid precursor solution, and the hydration time was 24 h.

(3) Bioaffinity Assembly of Biotinylated Janus Liposomes

Binding between liposomes was initiated by mixing these biotin-decorated liposomes with NeutrAvidin at a mixing ratio of 5 (biotin) to 1 (protein), with the final biotin concentration

typically held at ~25 nM. The resulting mixture was briefly vortexed and then incubated at room temperature in the dark for durations specified in the next section.

(4) Confocal Fluorescence Microscopy

Fluorescence images of giant liposomes were acquired on a Nikon A1+/MP confocal scanning laser microscope (Nikon Instruments, Inc., Melville, NY) using 10× objective and excitation laser lines at 488 and 561 nm. The corresponding green and red emission signals were filtered at 525 ± 25 and 595 ± 25 nm. For each measurement, a 10−15 μL liposome solution was first pipetted into a home-prepared PDMS microwell reversibly sealed to a precleaned microscope cover slide (Corning No. 1, 22 × 22 mm, Corning, NY) and then given 1 h to settle under 100% humidity.

4.3 Results and Discussion

Following the procedure described in Experimental Section, three kinds of biotin-DOPE decorated GJLs were produced (Figure 4-1). These results thus put me in position to start examining the influence of domain configuration on the interactions and assembling behavior of Janus liposomes.

4.3.1 Biotin placement in Janus liposomes

To render these GJLs surface-binding capability, I have looked into several phosphoethanolamine (PE) lipids with their amine headgroups conjugated to biotin. To realize biotin/avidin binding specific to liposome domains, I hypothesized that these biotin PE could be sorted into lo (or ld) domains according to their acyl chains, that was, 1,2-dipalmitoyl-sn-glycerol-3-phosphoethanolamine (DPPE) into DPPC, or 1,2-dioleoyl-sn-glycerol-3-phosphoethanolamine DOPE into DOPC. This required a low biotin-DOPE doping level in liposomes so that its presence would not significantly impact the phase separation established by

the three main lipid components. In this study, I have chosen to keep the biotin-DOPE doping level constant at 1 mol %. Also important was the potential reorganization/redistribution[128] of biotin-PE within the liposomes upon binding to avidin, which needed to be checked after liposome production.

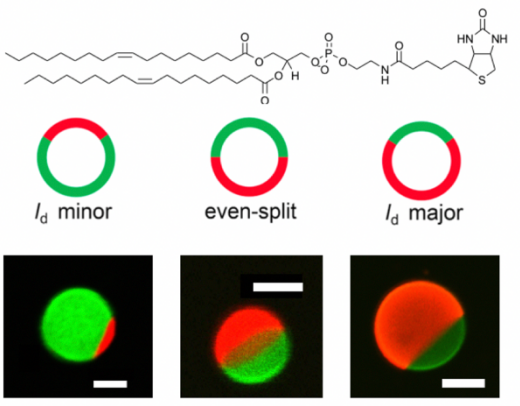

Figure 4-1. Biotinylated GJLs with controlled domain configurations. The molecular structure of biotin-DOPE used for fabricating biotinylated GJLs is presented at top, and other lipids see Chapter 2 (Figure 2-6). Bottom: confocal fluorescence micrographs of biotinylated GJLs, and the corresponding cartoon drawing is also included. DPPC/DOPC/cholesterol mixing ratio (in mol %): ld-minor, 50/20/30; even-split, 35/35/30; and ld-major, 30/50/20. All liposomes, in addition, contained 1 mol % biotin-DOPE and 0.2 mol % rho-DOPE and Bodipy-chol. The scale bar: 10 μm.

Guided by these considerations, biotin-DOPE (Figure 4-1 top) was found to be a suitable biotin lipid conjugate for DPPC/DOPC/cholesterol Janus liposomes. As shown in Figure 4-2, high-quality liposomes displaying uniform phase separation could still be prepared when this lipid was included in the formation. Using a green-labeled avidin to bind these liposomes, moreover, a strong colocalization between avidin and rho-DOPE were observed, indicating that the incorporated biotin-DOPE almost exclusively resided in the ld domains of these Janus

liposomes. Importantly, this exclusive phase preference persisted even when these biotinylated liposomes were challenged with high dosages of avidin, *e.g.*, at 1:1 biotin/ avidin mixing ratio.

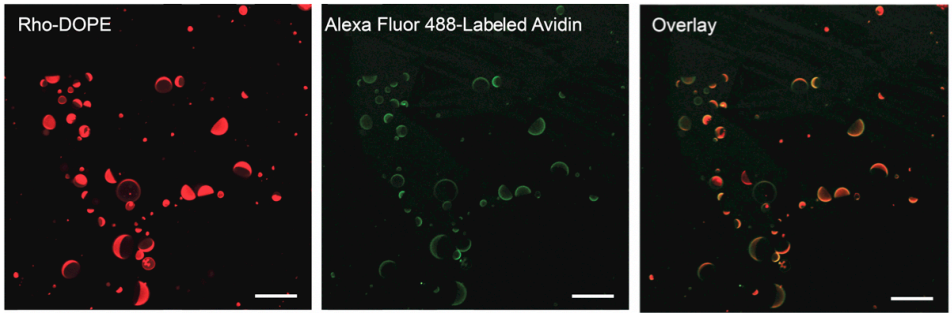

Figure 4-2. Phase preference of biotin-DOPE in DPPC/DOPC/cholesterol Janus liposomes. (left) Confocal fluorescence image of rho-DOPE displaying the ld phase; the lo domains were not labeled. (middle) Green channel showing avidin location of the same liposome sample. (right) Merged image displaying both red and green fluorescence. The scale bar is 50 μm.

4.3.2 Self-assembly

Bringing these findings together, the next step was to examine the assembling behavior of biotinylated Janus liposomes carrying different domain configurations. Successful binding between liposomes was observed in all cases when they were incubated with avidin, which, as expected, occurred exclusively through ld domains. Such formation, in addition, proceeded in a time-dependent fashion, producing first low populations of small liposome clusters among unbound individual liposomes and then aggregates that may engage more liposomes. Accordingly, I present these results in two parts below.

(1) Clustering upon short-term incubation

Summarized in Figure 4-3 are the main observations on the initial liposome cluster formation, taken after 2-day liposome/avidin incubation. For Janus liposomes with their binding ld domain as the minor domain, dimer formation predominated (Figure 4-3 a–c). The same also

held true for Janus liposomes with roughly equal lo/ld domains (Figure 4-3 f–h). In either case, clusters with more than two members were only seen when there existed a significant size mismatch among binding partners such that small liposomes either fitted into the grooves formed by large ones (Figure 4-3 d, e) or co-bound a giant host (Figure 4-3 i). In contrast, three-member clusters were routinely found to form alongside dimers for ld-major Janus liposomes (Figure 4-3 l–n vs j, k). Such disparity in assembling behavior most likely resulted from the larger portion of binding sites carried by ld-major Janus liposomes, which not only increased the chance of successful binding upon liposomes' encounter, but also provided more room to accommodate multi-liposome binding. Of the three types of liposomes tested, on the other hand, no preferred angles or locations (*e.g.*, cap *vs* phase boundary) for binding between ld domains were noticed, suggesting uniform biotin distribution therein.

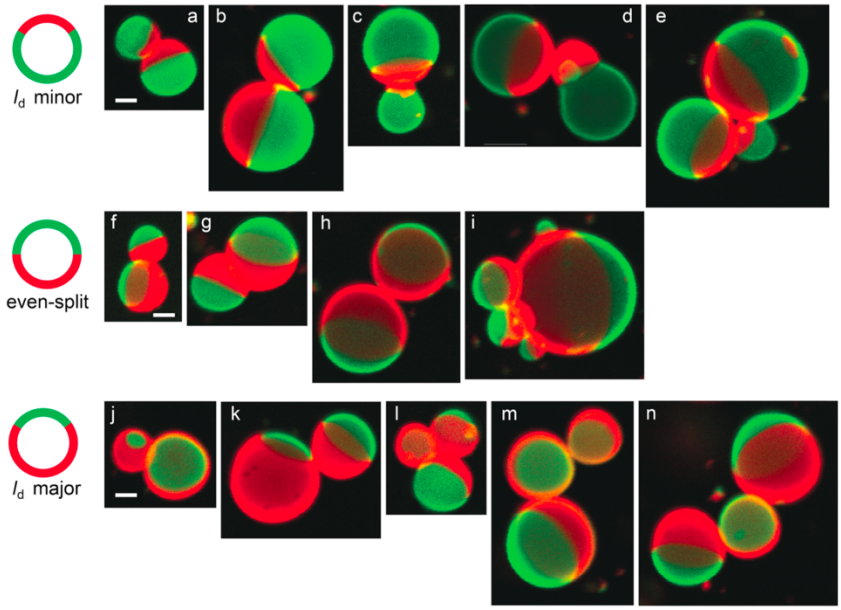

Figure 4-3. Clustering of biotin-decorated GJLs upon incubation with avidin in 2 d. Confocal fluorescence images of these clusters are presented in three rows according to liposome domain configuration. Scale bars represent 5 μm and apply to all images.

(2) Clustering upon long-term incubation

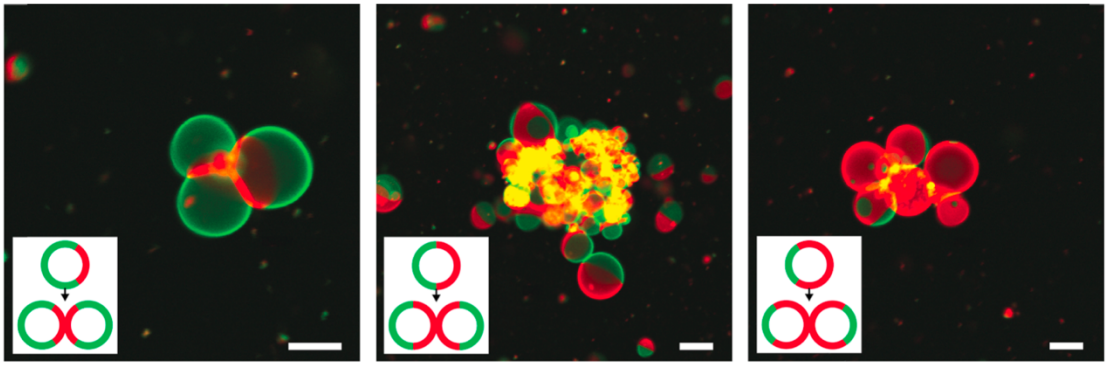

Figure 4-4. Aggregation and lipid fusion of biotin-decorated Janus liposomes upon extended (typically 1 week) incubation with avidin. DPPC/DOPC/cholesterol mixing ratios (in mol %): (left) ld-minor, 50/20/30; (middle) even-split, 35/35/30; (right) ld-major, 30/50/20. All liposomes, in addition, contained 1 mol % biotin-DOPE and 0.2 mol % rho-DOPE and Bodipy-chol. The scale bar is 20 μm. Drawing embedded in the images illustrate a comparable clustering scenario for the three types of liposomes, in which a free liposome approaches a symmetrically bound liposome dimer from the top in an ideal manner.

Next, the clustering of biotinylated Janus liposomes at longer avidin incubation times was examined. For ld-minor liposomes, dimers and trimers remained the most common clusters formed after 7 days, which was likely due to their relatively small binding domains spatially limiting further growth of the seed clusters, as discussed earlier. Larger clusters were only occasionally found, and one of such, a tetramer, is shown in Figure 4-4 left. Compared to clusters obtained after 2-day incubation, a distinct feature here was the significantly larger areas of contact between ld domains. This clearly results from the extended incubation, which enables avidin to continue to arrive at the interface and cross-link the remaining ld domains between binding liposomes. In the case of ld-major liposomes, larger clusters containing 5−7 members

were routinely observed after 7 days (Figure 4-4 right), confirming the capability of their larger biotin-occupying domains to promote further liposome binding. Similar to ld-minor liposomes, diaphragms form between contacting liposomes, which were accompanied by minor lipid exchange between lo and ld domains, as evident from the resultant yellow fluorescence. In marked contrast to these two cases, much larger liposome aggregates often consisting of dozens of binding members were consistently found to form for even-split Janus liposomes when similarly treated (Figure 4-4 middle). In each of these aggregates, I also observed substantial lipid interfusion, which appeared to occur both within individual liposomes and between neighboring liposomes. This exclusive formation tended to reoccur when these liposomes were tested at different concentrations or biotin/ avidin mixing ratios.

It is reasonable to believe that this intriguing behavior of even-split liposomes resulted from a cascade of effects. It started with their even-split geometry, which placed the lo/ld phase boundary near the liposome equator, the longest one of the three. This meant that, on average, these even-split liposomes bearded the largest line tension, which scaled linearly with the length of the phase boundary. Such high built-in tension made these even-split liposomes more susceptible to external perturbations. Geometry also made another critical difference when an unbound even-split liposome approached an existing liposome cluster – it provided the newcomer maximal chance to contact the cluster on the opposite domains (Figure 4-4 middle, inset). In comparison, such access was significantly compromised in the other two types of liposomes, whose major domains dominated their interactions (Figure 4-4 left and right, insets). Establishing contacts between opposite domains was critical, simply because it triggered cross-phase lipid exchange. While such lipid exchange could only occur along the phase boundary in individual liposomes, a largely one-dimensional process, the same process took place across the

entire contacting surfaces between liposomes and thus was expected to be more efficient. A direct outcome of such lipid exchange was the homogenization of biotin, which enabled global avidin binding and hence continual growth of the seed clusters in an uncontrolled manner, analogue to homogeneous liposome aggregation.[68,129] This eventually led to the formation of large aggregates. Taken this together, this mechanism may be summarized as follows: geometry → high susceptibility/access → lipid exchange → biotin homogenization → global binding → aggregation. To put this mechanism on a firm footing, further work is clearly needed.

(3) ld-minor GJLs deformation

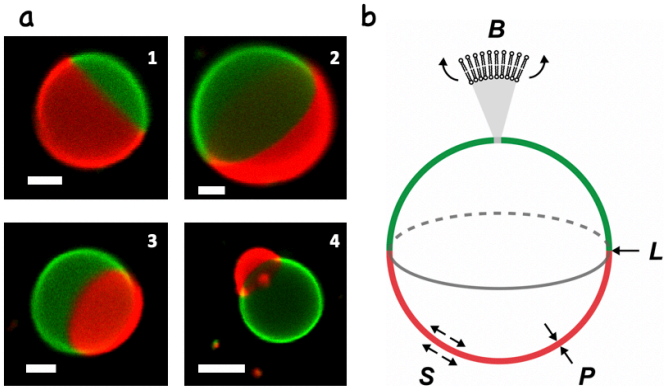

Figure 4-5. The response of biotinylated GJLs with various Janus configurations to avidin. (a) Confocal fluorescence micrographs of biotinylated GJLs incubated with avidin 2 d: (1) ld major, (2) even-split, and (3-4) ld minor. Scale bar: 5 μm. (b) Schemes main forces that govern the shape and shape transformation of biphasic liposomes according to the curvature elasticity model. B, lipid-bending force; L, line tension; S, lateral surface tension; P, osmotic pressure. Except for line tension, which operates on and around the phase boundary (circle in gray), all other forces act across the whole surface/body of the liposome.

Another observed formation was the bulging of ld domains in biotinylated Janus liposomes upon incubation with avidin, which, interestingly, occurred only in ld-minor liposome

samples. Similar formation has been observed from phase-separated liposomes before, when these liposomes were subjected to certain physical perturbations,[73,130] *e.g.*, temperature or osmotic pressure. According to the curvature elasticity model,[129,131-133] the shape of phase-separated liposomes at equilibrium is governed by the dynamic balance of two opposing forces: lipid bilayer bending *vs* line tension. The former originates from the curvature carried by the spherical liposome, whose departure from the ideally packed, planar bilayer configuration induces a mechanical stress across the entire liposome surface. Line tension, on the other hand, emanates from the size/chemical mismatch between lipids making up the phase boundary of the liposome, which scales linearly with the length of the boundary. These two oppose each other in that the bending force intends to lower the liposome curvature, a process necessarily causing the phase boundary to expand, which line tension always acts to minimize (Figure 4-5). Thus-established shape equilibrium, moreover, is quite delicate in that the force balance is very susceptible to additional sources of perturbation that may arise in and around the liposome. Such perturbations include lipid lateral tension and osmotic pressure, which enter the equation by modifying the liposome area and volume, respectively (Figure 4-5). Complicating the phase transformation further is the different mechanical strength, or bending rigidity, built into different lipid domains. The lo domains, comprising mainly DPPC and cholesterol, displayed a bending rigidity several times greater than that of the ld domains[133] and thus were more resistant to a perturbation.

Considering its multi-binding ability[126] as well as added protein mass, avidin binding was expected to exert a significant perturbation to the organization/motion of biotin-DOPE within the ld domains. This, in effect, raised the lateral tension of the outer ld domains, which could drive liposome shape transformation. Because bulging produced more curved ld domains that could

directly offset the lateral tension increase, it stood as a thermodynamically favored transformation pathway. On the other hand, two factors may account for its exclusive occurrence in ld-minor liposomes. First was in the membrane mechanics. Compared to Janus liposomes with even-split domains, ld-minor liposomes had smaller phase boundaries, which produced lower line tensions and thus less resistance to shape transformation. Similar argument also held true for the lo-minor liposomes, whose bulging would require significant binding of the lo domains, an unlikely event considering their higher bending rigidity and lack of local perturbation, *i.e.*, avidin binding. Second, assuming exclusive biotin-DOPE partitioning into the ld domains, its effective concentration should be the highest in the ld-minor liposomes (due to the same 1% being concentrated into a smaller area of liposomes). This could lead to a denser avidin binding and hence a stronger perturbation.

4.4 Conclusion

The work presented in this Chapter has further demonstrated the versatility of PVA gel-assisted lipid swelling. This method enabled straightforward incorporation of biotin-conjugated lipids (biotin-DOPE) into the formation of Janus liposomes. Specifically, all three kinds of GJLs with various Janus configurations, including ld-minor, ld-major, and even-split GJLs, were successfully obtained by adding a limited amount of biotin-DOPE (1 mol %) into the DPPC/DOPC/cholesterol ternary lipid system which was followed by the procedure of PVA gel-assisted hydration as reported in Chapter 2. The fluorescent Alexa Fluor 488-labeled avidin was employed for further detecting the location of biotin-DOPE based on specific biotin-avidin binding. The result from this experiment showed that biotin-DOPE preferentially partitioned into the less ordered ld phase of the lipid matrix, rendering these Janus liposomes asymmetrical binding capacity toward avidin. Finally, it was found that such affinity binding drove irreversible

and domain-specific clusters formation among Janus liposomes, whose structure and size depended on the domain configuration of individual liposomes and incubation time. One marked difference among three kinds of biotin-modified GJLs was the formation of large liposome aggregates consisting of dozens of even-split biotinylated GJLs upon incubating with avidin for 7 days, whereas clusters with a limited number of binding members were routinely observed for the other two kinds of biotinylated GJLs under the same experiment conditions. Furthermore, another finding was that biotin-avidin affinity binding could induce physical-chemical perturbations on the lipid bilayer membrane leading to a bulging of the ld domain in the ld-minor biotinylated GJLs, which behavior were not noticed in either ld-major or even-split biotinylated GJLs.

CHAPTER 5. CHARGED GIANT JANUS LIPOSOMES

5.1 Introduction

Mono-charged liposomes have been widely prepared and utilized. Other than ref. 83 described in section 1.3, in which the homogeneous negatively and positively charged GUVs were employed to study membrane adhesion, Lei and co-workers[49] did similar research but used DPPE-PEG decorated homogenous oppositely charged GUVs. From systematically investigating the effect that the presence of PEG on the lipid bilayer membrane had on the interactions of positively charged EDOPC/DOPC GUVs and negatively charged DOPG/DOPC GUVs, they found that PEG-modified oppositely charged GUVs exhibited a slower adhesion and fusion process as compared to PEG-free ones. This could be interpreted by the role of PEG: 1) PEG could suppress the lipids diffusion in the plane of the membrane leading to the slowed migration of charged lipids; 2) PEG chains could significantly prevent the intermembranes' close contact rendering reduced electrostatic interactions among oppositely charged membranes.

Apart from the researches using homogeneous charged GUVs, phase-separated charged GUVs have also been studied. Working with several ternary lipid systems containing cholesterol together with DPPC and low-melting anionic lipid 1,2-diphytanoyl-*sn*-glycero-3-phosphoglycerol (DiPhyPG), Keller and co-workers[134] found that addition of anionic PG lipids (to replace PCs of identical acyl chains), even up to 60 mol % (the composition of this GUVs was DPPC/DiPhyPG/cholesterol = 60/20/20 in mol %), only had a minimal influence on the primary phase separation of the system. To account for similarly dominating charge repulsion, these authors suggested several possible scenarios where the negative charge might be compensated, such as ion condensation and H-bonding between PG lipids. However, in another ternary lipid system consisting of egg sphingomyelin (eSM), DOPG, and cholesterol, Dimova

and co-workers[135] declared the presence of anionic charged DPPG could significantly decrease the lo-ld coexistence region as compared to the DPPC/eSM/cholesterol system. This observation was the consequence of phase separation suppression induced by the repulsion among the like charged DPPG. For example, the GUVs with the composition of DPPG/eSM/cholesterol = 40/40/20 in mol % were in the fluid one-phase region at room temperature. In further work, they found the charged domains could be stabilized by adding salt (*e.g.*, NaCl, $CaCl_2$). Furthermore, they injected DOTAP LUVs in the vicinity of negatively charged GUVs which resulted in 1) increased area fraction of the ld DPPG-rich domains in the phase-separated GUVs, and 2) the formation of domains in the non-phase-separated GUVs. Strong interactions between oppositely charged liposomes could induce the process of adhesion-fusion as reported in other works[49,83] and thus alter lipid composition on the membranes, rendering phase behaviors change. In addition, the usefulness of phase-separated charged liposomes has been confirmed. Imam and co-workers[136] took advantage of the capability of fusion DOTAP-contained GUVs with endosomal membrane as well as cellular plasma membrane to deliver red fluorescent dextran polymer to live cells. As compared to cells untreated with GUVs, approximately 40 times and 10 times higher red fluorescence were detected by treating cells with phase-separated and homogenous DOTAP-contained GUVs, respectively. I have covered a few examples of studying mono-charged liposomes, however, to the best of my knowledge, there is no published work about phase-separated liposomes containing both anionic and cationic lipids.

Based on the results in the last Chapter, it is appropriate to ask if opposite charges can be configured face-to-face on the same colloidal body to yield dipolar Janus liposomes. To answer this curiosity, in this Chapter, anionic lipid DPPG and cationic lipid DOTAP have been introduced into the DPPC/DOPC/cholesterol ternary lipid system, whose composition falls

within the lo-ld coexistence region, to prepare dual-charged GJLs. Assuming the acyl chain determined hydrophobic mismatch is the predominant factor to govern the interactions among lipids, thus, in phase-separated liposomes, the negatively charged DPPG (di16:0) preferentially sort into the DPPC (di16:0)-enriched lo phase, whereas the positively charged DOTAP (di18:1) selectively partition into the DOPC (di18:1)-enriched ld phase (Figure 5-1). Therefore, GJLs in which the opposite surface charges are confined in two fluid domains can be expected, which are named as dipolar GJLs.

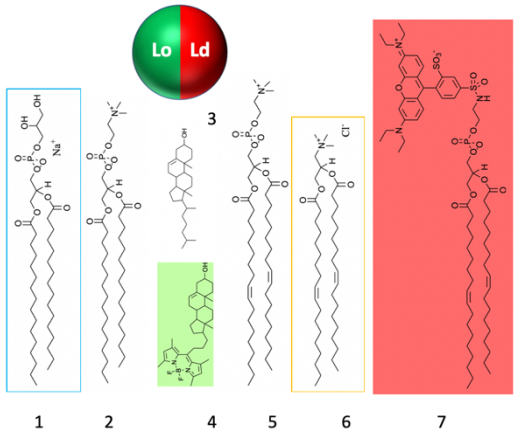

Figure 5-1. Lipids preference partitions in lo and ld phases of dipolar GJLs. 1- DPPG, 2-DPPC, 3- cholesterol, and 4- Bodipy-chol are enriched in lo phase, whereas, 5- DOPC, 6-DOTAP, and 7- rho-DOPE are enriched in ld phase.

Besides the fundamental interest for preparing dipolar GJLs, *e.g.*, in lipid-based colloid chemistry and self-assembly, this effort was also inspired by many attractive features demonstrated by solid/polymer Janus particles carrying heterogeneous surface charges. For example, the dipolar Janus particles from ref. 17 were found to form clusters of various shapes and sizes under low electrolyte conditions, which were well captured by Monte Carlo simulation. In another study, Nisisako and co-workers[23] prepared heterogeneously charged polyacrylate

Janus microparticles and further demonstrated a black-and-white electrical display device using these Janus particles. As detailed below, the successful preparation of dipolar GJLs following lipid sorting is first confirmed by using charged fluorescent nanospheres to track charge location on liposomes. Similar to their solid/polymeric counterparts, these dipolar GJLs can also self-assemble electrostatically into more complex clusters. The dipolar charge configuration in these Janus liposomes is further confirmed by their distinctive electrokinetic motion behavior.

5.2 Experimental Section

(1) Regents

All lipids, including DPPC, DOPC, DPPG, DOTAP, rho-DOPE, and Bodipy-chol were obtained from Avanti Polar Lipids (Alabaster, AL). Aqueous suspensions of green fluorescent polystyrene nanospheres were obtained from Bangs Laboratories, Inc. (carboxylic acid terminated, PS-COOH, mean diameter: 0.196 μm; excitation/emission maximum: 480/520 nm; charge density: ~0.5 milliequivalents/g) and Thermo Fisher Scientific (amine-terminated, PS-NH_2, mean diameter: 0.19 μm; excitation/emission maximum: 505/515 nm; charge density: 0.1-2.0 milliequivalents/g). Other chemicals, including PVA (MW: 145,000), cholesterol, chloroform, and methanol were obtained from Sigma-Aldrich. Deionized (DI) water of 18.2 MΩ × cm (Millipore) was used throughout this work.

(2) Liposome preparation

Giant liposomes of various compositions and configurations were prepared via gel-assisted hydration[92] as previously detailed (Chapter 2) with three modifications: 1) charged lipids directly mixed with DPPC, DOPC and cholesterol in lipid precursor chloroform solution; 2) starting lipid concentration decreased to 1 mM (*vs.* 5 mM in Chapter 2); and 3) The final hydration step was carried out by incubating the dried lipid films in 1 mL DI water at 45 °C for

2.5 h. Thus-produced liposomes were harvested with a pipette and stored at room temperature. Incubation at higher temperatures (50 or 60 °C) was found to yield liposome products of similar yields and quality, and thus was not pursued further.

(3) Confocal fluorescence microscopy

Fluorescence images and videos of giant liposomes were acquired on a Nikon A1+/MP confocal scanning laser microscope (Nikon Instruments, Inc. Melville, NY) using 10× objective and excitation laser lines at 488 and 561 nm. The corresponding green and red emission signals were filtered at 525 ± 25 and 595 ± 25 nm, respectively, before being detected by photomultiplier tubes. The confocal pinhole was typically set at 50 μm. As imaging cells, home-prepared PDMS microwells (diameter: 3 mm; depth: 2 mm) fixed on glass slides were employed. All liposome samples were given 0.5 h to settle in the PDMS cells under ~100% humidity before being imaged.

(4) Zeta potential measurement

Zeta potential values of liposomes and polystyrene nanospheres suspended in DI water were obtained from a Malvern Zetasizer (Nano-ZS90, Malvern Instruments, Worcestershire, UK) using capillary cells (DTS1060/DTS1061) operated under a 150-V bias. For liposomes, the measurements were made on diluted samples of freshly prepared liposomes with a total lipid concentration of ~1 μM. The final concentrations of nanospheres were controlled to be ~1×10^9 beads per mL. In both cases, typically five parallel readings were taken for each sample.

(5) General characterization of giant liposomes produced by gel-assisted hydration

The liposome size distribution reported in Figure 5-3 was based on size analysis of 500 Janus liposomes arbitrarily sampled from multiple liposome batches. In order to reliably call their domain configuration, only liposomes with diameter >2 μm were included in this analysis.

Similarly, the percent area occupied by the liquid-ordered lipid domain (%lo) in these liposomes was determined by analyzing 100 such particles.

(6) Characterization of charge distribution in dipolar GJLs

Placement of DOTAP and DPPG in dipolar GJLs was characterized by following their electrostatic binding with carboxyl- or amine- terminated, fluorescent polystyrene nanospheres (diameter: ~0.2 μm) with confocal fluorescence microscopy. To afford such binding, small quantities of these nanospheres were added into dipolar GJLs solutions, briefly vortexed and subsequently incubated at room temperature in dark for 1-3 days. Typically, the total lipid and nanosphere concentrations in the final mixtures were controlled at 0.5 μM and 1×10^9 beads per mL, respectively.

(7) Self-assembly of dipolar GJLs

Electrostatic self-assembly events of dipolar GJLs in DI water were followed in liposome-density and time-dependent manner using confocal fluorescence microscopy. Of the former condition, liposome interactions were allowed to proceed either at the as-prepared density, *i.e.*, with a total lipid concentration of ~5 μM in the final liposome products, or at a 4-time dilution of the original. Before imaging, these samples were incubated at room temperature in dark for various time periods specified in the next section.

(8) Electrokinetic motion of GJLs

Electrokinetic motion of various Janus liposomes under DC electric field was conducted in cyclic olefin copolymer microfluidic channels (thinXXS 100182 microfluidic linear channel slide; dimensions: 200 μm × 200 μm × 18 mm; Cole- Parmer, Vernon Hills, IL) and recorded by the same confocal fluorescence microscope. Before each measurement, the microchannel was first cleaned by sonication in methanol and then DI water, 30 min each, rinsed with methanol and

DI water, and blow-dried with a nitrogen stream. Following sample injection, two platinum wires (diameter: 0.5 mm) were inserted into the inlets of the microchannel and subsequently fixed in position with parafilm, which in turn sealed the liposome solution inside the channel. The magnitude and polarity of applied potential were controlled by a direct current (DC) power supply (BK Precision 9122A) connected directly to the platinum wires.

5.3. Results and Discussion

5.3.1 Design and formation of dipolar Janus liposomes

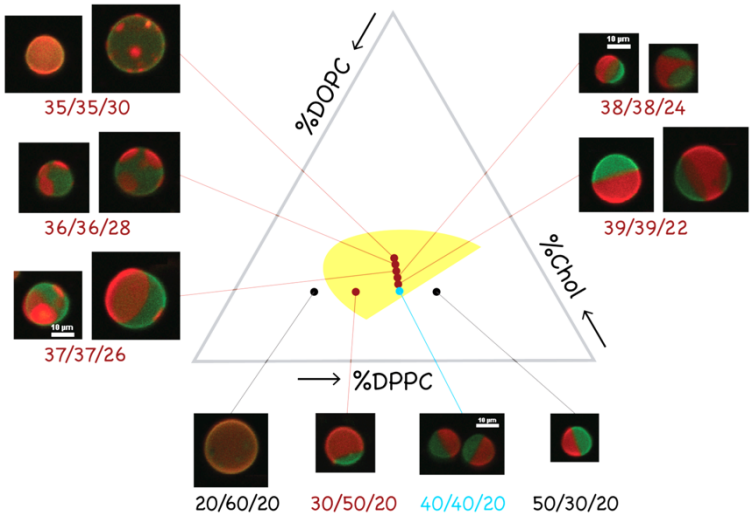

Figure 5-2. Optimization of lipid composition for the production of GJLs containing 2 mol % DPPG and DOTAP. (center) Generic triangle phase diagram of DPPC/DOPC/cholesterol system at room temperature; for clarity, only the lo-ld coexistence region is marked out (in yellow). Images surrounding the phase diagram are confocal fluorescence micrographs of liposomes produced at different lipid compositions, which are specified below images in ratios of total saturated lipids (DPPC, DPPG) *vs.* total unsaturated lipids (DOPC, DOTAP) *vs.* cholesterol. All samples in addition included 0.2 mol % rho-DOPE and Bodipy-chol; the scale bars included in the images are 10 μm and apply to all samples.

Same reason as described in Chapter 2 was employed here for setting out to build dipolar GJLs with the DPPC/DOPC/cholesterol ternary system.[66,106] To configure these Janus liposomes with a dipolar charge arrangement, in addition, the anionic DPPG and cationic DOTAP were incorporated into the formation. While DPPG is naturally occurring, *e.g.*, as a major lung surfactant component,[137] DOTAP is a synthetic cationic lipid frequently used in gene transfection and delivery[48] through electrostatic complexation with DNAs and RNAs. Both lipids, in addition, are expected to be highly charged in water, as the pK_a of DPPG[138] is ~1 and DOTAP is a quaternary ammonium cation. As Chapter 4 and discussion in introduction section of this Chapter (Figure 5-1), the DPPG partitions into DPPC-enriched lo domain and the DOTAP partitions into DOPC-enriched ld domain. Finally, in order to examine these liposome products with fluorescence microscopy, fluorescent lipid phase probes, rho-DOPE (ld, red) and Bodipy-chol (lo, green), were also included in the formation.

I started with liposome products composed of 35/35/30 DPPC/DOPC/cholesterol (mole %), which, used previously in Chapter 2, 3, and 4, yielded mostly Janus liposomes with roughly even-split lo/ld domains. When 2 mol % DPPG and DOTAP each were added into the lipid precursor, spherical liposomes could still be produced, but they seldom reached a satisfactory level of global phase separation (Figure 5-2). This negative but interesting result could be understood on the grounds of electrostatic interactions emanating from these charged lipids, which discouraged phase separation (which acted to pull attracting DPPG and DOTAP apart) on one hand, and raised the kinetic barrier for merging among small ld domains (each now bearing like charge) on the other.

To counterbalance such electrostatic interactions so that the lipid coalescence could proceed unhindered, I increased the share of DPPC/DOPC stepwise in the lipid makeup at the

expense of cholesterol, while keeping the charge loading constant (Figure 5-2). Iteration as such then led to the composition of DPPC/DOPC/cholesterol/DPPG/DOTAP mixed at 38/38/20/2/2 mole %, which produced Janus liposomes at a high yield of ~80% (Figure 5-3 a). Moreover, the majority of the giant liposomes thus formed had diameters in the range of 5–20 μm (Figure 5-3 b). On average, these liposomes contained in their structures a smaller lo domain, *i.e.*, 46% *vs.* 54% associated with the ld domain (Figure 5-3 b inset). Thus, the first goal of this investigation has achieved – a lipid formula that contained both anionic and cationic lipids and at the same time still afford good Janus liposome formation.

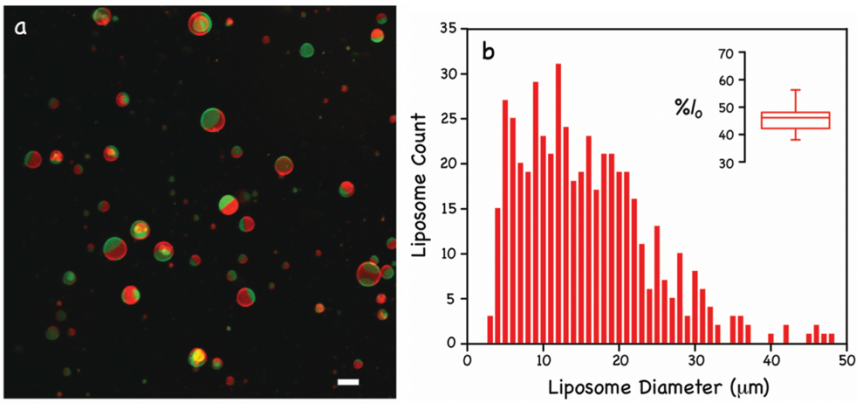

Figure 5-3. Dual-charged GJLs. (a) Fluorescence micrograph of liposomes freshly formed from a lipid precursor of DPPC/DOPC/cholesterol/DPPG/DOTAP/Bodipy-chol/rho-DOPE mixed at 38/38/20/2/2/0.2/0.2 mole %; the total lipid concentration in the final liposome product was ~5 μM. Scale bar: 10 μm. (b) Size distribution of dual-charged Janus liposomes (n = 500). The liposome diameter was determined from fluorescence micrographs similar to (a) and reported to the closest micrometers. Inset: Percent area occupied by the liquid-ordered hemisphere (%lo) in dual-charged Janus liposomes (n = 100).

As the percentage of charged lipids increased, the electrostatic interactions would increase in magnitude, eventually dominating the energetics in the system. This shift of

dominance could be seen, for example, when 10 mol % DPPG/DOTAP each were added into the formation (Figure 5-4 a). While liposomes were still being produced with a good yield at this high doping level, very few of them possess the desired Janus configuration, which was likely due to compromised lipid phase separation caused by strong electrostatic interactions. At the intermediate doping level of 5 mol %, by contrast, Janus liposome formation remained feasible (Figure 5-4 b). Taken together, these results pointed to the existence of an upper limit on the amount of oppositely charged lipids that could be sorted into immiscible liquid/liquid lipid domains. In addition to the charge doping level, this limit was expected to also depend on other factors, such as the structure and mixing ratio of charged lipids and host lipids.

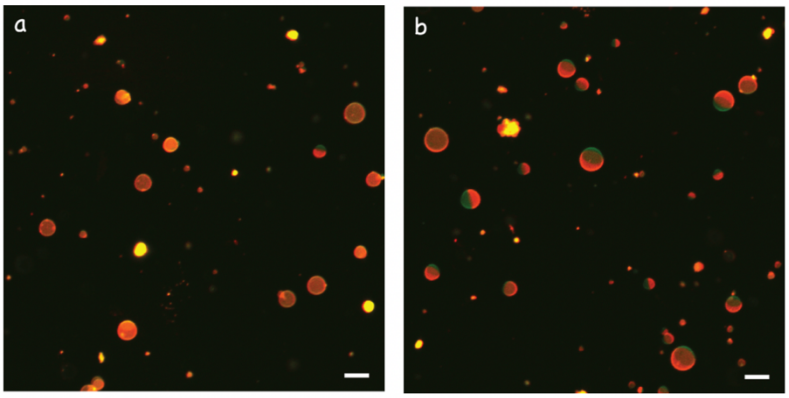

Figure 5-4. Effect of the charge loading level on Janus liposome production. (a) Fluorescence micrograph of liposomes prepared from a lipid precursor of DPPC/DOPC/cholesterol/DPPG/DOTAP/Bodipy-chol/rho-DOPE mixed at 30/30/20/10/10/0.2/0.2 mole %. (b) Fluorescence micrograph of liposomes prepared from a lipid precursor of DPPC/DOPC/cholesterol/DPPG/DOTAP/Bodipy-chol/rho-DOPE mixed at 35/35/20/5/5/0.2/0.2 mole %. In both cases, the total lipid concentration in the final liposome product was ~5 μM. Scale bar: 20 μm.

5.3.2 Charge placement in liposomes

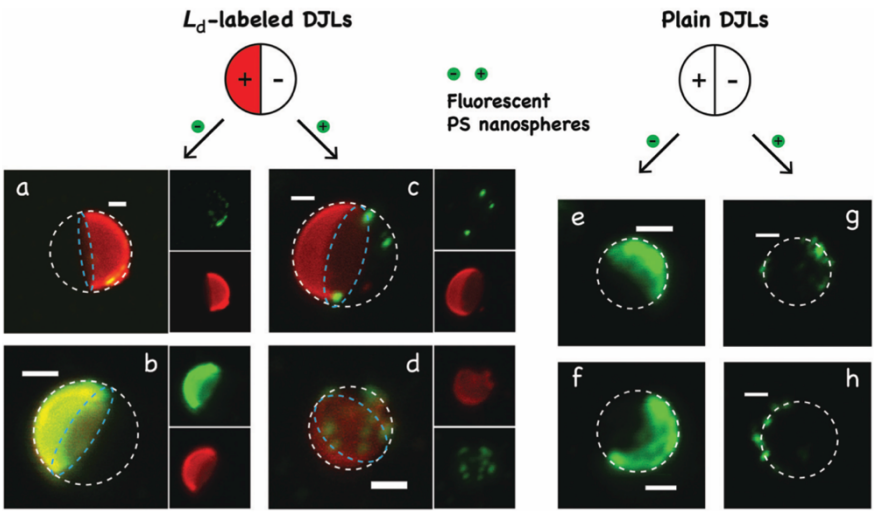

Figure 5-4. Placement of charged lipids in GJLs as revealed by fluorescent PS nanosphere binding. (left) Fluorescence micrographs of dual-charged, rho-DOPE-labeled Janus liposomes upon incubation with either PS-COOH nanospheres (a and b) or PS-NH_2 nanospheres (c and d). Broken circles in white and blue outline the estimated circumference and phase boundary of the liposomes, respectively. Each liposome sample is shown by three images, one by dual (the image on the left) and the other two by single-channel excitation. Images (a and c) were acquired after overnight liposome/nanosphere incubation, whereas (b and d) were obtained after 3-day incubation. (right) Fluorescence micrographs of unlabeled, dual-charged Janus liposomes upon binding with either PS-COOH nanospheres (images e and f) or PS-NH_2 nanospheres (images g and h) after 3-day incubation. Broken circles are added in the images as a visual guide of the liposome contour. Scale bars in all images represent 5 μm.

The next step was the identification of DPPG/DOTAP distribution in these Janus liposomes. To do so, fluorescent PS nanospheres were employed whose surfaces were terminated with either –COOH or –NH_2 groups (see section 5.2 (1)). Through electrostatic binding, these charged fluorescent particles were expected to coat the surface of Janus liposomes and thus

revealed the location of charged lipids in the latter. The zeta potentials of these nanospheres are included in Table 5-1.

As shown in Figure 5-5, green fluorescent nanospheres bound these dual-charged liposomes in a domain-specific fashion, *i.e.*, PS-COOH to the lo domain and PS-NH_2 to the ld domain, in accordance with the designated placement of DPPG (lo) and DOTAP (ld). Here, an interesting distinction could be made between the two charged lipids. While dotted nanosphere attachments were detected in both cases upon overnight incubation (Figure 5-5 a and c), the binding between PS-COOH and the positively-charged ld domain clearly proceeded further. This, for example, produced an even, half-moon shaped nanosphere layer covering the ld domain after 3 days (Figure 5-5 b). By contrast, no such full coverages were seen when PS-NH_2 nanospheres were used instead (Figure 5-5 d). A similar trend was also observed when plain (unlabeled) liposomes were incubated with these charged nanospheres (Figure 5-5 e–h), thus ruling out the possibility of fluorescent dyes being responsible for the observed formations. On the other hand, no nanosphere binding was detected when Janus liposomes free of DPPG/DOTAP were tested. Taken together, these results confirmed the domain-associated distribution of opposite charges in Janus liposomes, and hence the successful formation of the intended dipolar GJLs.

It is interesting that the dipolar GJLs displayed the nonuniform, domain-specific electrostatic binding (Figure 5-5). Such discreteness cannot be attributed entirely to the different charge density carried by the two types of nanospheres (Table 5-1), which would only alter the extent of their attachment, but not their location or binding pattern, on liposomes. Rather, it is the structural dissimilarity between DOTAP and DPPG, as well as the different lipid environments in which they are situated, that are directly responsible for the observed contrasts. Owing to their

phosphate and glycerol groups, DPPG hydrogen bonds extensively with neighboring lipids as well as water molecules, which in turn causes its tight packing in bilayers, *e.g.*, an area of 0.48 nm^2 occupied per lipid,[139] as compared to 0.73 nm^2 for DOTAP[139] or 0.64 nm^2 for DPPC[140]. To the aqueous-suspended nanospheres, this structural arrangement of DPPG poses a constraint not only on the binding accessibility, but also on its efficiency. Complicating the matter further were the lo *vs.* ld domains hosting DPPG and DOTAP, which represented two drastically different lipid environments,[141-143] *e.g.*, in lipid packing density, lateral mobility and hydration level. To evaluate the impact of these factors with any certainty, further work is clearly needed.

5.3.3 Zeta potential measurement of dipolar GJLs

To further characterize the charge distribution in these dipolar GJLs, zeta potential measurement was carried out next. As summarized in Table 5-1, Janus liposomes comprising DPPC/DOPC/cholesterol displayed a slightly negative zeta potential of –2.5 mV. While there existed no published zeta potential data on Janus liposomes, this number was within the range of reported values for homogeneous zwitterionic liposomes containing cholesterol.[144,145] The polar heads of zwitterionic lipids are not strictly parallel to the liposome surface, where the negative charge from phosphate group cannot be entirely canceled by the positive choline group, and their reorientation can cause partial surface charge, thus the zeta potential is not zero.[146] Specifically, after the reorientation, the choline group got shielded by the phosphate group in DI water, that was why the sign of zeta potential was negative.

Furthermore, when the ld-domain indicator dye, rho-DOPE, was included in the sample at a 0.2 mol % level, the zeta potential became more negative, –5.7 mV, apparently due to its intrinsic negative charge. In contrast, the lo-domain indicator, Bodipy-chol, was found to modify the zeta potential toward more positive values, though to a lower extent compared to rho-DOPE

(–4.4 mV). For charge-loaded samples, it was found Janus liposomes singly charged with 2 mol % DPPG or DOTAP (together with both dyes) to yield zeta potentials of comparable magnitude (–19.1 mV *vs.* 18.7 mV). Finally, for DJLs that included both DPPG and DOTAP (again with both dyes present), a positive zeta potential of 5.2 mV was recorded.

Table 5-1. Zeta potential (ζ) values of aqueous-suspended GJLs and polystyrene (PS) nanoparticles.

Sample	ζ (mV)	Sample	ζ (mV)	Sample	ζ (mV)
Zwitterionic		*Dual-charged*		*Anionic*	
Unlabeled[a]	–2.5 ± 0.2[j]	Unlabeled[e]	9.1 ± 1.2[j]	Dual-Labeled (45 °C)[h]	–19.1 ± 0.8[j]
Ld-Labeled[b]	–5.7 ± 0.2[j]	Ld-Labeled[f]	2.5 ± 0.6[j]	Dual-Labeled (50 °C)[h]	–19.7 ± 0.7[j]
Dual-Labeled[c]	–4.4 ± 0.3[j]	Dual-Labeled (45 °C)[g]	5.2 ± 0.7[j]	Dual-Labeled (60 °C)[h]	–19.3 ± 1.0[j]
PS nanospheres[d]		Dual-Labeled (50 °C)[g]	5.6 ± 0.5[j]	*Cationic*	
-COOH	–42.6 ± 0.4[j]	Dual-Labeled (60 °C)[g]	5.4 ± 0.4[j]	Dual-Labeled (45 °C)[i]	18.7 ± 0.4[j]
-NH_2	18.4 ± 1.0[j]			Dual-Labeled (50 °C)[i]	18.6 ± 0.7[j]
				Dual-Labeled (60 °C)[i]	19.2 ± 0.8[j]

[a] DPPC/DOPC/cholesterol = 40/40/20 mol %.

[b] Composition as in a plus 0.2 mol% RhO-DOPE.

[c] Composition as in a plus 0.2 mol% RhO-DOPE and Bodipy-Chol each.

[d] The final concentrations of PS nanospheres were controlled to be ~1×10^9 beads per mL.

[e] DPPC/DPPG/DOPC/DOTAP/cholesterol = 38/2/38/2/20 mol%.

[f] Composition as in d plus 0.2 mol% RhO-DOPE.

[g] Composition as in d plus 0.2 mol% RhO-DOPE and Bodipy-Chol each.

[h] DPPC/DPPG/DOPC/cholesterol/RhO-DOPE/Bodipy-Chol = 38/2/40/20/0.2/0.2 mol%.

[i] DPPC/DOPC/DOTAP/cholesterol/RhO-DOPE/Bodipy-Chol = 40/38/2/20/0.2/0.2 mol%.

[j] Standard deviation (n = 5).

5.3.3 Electrokinetic motion of dipolar GJLs

To corroborate the above zeta potential data, which measured the collective electrophoretic behavior of liposome populations, the electrokinetic motion of individual Janus liposomes subjected to a DC field was further monitored. As described in the section 5.2 (8), this was carried out in linear microchannels made of cyclic olefin copolymers, which are known to

sustain significant cathodic electroosmotic flow (EOF).[147] Since the liposome solution was confined in the microchannel, which sustained no net fluid flow across, a counter flow developed at the center of the microchannel to balance out the surface-originated EOF running in the opposite direction.[148] As shown in Figure 5-6, this counter flow dominated the fluid movement at and near the midplane of the channel, carrying both zwitterionic and dipolar Janus liposomes toward the anode. Concurrent to migration, interestingly, both types of liposomes also underwent rotation. While the rotation of these liposomes did not follow any particular ordered sequence – due to their random initial orientations, it always acted to align the two hemispheres of these liposomes along the electric field.

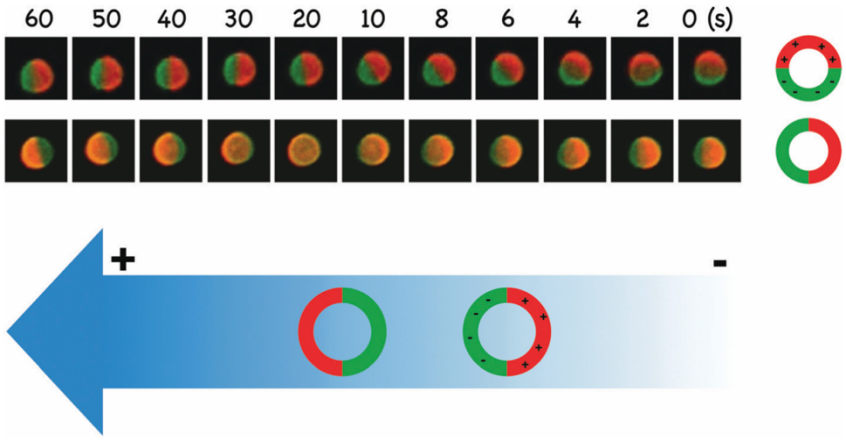

Figure 5-6. Characteristic rotation and alignment of individual dipolar (top row) and zwitterionic (second row) Janus liposomes in response to an electric field (1 V cm^{-1}). The numbers given at the top of the images indicate the time elapsed (in seconds) since the field was turned on at time 0. (bottom) Schematic of the direction (indicated by the blue arrow) and relative mobility of liposome movement in relation to polarity of the applied field. Their domain-specific alignments with the field are also shown; both liposomes are ~11 μm in diameter.

Upon close inspection, however, several distinctive features between the two liposomes could be identified:

(1) Terminal liposome orientation. In the case of dipolar GJLs, the lo(–) domain always pointed to the anode and the ld(+) domain pointed to the cathode, thus behaving like a giant electric dipole in a DC field. While not as highly loaded as dipolar GJLs, charge was nevertheless unevenly distributed between the two hemispheres of zwitterionic Janus liposomes, mainly due to the negatively-charged rhodamine residing in the ld domain, which preferentially pointed to the anode (Figure 5-6). Once aligned, both liposomes rotated no further and thereafter migrated onward with their respective fixed orientations. In other words, the rotation of these liposomes only occurred at the beginning of their electrokinetic motion, when their charged domain(s) were not yet fully aligned with the electric field.

(2) Alignment time. In general, it took less time for dipolar GJLs to achieve their steady terminal orientation, *e.g.*, ~20 s as compared to ~40 s observed for the zwitterionic liposome (Figure 5-6). This made sense – with their higher charge level and dipolar charge distribution, dipolar GJLs experienced a stronger electrostatic torque when not aligned with the external field than the zwitterionic liposome – under otherwise comparable conditions.

(3) Electrokinetic mobility. While both types of liposomes migrated toward the anode, dipolar GJLs consistently registered a lower mobility: $2.2 \pm 0.5 \times 10^{-4}$ cm^2 V^{-1} s^{-1} (n=12), as compared to $3.3 \pm 0.2 \times 10^{-4}$ cm^2 V^{-1} s^{-1} (n=12), for zwitterionic liposomes. This mobility difference was clearly caused by their electrophoresis running in opposite directions (Table 5-1), one against (in the case of dipolar GJLs) and the other along the same direction as the counter flow of EOF.

5.3.4 Electrostatic self-assembly of dipolar GJLs

Unlike solid dipolar Janus particles, whose binding occurs exclusively via oppositely-charged hemispheres,[17] clustering of dipolar GJLs apparently occurred between both dissimilar (Figure 5-7 a–d) and similar domains (Figure 5-7 e–h). In the former case, the lo and ld domains were further found to join each other in either head-to-head (Figure 5-7 a and b), or head-to-side (Figure 5-7 c) or side-to-side (Figure 5-7 d) fashion, with the last configuration less frequently observed. On the other hand, liposome clustering via similar lipid domains was somewhat surprising, as it implied binding between like charges – a thermodynamically disfavored scenario.

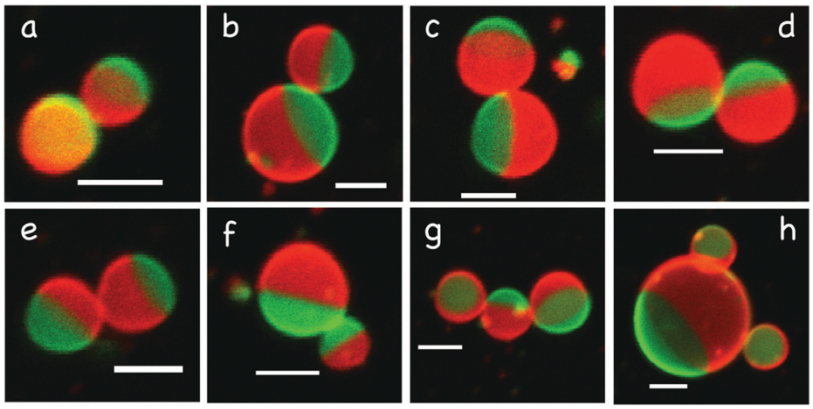

Figure 5-7. Dipolar GJL dimer (images a–f) and trimer (g and h) formation under a relatively low liposome density (total lipid concentration: ~1.25 μM). Before imaging, these liposomes were incubated for 2 h at room temperature in the dark. Scale bar: 10 μm.

To account for such unexpected formations, a pair of unique features associated with the current liposome system were considered. (1) The presence of smaller lipid particles. As evident from Figure 5-7 b, g and h, these particles were also being produced by the hydration process alongside the micro-sized dipolar GJLs. Being charged and more mobile, these small particles often found larger liposomes to bind and, in doing so, could modify the surface charge composition of the latter. (2) Small lipid domains presented in the ‘‘wrong’’ hemispheres, which

could exist as kinetically trapped local states as a result of incomplete coalescence. As noted previously by other workers, these local states may persist in phase-separated lipid systems either due to high membrane viscosity[73] or interdomain repulsion.[149] Conceivably, the like charged present in these small domains added electrostatic repulsion between them, thus discouraging their merging even more.[135] Since these small domains bearded the opposite charge of the hemispheres in which they were situated, they in effect served as binding sites to link similar domains of dipolar GJLs in proximity.

When incubated at a relatively high liposome concentration, the increased number of dipolar GJLs presented promotes more frequent liposome encounters and hence the formation of more extended clusters. A very informative sequence of images capturing such assembling events is included in Figure 5-8 (top section). At the beginning of this sequence, there were about a dozen separate DJLs sitting on the floor of the imaging chamber. Two pairs of dimers were formed in the first two minutes near the center of the view (marked by a broken circle), as these dipolar GJLs bound ‘‘head-to-head’’ with their neighbors just a few microns away. The close proximity between the two dimers allowed them to further approach each other to make contact in the next few minutes – this time between ld domains with the assistance of a smaller liposome, producing a tetramer. This tetramer was later joined by a third dimer coming from the lower left (marked by broken oval, 8 min), and the new contact appeared to be between lo domains. Not too far behind, there was also another larger liposome (marked by asterisk, 8 min) approaching the tetramer from the right side. Since the size/orientation of this newcomer’s lo domain matched well with the ld domain of the tetramer, they bound and subsequently fused into each other (16 and 18 min). This interaction was so powerful that it appeared to cause the third dimer to detach from the tetramer (21 to 30 min). Intriguingly, prior to its merging, this (bigger) liposome not

only rolled directly toward its binding partner but at the same time, also rotated so as to achieve a favorable orientation for binding. Such ‘‘docking’’-like movement was absent in electrostatic binding between homogeneous anionic/cationic liposomes,[83,150] and once again confirmed the dipolar charge configuration in these liposomes.

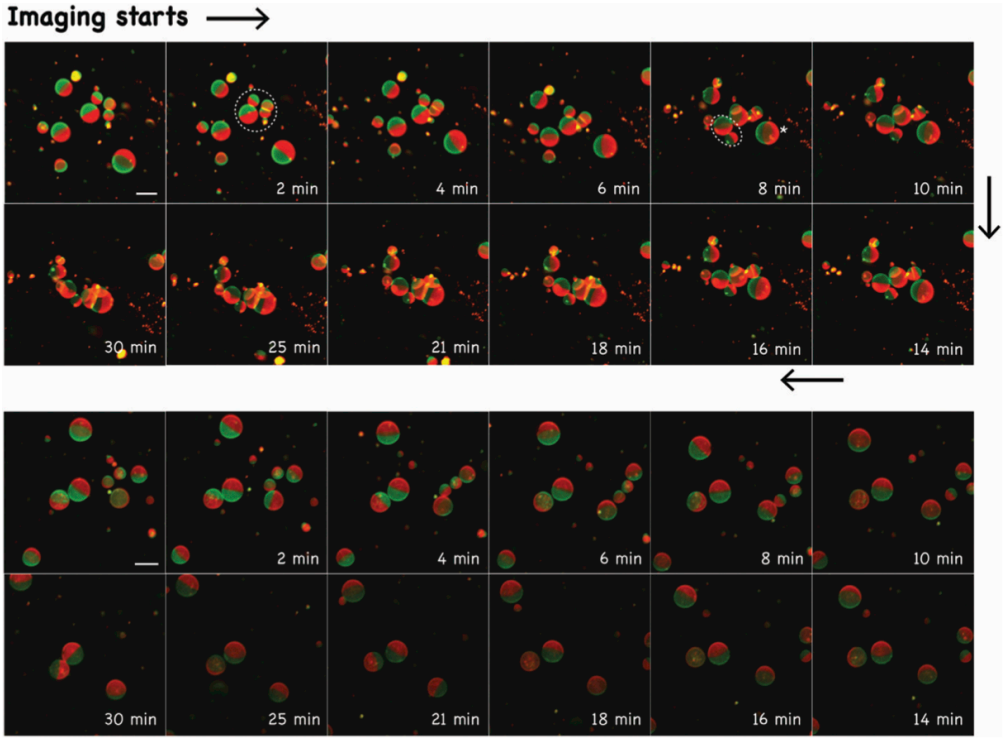

Figure 5-8. GJLs motions under a relatively high liposome density. (top) Time-sequenced fluorescence micrographs of dipolar GJLs undergoing aggregation. Liposomes were imaged right after their formation; total lipid concentration: 5 μM. (bottom) A similar sequence recorded for zwitterionic Janus liposomes (lipid composition: DPPC/DOPC/cholesterol/Bodipy-chol/rho-DOPE, 40/40/20/0.2/0.2 mol %) as a control. Scale bar: 20 μm.

A drastically different interaction behavior was displayed by Janus liposomes bearing no DPPG or DOTAP. With a comparable liposome density to start with, these particles diffused around and would temporarily get so close to each other to appear in direct contact, but always

parted their ways afterwards (Figure 5-8, bottom section). Clearly, being in close proximity alone was insufficient for the two zwitterionic lipid bilayers to initiate fusion. Since lipid fusion involves extensive lipid/water reorganization at the interfaces, some more forceful binding mechanism has to be in place to overcome the associated energy barriers. In cell biology, for example, this task is often fulfilled by the soluble N-ethylmaleimide-sensitive factor attachment protein receptor (SNARE)[151] complexes located on cargo vesicles and the target membrane. There, interestingly, electrostatic attraction is also found to play a central role in complementary binding between SNARE complexes, a process facilitated specifically by protein motifs enriched with cationic lysine and anionic glutamic acid residues.[152]

5.4 Conclusion

As far as I am aware, this new type of liposome that contains opposite surface charges decorating the two hemispheres of the same colloidal body – dipolar Janus liposomes – is the first time to be presented. Such heterogeneous organization of surface charge was achieved through cholesterol-modulated lipid phase separation, which sorted anionic lipid (DPPG) and cationic lipid (DOTAP) into coexisting liquid-ordered/liquid-disordered domains. The detailed experimental conditions to produce these liposomes in high (>80%) yields have been presented, based on hydration of a ternary lipid system consisting of DPPC/DOPC/cholesterol. The size and domain configuration of thus produced liposomes were then characterized with confocal fluorescence microscopy. Using the same technique, the charge distribution of the dual-charged GJLs were identified by employing functionalized fluorescent PS nanospheres to incubate with these Janus particles. Upon electrostatic interaction governed adsorption, for dual-charged GJLs, the negatively PS-COOH particles were specifically loaded on the ld domain, whereas, the positively PS-NH_2 particles selectively attached onto the lo domain, suggesting that these dual-

charged GJLs were dipolar Janus particles. This dipolar structure was further confirmed in the experiment of electrokinetic motion of dipolar GJLs in which the dipolar GJLs showed fixed liposome orientation after achieving a stable state. In addition, taking advantage of a confocal microscope, I also followed, in detail, the electrostatic self-assembly of these new dipolar colloidal particles whose size were found to depend on the density of liposomes. Specifically, dimers and trimers with various binding fashions were observed in the case of using low density dipolar GJLs, and the formation of extended clusters were captured by using a high density dipolar GJLs solution. This unique molecular assembly formation may be of fundamental interest in the areas of lipid colloid chemistry and self-assembly and moreover adds an all-lipid-based soft material into the fast-growing inventory of patchy particles.

CHAPTER 6. SUMMARY AND OUTLOOK

6.1 Summary

Motivated by the technical promises of micro-sized Janus liposomes as well as the lack of general methods to synthesize such asymmetrical lipid colloids, a facile, robust, and reliable procedure for preparing GJLs via PVA gel-assisted hydration have been developed.[1] Combining this method with membrane-based lipid extrusion, an efficient upper-limit-size-controlled procedure for preparing giant liposomes has been established, named PC membrane-gated, PVA gel-assisted hydration. Furthermore, (bio)chemically reactive or physically responsive functionalities have been straightforwardly imparted on the prepared GJLs and thus obtained biotinylated GJLs or dipolar-charged GJLs, respectively. Finally, I have carefully monitored and interpreted the biotin-avidin affinity binding directed clustering of biotin-decorated GJLs[1] as well as the electrokinetic motions and electrostatic interaction governed self-assembly of dipolar-charged GJLs[2].

(1) GJLs preparation

In the chosen ternary lipid systems, DPPC/DOPC/cholesterol and DPPC/DPhPC/cholesterol, the hydrophobic mismatch among high-melting saturated phospholipid (DPPC) and low-melting unsaturated (DOPC) or branched (DPhPC) phospholipid together with cholesterol-induced liquid-liquid immiscibility drive the lipid phase segregation.[53,88] The phase separation but coexisting lo-ld phases render these liposomes their Janus configuration. The GJLs in principle share many of the features promised by Janus particles, therefore, the first step should be to call for a robust method to make such colloidal particles.

There have been several evidences showing that gel-assisted lipid swelling approach can overcome several issues arising from other commonly used giant liposomes preparation methods, such as residual organic solvent contamination, high fraction of multilamellar liposomes and lipids usage limitation.[89,92] Considering this, the procedure of gel-assisted hydration was employed and modified for fabricating GJLs. Presented in Chapter 2, high-yield and high-quality DPPC/DOPC/cholesterol giant liposomes with polymorphic patches were obtained after a short-time (typically 1 h) hydration, and then these domains underwent coalescence to evolve into two hemispheres showing distinctive fluidic characteristics (lo and ld phases) and thus GJLs formed. The versatility and robustness of this procedure has been further demonstrated through successfully preparing (1) Janus configuration tunable GJLs, (2) modified DPPC/DOPC/cholesterol GJLs, including biotinylated GJLs (Chapter 4) and charged GJLs (Chapter 5), (3) DPPC/DPhPC/cholesterol GJLs, and (4) homogeneous liposomes (Chapter 3). This is the first reported work to fabricate Janus particles via gel-assisted hydration method.

Not surprisingly, the giant liposomes generated from PVA gel-assisted lipid swelling bear wide size distributions which may hinder their further applications[99] (*e.g.*, drug delivery). The membrane-gated gel-assisted hydration procedure developed in Chapter 3 has shown the capability to address this issue. Specifically, the planar lipid stacks deposited on PVA gel were laminated atop with PC membranes featuring with uniform-sized pores, and then the underlying lipids could only pass through the pores to form liposomes in the main aqueous phase upon hydration. This method has exhibited efficient upper-limit size controlment for producing liposomes consisting with various components, and more importantly, both the lamellarity and the Janus structure of GJLs were retained via this procedure which is quite challenging for extrusion method.

(2) Self-assembly and motion

Low-density DPPC/DOPC/cholesterol GJLs are not prone to cluster/aggregate in DI water. However, by incorporating lipids containing functional characteristics with this primary three-component lipid system, features of other functionalized Janus particles posed have been observed, including self-assembly and electrokinetic motion.

As shown in Chapter 4, biotin-conjugated lipid (biotin-DOPE 1 mol %) was straightforwardly added into DPPC/DOPC/cholesterol precursor chloroform solution at first, and then underwent the same routine described in Chapter 2 resulting in biotinylated GJLs. This work further demonstrates that biotin-DOPE preferentially partition into ld phase of the lipid matrix mainly due to the fact that this molecule shares the same dioleoyl chains with the main lipid component (DOPC) in ld phase. The selective sorting feature renders the biotin-decorated GJLs asymmetrical binding capacity toward avidin. This affinity binding drives irreversible and domain-specific cluster formation among GJLs, whose structure and size are found to depend on the domain configuration of individual liposomes and incubation time.

An alternative route has been taken to achieve self-assembly of GJLs which is presented in Chapter 5. Analogous with Chapter 4, charged lipids, including anionic DPPG and cationic DOTAP, were directly introduced into DPPC/DOPC/cholesterol lipid matrix for forming charged GJLs via PVA gel-assisted lipid swelling procedure. Through charged PS nanospheres binding experiment, this kind of dual-charged GJLs have been further confirmed to be a kind of dipolar Janus particles that contain opposite surface charges decorating two hemispheres of the same colloidal body. This feature of dipolar-charged GJLs has also been demonstrated in electrokinetic motion in which liposomes underwent cathode to anode migration while holding a fixed terminal orientation (the lo phase pointed to anode, whereas the ld domain faced to

cathode). The imparted extra electrostatic interactions among these GJLs can drive clusters formation, whose structure and size are found to depend on the liposome density. The significant contribution of this work is that such type of all-lipid-based dipolar colloidal Janus particles has never been fabricated before this work. The facile, efficient preparation procedure combined with the unique surface charge structure opens a new window for patchy particles research.

6.2 Outlook

Thus far, GJLs with or without functionalities have been successfully prepared via PVA gel-assisted lipid swelling in DI water and their properties/behaviors have been investigated and interpreted as well. However, the supporting electrolytes have not been involved in the work reported here which is essential for extending the capability of this method as well as further applications of GJLs. This will be the major direction to be exploited in the future.

Nevertheless, the preparation routines of giant liposomes presented in this Dissertation demonstrate the highlights including good reproducibility, a special-equipment-free and easy-to-follow procedure, high-yield and high-quality liposome formation, as well as versatile lipids applicability. These may be of interest to researchers in patchy particle community. With reliable preparation methods in hand, it is now feasible to test these Janus liposomes alongside their inorganic/polymer cousins as building blocks and motors. Understanding the physicochemical similarities and differences between various types of patchy particles, for one, will help researchers design better applications according to their strengths. In addition, the membrane-gated gel-assisted hydration approach further provides an opportunity to examine size-dependent characteristics of giant liposomes which are anticipated to be beneficial for developing novel patchy materials.

Successful fabricating both biotin-decorated and charged lipids-contained GJLs presented in this work are good examples for selectively sorting functional lipids into phase-separated lipid systems. Thus, other kinds of lipids containing special functions are able to be involved for creating new types of multifunctional, lipid-based colloidal patchy particles. Moreover, these modified GJLs may find applications in several areas.

(1) Bioanalytical/biomedical applications. A good number of homogeneous/heterogenous biodetection schemes have been developed using symmetrical liposomes,[153] taking advantages of their aqueous core and soft, modifiable surfaces combined in a small package. Janus liposomes are expected to work equally well in many of these bioassays. Furthermore, the biocompatible, biodegradable GJLs will add new capabilities into the fast-growing inventory of drug delivery. The electrokinetic motions of dipolar GJLs indicate the potential to be used to develop display devices and electric field responsive probers which have been realized by other kinds of Janus particles[10,23] and moreover may overcome several challenges the current materials face in biological environment.

(2) Micromotors. The fact that biotin-DOPE preferentially partition into ld domain as well as specific binding affinity hint at the possibility to locate enzymes, like horseradish peroxidase,[30] on ld-domain hemisphere rendering the new functional GJLs asymmetrical reaction feature in the presence of substrates. These GJLs will be recognized as a kind of micromotor if gas is produced during the process.

(3) Membrane biophysics. The majority of phase-separated liposomes that have appeared in the biophysical literature are prepared using electroformation, which is known to suffer several limitations, such as potential lipid damage and biases toward charged lipids.[40] In this regard, the field can clearly benefit from having a robust alternative. On the other hand, the

results from Chapter 4 point to the possibility of inducing liposome shape transformation by protein adhesion and, moreover, the importance of liposome domain configuration and mechanical properties leading to such changes. This may be further developed into a model system for studying lipid bulging/budding, a fundamental process essential to many biological functions.[154,155]

(4) Synthetic biology. Apart from the top-down strategy used in the state-of-the-art field for engineering biochemical components to construct biological systems, liposome self-assembly, especially domain-specific clustering, implies feasibility to be employed in a bottom-up strategy for synthetic biology research.[156,157] Together with pursued application of giant liposomes for building artificial cells, the self-assembled GJLs encapsulating biomolecules will find their special role in this area.

6.3 Contributions of The Dissertation

The experimental findings presented in this Dissertation devote contributions to both Janus particle and liposome communities. First of all, the success of fabricating GJLs firmly identified the feasibility to produce all-lipid-based Janus particles through the novel but facile procedures: PVA gel-assisted hydration as well as membrane-gated and gel-assisted hydration. These biomaterial-based soft Janus particles should be an appealing material when considering the promising features of Janus particles as well as the suitableness of biomaterials in bio-related applications, however, these particles have rarely been prepared and utilized for purposes which have been covered by the researches from Chapter 2 to 5. Moreover, the results of producing high-yield and high-quality GJLs by using a gel-assisted hydration approach offer a reliable routine to prepare soft Janus particles by following the strategy of phase separation. Another significant contribution to the Janus particle field is that the example of the first reported dipolar

charged liposomes 1) provides a practical means to fabricate dipolar soft colloidal particles which, to my knowledge, have been rarely reported and are very challenging for other sophisticated methods to fabricate; 2) adds a biomaterial-based charged material into the fast-growing inventory of Janus particles. With respect of the contributions to the liposome community, the work presented here 1) displays the viability to selectivity incorporate functionalities into the desired domains through the hydrophobic mismatch regulated partition preferences; 2) demonstrates two practicle strategies to achieve self-assembly of giant liposomes which may be highly beneficial for building/designing novel materials with desired features through a bottom-up approach; 3) gives inspiration to prepare other types of functionalized liposomes by employing different lipid species and/or introducing various functional compartments.

This Dissertation has introduced reliable strategies to prepare giant Janus liposomes displaying tunable patchy geometry, size and function. These lay a good foundation as a starting point for future researches to develop new types of biomaterial-based patchy particles. This also opens up exciting new possibilities for applications of biocompatible multifunctional materials as well as fundamental researches.

References

1. Wang M.; Liu, Z.; Zhan, W. Janus Liposomes: Gel-Assisted Formation and Bioaffinity-Directed Clustering. *Langmuir* **2018**, *34*, 7509-7518.

2. Liu, Z.; Cui, J.; Zhan, W. Dipolar Janus Liposomes: Formation, Electrokinetic Motion and Self-Assembly. *Soft Matter* **2020**, *16*, 2177-2184.

3. Perro, A.; Reculusa, S.; Ravaine, S.; Bourgeat-Lami, E.; Duguet, E. Design and Synthesis of Janus micro- and nanoparticles. *J. Mater. Chem.* **2005**, *15*, 3745-3760.

4. Jiang, S.; Chen, Q.; Tripathy, M.; Luijten, E.; Schweizer, K. S.; Granick, S. Janus Particle Synthesis and Assembly. *Adv. Mater.* **2010**, *22*, 1060-1071.

5. Pawar, A. B.; and Kretzschmar, I. Fabrication, Assembly, and Application of Patchy Particles. *Macromol. Rapid Commun.* **2010**, *31*, 150-168.

6. Du, J.; O'Reilly, R. K. Anisotropic Particles with Patchy, Multicompartment and Janus Architectures: Preparation and Application. *Chem. Soc. Rev.* **2011**, *40*, 2402-2416.

7. Loget, G.; Kuhn, A. Bulk Synthesis of Janus Objects and Asymmetric Patchy Particles. *J. Mater. Chem.* **2012**, *22*, 15457-15474.

8. Walther, A.; Müller, A. H. E. Janus Particles: Synthesis, Self-Assembly, Physical Properties, and Applications. *Chem. Rev.* **2013**, *113*, 5194-5261.

9. Pang, X.; Wan, C.; Wang, M.; Lin, Z. Strictly Biphasic Soft and Hard Janus Structures: Synthesis, Properties, and Applications. *Angew. Chem., Int. Ed.* **2014**, *53*, 5524-5538.

10. Yi, Y.; Sanchez, L.; Gao, Y.; Yu, Y. Janus Particles for Biological Imaging and Sensing. *Analyst* **2016**, *141*, 3526-3539.

11. Zhang, J.; Grzybowski, B. A.; Granick, S. Janus Particle Synthesis, Assembly, and Application. *Langmuir* **2017**, *33*, 6964-6977.

12. Kirillova, A.; Marschelke, C.; Synytska, A. Hybrid Janus Particles: Challenges and Opportunities for the Design of Active Functional Interfaces and Surfaces. *ACS Appl. Mater. Interfaces* **2019**, *11*, 9643-9671.

13. Casagrande, C.; Fabre, P.; Raphaël, E.; Veyssié, M. Janus Beads: Realization and Behavior at Water/Oil Interfaces. *Europhys. Lett.* **1989**, *9*, 251-255.

14. de Gennes, P. G. Soft Matter (Nobel Lecture). *Angew. Chem., Int. Ed. Engl.* **1992**, *31*, 842-845.

15. Sabapathy, M.; Mathew K, R. A.; Mani, E. Self-Assembly of Inverse Patchy Colloids with Tunable Patch Coverage. *Phys. Chem. Chem. Phys.* **2017**, *19*, 13122-13132.

16. Nie, Z.; Li, W.; Seo, M.; Xu, S.; Kumacheva, E. Janus and Ternary Particles Generated by Microfluidic Synthesis: Design, Synthesis, and Self-Assembly. *J. Am. Chem. Soc.* **2006**, *128*, 9408-9412.

17. Hong, L.; Cacciuto, A.; Luijten, E.; Granick, S. Clusters of Charged Janus Spheres. *Nano Lett.* **2006**, *6*, 2510-2514.

18. Smoukov, S. K.; Gangwal, S.; Marquez, M.; Velev, O. D. Reconfigurable Responsive Structures Assembled from Magnetic Janus Particles. *Soft Matter*, **2009**, *5*, 1285-1292.

19. Li, M; L, D. Vortices around Janus Droplets Under Externally Applied Electric Field. *Microfluid Nanofluid* **2016**, *20*, 79.

20. Reculusa, S.; Poncet-Legrand, C.; Perro, A.; Duguet, E.; Bourgreat-Lami, E.; Mingotaud, C.; Ravaine, S. Hybrid Dissymmetrical Colloidal Particles. *Chem. Mater.* **2005**, *17*, 3338-3344.

21. Tanaka, T.; Nakatsuru, R.; Kagari, Y.; Saito, N.; Okubo, M. Effect of Molecular Weight on the Morphology of Polystyrene/Poly(methyl methacrylate) Composite Particles Prepared by the Solvent Evaporation Method. *Langmuir* **2008**, *24*, 12267-12271.

22. Nie, Z.; Li, W.; Seo, M.; Xu, S.; Kumacheva, E. Janus and Ternary Particles Generated by Microfluidic Synthesis: Design, Synthesis, and Self-Assembly. *J. Am. Chem. Soc.* **2006**, *128*, 9408-9412.

23. Nisisako, T.; Torii, T.; Takahashi, T.; Takizawa, Y. Synthesis of Monodisperse Bicolored Janus Particles with Electrical Anisotropy Using a Microfluidic Co-Flow System. *Adv. Mater.* **2006**, *18*, 1152-1156.

24. Yoshida, M.; Roh, K. -H.; Mandal, S.; Bhaskar, S.; Lim, D.; Nandivada, H.; Deng, X.; Lahann, J. Structurally Controlled Bio-hybrid Materials Based on Unidirectional Association of Anisotropic Microparticles with Human Endothelial Cells. *Angew. Chem. Int. Ed.* **2009**, *21*, 4920-4925.

25. Hwang, S.; Roh, K. -H.; Lim, D. W.; Wang, G.; Ctirad U.; Lahann, J. Anisotropic Hybrid Particles Based on Electrohydrodynamic Co-Jetting of Nanoparticle Suspensions. *Phys. Chem. Chem. Phys.* **2010**, *12*, 11894-11899.

26. Walther, A.; Hoffmann, M.; Müller, A. H. E. Emulsion Polymerization Using Janus Particles as Stabilizers. *Angew. Chem. Int. Ed.* **2008**, *47*, 711-714.

27. Lin, F.; Doong, R. Bifuncitonal Au-Fe_3O_4 Heterostructures for Magnetically Recyclable Catalysis of Nitrophenol Reduction. *J. Phys. Chem. C* **2011**, *115*, 6591-6598.

28. Ma, X.; Jannasch, A.; Albrecht, U. R.; Hahn, K.; Miguel-López, A.; Schäffer, E.; Sánchez, S. Enzyme-Powered Hollow Mesoporous Janus Nanomotors. *Nano Lett.* **2015**, *15*, 7043-7050.

29. Howse, J. R.; Jones, R. A. L.; Gough, T.; Vafabakhsh, R.; Golestanian, R. Self-Motile Colloidal Particles: From Directed Propulsion to Random Walk. *Phys. Rev. Lett.* **2007**, *99*, 048102.

30. Ma, X.; Hortelão, A. C.; Patiño, R.; Sánchez, S. Enzyme Catalysis To Power Mico/Nanomachines. *ACS Nano* **2016**, *10*, 9111-9122.

31. Moran, J. L.; Posner, J. D. Phoretic Self-Propulsion. *Annul. Rev. Fluid Mech.* **2017**, *495*, 511-540.

32. Yu, H.; Chen, M.; Rice, P. M.; Wang, S. X.; White, R. L.; Sun, S. Dumbbell-like Bifunctional Au-Fe_3O_4 Nanoparticles. *Nano Lett.* **2005**, *5*, 379-382.

33. Xu, C.; Eang, B.; Sun, S. Dumbbell-like Au-Fe_3O_4 Nanoparticles for Target-Specific Platin Delivery. *J. Am. Chem. Soc.* **2009**, *131*, 4216-4217.

34. Xu, C.; Xie, J.; Ho, D.; Wang, C.; Kohler, N.; Walsh, E. G.;; Morgan, J. R.; Chin, Y. E.; Sun, S. Au-Fe_3O_4 Dumbbell Nanoparticles as Dual-Functional Probes. *Angew. Chem. Int. Ed.* **2008**, *47*, 173-176.

35. Chen, Q.; Whitmer, J. K.; Jiang, S.; Bae, S. C.; Luijten, E.; Granick, S. Supercolloidal Reaction Kinetics of Janus Spheres. *Science*, **2011**, *331*, 199-202.

36. Kraft, D. J.; Ni, R.; Smallenburg, F.; Hermes, M.; Yoon, K.; Weitz, D. A.; van Blaaderen, A.; Grpenewold, J.; Dijkstra, M.; Kegel, W. K. Surface Roughness Directed Self-Assembly of Patchy Particles into Colloidal Micelles. *Proc. Natl. Acad. Sci. U.S.A.* **2012**, *109*, 10787-10792.

37. Gangwal, S.; Cayre, O.; Velev, O. D. Dielectrophoretic Assembly of Metallodielectric Janus Particles in AC Electric Fields. *Langmuir* **2008**, *24*, 13312-13320.

38. Takei, H.; Shimizu, N. Gradient Sensitive Microscopic Probes Prepared by Gold Evaporation and Chemisorption on Latex Spheres. *Langmuir* **1997**, *13*, 1865-1868.

39. Beales, P. A.; Nam, J.; Vanderlick, T. K. Specific Adhesion between DNA-Functionalized "Janus" Vesicles: Size-Limited Clusters. *Soft Matter* **2011**, *7*, 1747-1755.

40. Walde, P.; Cosentino, K.; Engel, H.; Stano, P. Giant Vesicles: Preparations and Applications. *ChemBioChem* **2011**, *11*, 848-865.

41. Meer, G. V.; Voelker, D.; Feigneson, G. Membrane Lipids: Where They Are and How They Behave. *Nature* **2008**, *9*, 112-124.

42. Heberle, F. A.; Feigenson, G. W. Phase Separation in Lipid Membranes. *Cold Spring Harb Perspect Biol* **2011**, *3*, a004630.

43. Li, J.; Wang, X.; Zhang, T.; Wang, C.; Huang, Z.; Luo, X.; Deng, Y. A Review on Phospholipids and Their Main Applications in Drug Delivery Systems. *Asian J. Pharm. Sci.* **2015**, *10*, 81-98.

44. Bangham, A. D.; Horne, R. W. Action of Saponin on Biological Cell Membranes. *Nature* **1962**, *196*, 952-955.

45. Simons, K.; Vaz, W. L. C. Model Systems, Lipid Rafts, and Cell Membranes. *Annu. Rev. Biophys. Struct.* **2004**, *33*, 269-295.

46. Sankaram, M. B.; Thompson, T. E. Cholesterol-Induced Fluid-Phase Immiscibility in Membranes. *Proc. Natl. Acad. Sci. U.S.A.* **1991**, *19*, 8686-8690.

47. Furse, S. Is Phosphatidylglycerol Essential for Terrestrial Life? *J. Chem. Biol* **2017**, *10*, 1-9.

48. Regelin, A. E.; Fankhaenel, S.; Gürtesch, L.; Prinz, C.; von Kiedrowski, G.; Massing, U. Biophysical and Lipofection Studies of DOTAP Analogs. *Biochim. Biophys. Acta* **2000**, *1464*, 151-164.

49. Lei, G.; MacDonald, R. C. Effects on Interactions of Oppositely Charged Phospholipid Vesicles of Covalent Attachment of Polyethylene Glycol Oligomers to Their Surfaces: Adhesion, Hemifusion, Full Fusion and “Endocytosis”. *J. Membrane Biol.* **2008**, *221*, 97-106.

50. Chan, Y. M.; van Lengerich, B.; Boxer, S. G. Lipid-Anchored DNA Mediates Vesicle Fusion as Observed by Lipid and Content Mixing. *Biointerphases* **2008**, *3*, FA17-FA21.

51. Evers, C. H. J.; Luiken, J. A.; Bolhuis, P. G.; Kegel, W. K. Self-Assembly of Microcapsules via Colloidal Bond Hybridization and Anisotropy. *Nature* **2016**, *534*, 364-368.

52. Has, C.; Pan, S. Vesicle Formation Mechanisms: An Overview. *J. Liposome Res.* **2020**, *104*, 1730401.

53. McConnell, H. M.; Vrljic, M. Liquid-Liquid Immiscibility in Membranes. *Annu. Rev. Biophys. Biomol. Struct.* **2003**, *32*, 469-492.

54. de Meyer, F.; Smit, B. Effect of Cholesterol on the Structure of a Phospholipid Bilayer. *Proc. Natl. Acad. Sci. U.S.A.* **2009**, *106*, 3654-3658.

55. Feigenson, G. W. Phase Diagrams and Lipid Domains in Multicomponent Lipid Bilayer Mixtures. *Biochim. Biophys. Acta* **2009**, *1788*, 47-52.

56. Nagle, J. F.; Tristram-Nagle, S. Structure of Lipid Bilayers. *Biochim. Biophys. Acta* **2000**, *1469*, 159-195.

57. Nagarajan, S.; Schuler, E. E.; Ma, K.; Kindt, J. T.; Dyer, R. B. Dynamics of the Gel to Fluid Phase Transformation in Unilamellar DPPC Vesicles. *J. Phys. Chem. B* **2012**, *116*, 13749-13756.

58. Poger, D.; Caron, B.; Mark, A. E. Effect of Methyl-Branched Fatty Acids on the Structure of Lipid Bilayers. *J. Phys. Chem. B* **2014**, *118*, 13838-13848.

59. Kara, S.; Afonin, S.; Babii, O.; Tkachenko, A. N.; Komarov, I. V.; Ulrich, A. S. Diphytanoyl Lipids as Model Systems for Studying Membrane-Active Peptides. *Biochim. Biophys. Acta* **2017**, *1859*, 1828-1837.

60. https://avantilipids.com/tech-support/physical-properties/phase-transition-temps

61. Takechi-Haraya, Y.; Sakai-Kato, K.; Abe, Y.; Kawanishi, T.; Okuda, H.; Goda, Y. Atomic Force Microscopic Analysis of the Effect of Lipid Composition on Liposome Membrane Rigidity. *Langmuir* **2016**, *32*, 6074-6082.

62. Almeida, P. F. F. Thermodynamics of lipid interactions in complex bilayers. *Biochim. Biophys. Acta* **2009**, *1788*, 72-85.

63. Momin, N.; Lee, S.; Gadok, A. K.; Busch, D. J.; Bachand, G. D.; Hayden, C. C.; Stachowiak, J. C.; Sasaki, D. Y. Designing Lipids for Selective Partitioning into Liquid Ordered Membrane Domains. *Soft Matter* **2015**, *11*, 3241-3250.

64. Marsh, D. Cholesterol-Induced Fluid Membrane Domains: A Compendium of Lipid-Raft Ternary Phase Diagrams. *Biochim. Biophys. Acta* **2009**, *1788*, 2114-2123.

65. Subramaniam, S.; McConnel, H. M. Critical Mixing in Monolayer Mixtures of Phospholipid and Cholesterol. *J. Phys. Chem.* **1987**, *91*, 1715-1718.

66. Veatch, S. L.; Polozov, I. V.; Gawrisch, K.; Keller, S. L. Liquid Domains in Vesicles Investigated by NMR and Fluorescence Microscope. *Biophys. J.* **2004**, *86*, 2910-2922.

67. Simons, K.; Ikonen, E. Functional Rafts in Cell Membranes. *Nature* **1997**, *387*, 569-572.

68. Valignat, M. -P.; Theodoly, O.; Crocker, J. C.; Russel, W. B.; Chaikin, P. M. Reversible Self-Assembly and Directed Assembly of DNA-Linked Micrometer-Sized Colloids. *Proc. Natl. Acad. Sci. U.S.A.* **2005**, *102*, 4225-4229.

69. Klymchenko, A. S.; Kreder, R. Fluorescent Probes for Lipid Rafts: From Model Membranes to Living Cells. *Chem Biol.* **2014**, *21*, 97-113.

70. Chiantia, S.; Ries, J.; Kahya, N.; Schwille, P. Combined AFM and Two-Focus SFCS Study of Raft-Exhibiting Model Membranes. *ChemPhysChem* **2006**, *7*, 2409-2418.

71. Veatch, S. L.; Soubias, O.; Keller, S. L.; Gawrisch, K. Critical Fluctuations in Domain-Forming Lipid Mixtures. *Proc. Natl. Acad. Sci. U.S.A.* **2007**, *104*, 17650-17655.

72. Sanderson, M. J.; Smith, I.; Parker, I; Bootman, M. D. Fluorescence Microscopy. *Cold Spring Harb Protoc*. **2014**, *10*, pdb.top071795.

73. Veatch, S. L.; Keller, S. L. Separation of Liquid Phases in Giant Vesicles of Ternary Mixtures of Phospholipids and Cholesterol. *Biophys. J.* **2003**, *85*, 3074-3083.

74. New, R. R. C. Liposome: A Practical Approach. Oxford University Press: Oxford, UK, 1990.

75. Lasic, D. D. Novel Applications of Liposomes. *Trends Bitechnol.* **1998**, *16*, 307-321.

76. Collier, J. H.; Messersmith, P. B. Phospholipid Strategies in Biomineralization and Biomaterials Research. *Annu. Rev. Mater. Res.* **2001**, *31*, 237-263.

77. Gibbs, B. F.; Kermasha, S.; Alli, I.; Mulligan, C. N. Encapsulation in the Food Industry: a Review. *Int. J. Food Sci. Nutr.* **1999**, *50*, 213-224.

78. Nohynek, G. J.; Lademann, J.; Ribaud, C.; Roberts, M. S. Grey Goo on the Skin? Nanotechnology, Cosmetic and Sunscreen Safety. *Crit. Rev. Toxicol.* **2007**, *37*, 251-277.

79. Chang, H. I.; Yeh, M. K. Clinical Development of Liposome-Based Drugs: Formulation, Characterization, and Therapeutic Efficacy. *Int. J. Nanomedicine* **2012**, *7*, 49-60.

80. Akashi, K.; Miyata, H.; Itoh, H.; Kinosita, K. Jr. Preparation of Giant Liposomes in Physiological Conditions and Their Characterization under an Optical Microscope. *Biophys. J.* **1996**, 71, 3242-3250.

81. McPhee, C. I.; Zoriniants, G.; Langbein, W.; Borri, P. Measuring the Lamellarity of Giant Lipid Vesicles with Differential Interference Contrast Microscopy. *Biophys. J.* **2013**, *105*, 1414-1420.

82. Chiba, M.; Miyazaki, M.; Ishiwata, S. Quantitative Analysis of the Lamellarity of Giant Liposomes Prepared by the Inverted Emulsion Method. *Biophys. J.* **2014**, 107, 346-354.

83. Menger, F. M.; Keiper, J. S.; Lee, S. J. Adhesion of Giant Liposomes as Observed by Light Microscopy. *Langmuir* **1997**, *13*, 4614-4620.

84. Parolini, L.; Mognetti, B. M.; Kotar, J.; Eiser, E.; Cicuta, P.; Michele, L. D. Volume and Porosity Thermal Regulation in Lipid Mesophases by Coupling Mobile Ligands to Soft Membranes. *Nat. Commun* **2015**, *6*, 5948.

85. Yang, S. -T.; Kiessling, V.; Tamm, L. K. Line Tension at Lipid Phase Boundaries as Driving Force for HIV Fusion Peptide-Mediated Fusion. *Nat. Commun* **2016**, *7*, 11401.

86. Frazier, M. L.; Wright, J. R.; Pokorny, A.; Almeida, P. F. F. Investigation of Domain Formation in Sphingomyelin/Cholesterol/POPC Mixtures by Fluorescence Resonance Energy Transfer and Monte Carlo Simulations. *Biophys. J.* **2007**, *92*, 2422-2433.

87. Heberle, F. A.; Buboltz, J. T.; Stringer, D.; Feigenson, G. W. Fluorescence Methods to Detect Phase Boundaries in Lipid Bilayer Mixtures. *Biochim. Biophys. Acta* **2005**, *1746*, 186-192.

88. Veatch, S. L.; Gawrisch, K.; Keller, S. L. Closed-Loop Miscibility Gap and Quantitative Tie-Lines in Ternary Membranes Containing Diphytanoyl PC. *Biophys. J.* **2006**, *90*, 4428-4436.

89. Rideau, E.; Wurm, F. R.; Landfester, K. Self-Assembly of Giant Unilamellar Vesicles by Film Hydration Methodologies. *Adv. Biosys.* **2019**, *3*, 1800324.

90. Horger, K. S.; Estes, D. J.; Capone, R.; Mayer, M. Films of Agarose Enable Rapid Formation of Giant Liposomes in Solutions of Physiologic Ionic Strength. *J. Am. Chem. Soc.* **2009**, *131*, 1810-1819.

91. Kamiya, K.; Takeuchi, S. Giant Liposome Formation Toward the Synthesis of Well-Defined Artificial Cells. *J. Mater. Chem. B* **2017**, *5*, 5911-5923.

92. Weinberger, A.; Tsai, F. C.; Koenderink, G. H.; Schmidt, T. F.; Itri, R.; Meier, W.; Schmatko, T.; Schröder, A.; Marques, C. Gel-Assisted Formation of Giant Unilamellar Vesicles. *Biophys. J.* **2013**, *105*, 154-164.

93. Mora, N. L.; Hansen, J. S.; Y.; Ronald, A. A.; Kieltyka, R.; Malmstadt, N.; Alexander Kros, A. Preparation of Size Tunable Giant Vesicles from Cross-Linked Dextran(Ethylene Glycol) Hydrogels. *Chem. Commun.* **2014**, *50*, 1953-1955.

94. Movsesian, N.; Tittensor, M.; Dianat, G.; Gupta, M.; Malmstadt, N. Giant Lipid Vesicle Formation Using Vapor-Deposited Charged Porous Polymers. *Langmuir* **2018**, *34*, 9025-9035.

95. Shum, H. C.; Lee, D.; Yoon, I.; Kodger, T.; Weitz, D. A. Double Emulsion Templated Monodisperse Phospholipid Vesicles. *Langmuir* **2008**, *24*, 7651-7653.

96. Nishimura, K.; Suzuki, H.; Toyota, T.; Yomo, T. Size Control of Giant Unilamellar Vesicles Prepared from Inverted Emulsion Droplets. *J. Colloid Interf. Sci.* **2012**, *376*, 119-125.

97. Deshpande, S.; Caspi, Y.; Meijering, A. E. C.; Dekker, C. Octanol-Assisted Liposome Assembly on Chip. *Nat. Commun.* **2016**, *7*, 1-9.

98. Deng, N.; Yelleswarapu, M.; Huck, W. T. S. Monodisperse Uni- and Multicompartment Liposomes. *J. Am. Chem. Soc.* **2016**, *138*, 7584-7591.

99. Zhu, T. F.; Szostak, J. W. Preparation of Large Monodisperse Vesicles. *PloS One* **2009**, *4*, e5009.

100. Lira, R. B.; Dimova, R.; Riske, K. A. Giant Unilamellar Vesicles Formed by Hybrid Films of Agarose and Lipids Display Altered Mechanical Properties. *Biophys J.* **2014**, *107*, 1609-1619.

101. Maoyafikuddin, M.; Pundir, M.; Thaokar, R. Starch Aided Synthesis of Giant Unilamellar Vesicles. *Chem Phys Lipids* **2020**, *226*, 104834.

102. Dao, T. P. T.; Fauquignon, M.; Fernandes, F.; Ibarboure, E.; Vax, A.; Prieto, M.; Le Meins, J. F. Membrane Properties of Giant Polymer and Lipid Vesicles Obtained by Electroformation and PVA Gel-Assisted Hydration Methods. *Colloid Surface A* **2017**, *533*, 347-353.

103. Mora, N. L.; Hansen, J. S.; Y.; Ronald, A. A.; Kieltyka, R.; Malmstadt, N.; Alexander Kros, A. Preparation of Size Yunable Giant Vesicles from Cross-Linked Dextran(Ethylene Glycol) Hydrogels. *Chem. Commun.* **2014**, *50*, 1953-1955.

104. Mora, N. L.; Gao, Y.; Gutierrez, M. G.; Peruzzi, J.; Bakker, I.; Peters, R. J. R. W.; Siewert, B.; Bonnet, S.; Kieltyka, R. E.; van Hest, J. C. M.; Malmstadt, N.; Kros, A. Evaluation of Dextran (Ethylene Glycol) Hydrogel Films for Giant Unilamellar Lipid Vesicle Production and Their Applications for the Encapsulation of Polymersomes. *Soft Matter* **2017**, *13*, 5580-5588.

105. Schultze, J.; Vagias, A.; Ye, L.; Prantl, E.; Breising, V.; Best, A.; Koynov, K.; Marques, C. M.; Butt, H. J. Preparation of Monodisperse Giant Unilamellar Anchored Vesicles Using Micropatterned Hydrogel Substrates. *ACS Omega* **2019**, *4*, 9393-9399.

106. Davis, J. H.; Clair, J. J.; Juhasz, J. Phase Equilibria in DOPC/DPPC-d_{62}/Cholesterol Mixtures. *Biophys. J.* **2009**, *96*, 521-539.

107. Juhasz, J.; Sharon, F. J.; Davis, J. H. Quantitative Characterization of Coexisting Phase In DOPC/DPPC/Cholesterol Mixture: Comparing Confocal Fluorescence Microscopy and Deuterium Nuclear Magnetic Resonance. *Biochim. Biophys. Acta* **2009**, *1788*, 2541-2552.

108. Ariola, F. S.; Li, Z.; Cornejo, C.; Bittman, R.; Heikal, A. A. Membrane Fluidity and Lipid Order in Ternary Giant Unilamellar Vesicles Using a New Bodipy-Cholesterol Derivative. *Biophys. J.* **2009**, *96*, 2696-2708.

109. Gudheti, M. V.; Mlodzianoski, M.; Hess, S. T. Imaging andShape Analysis of GUVs as Model Plasma Membranes: Effect of Trans DOPC on Membrane Properties. *Biophys. J.* **2007**, *93*, 2011-2023.

110. Garten, M.; Prévost, C.; Cadart, C.; Gautier, R.; Bousset, L.; Melki, R.; Bassereau, P.; Vanni, S. Methyl-Branched Lipids Promote the Membrane Adsorption of α-Synuclein by Enhancing Shallow Lipid-Packing Defects. *Phys. Chem. Chem. Phys.* **2015**, *17*, 15589-15597.

111. Taylor, P.; Xu, C.; Fletcher, P. D. I.; Paunov, V. N. A Novel Technique for Preparation of Monodisperse Giant Liposomes. *Chem. Comm.* **2003**, *14*, 1732-1733.

112. Diguet, A.; Le Berre, M.; Chen, Y.; Baigl, D. Preparation of Phospholipid Multilayer Patterns of Controlled Size and Thickness by Capillary Assembly on a Microstructured Substrate. *Small* **2009**, *5*, 1661-1666.

113. Osaki, T.; Kuribayashi-Shigetomi, K.; Kawano, R.; Sasaki, H.; Takeuchi, S. Uniformly-Sized Giant Liposome Formation with Gentle Hydration. *Proc. IEEE MEMS* **2011**, Cancun, 103-106.

114. Fan, T.; Wang, Q.; Hu, N.; Liao, Y.; Chen, X.; Wang, Z.; Yang, Z.; Yang, J.; Qian, S. Preparation of Giant Lipid Vesicles with Controllable Sizes by a Modified Hydrophilic Polydimethylsiloxane Microarray Chip. *J. Colloid Interf. Sci.* **2019**, *536*, 53-61.

115. Kang, Y. J.; Wostein, H. S.; Majd, S. A Simple and Versatile Method for the Formation of Arrays of Giant Vesicles with Controlled Size and Composition. *Adv. Mater.* **2013**, *25*, 6834-6838.

116. Zhu, C.; Li, Q.; Dong, M.; Han, X. Giant Unilamellar Vesicle Microarrays for Cell Function Study. *Anal. Chem.* **2018**, *90*, 14363-14367.

117. Mui, B. L. S.; Cullis, P. R.; Evans, E. A.; Madden, T. D. Osmotic Properties of Large Unilamellar Vesicles Prepared by Extrusion. *Biophys. J.* **1993**, *64*, 443-453.

118. Evans, E.; Needham, D. Physical Properties of Surfactant Bilayer Membranes: Thermal Transitions, Elasticity, Rigidity, Cohesion, and Colloidal Interactions. *J. Phys. Chem.* **1987**, *91*, 4219-4228.

119. Rawicz, W.; Olbrich, K. C.; McIntosh, T.; Needham, D.; Evans, E. Effect of Chain Length and Unsaturation on Elasticity of Lipid Bilayers. *Biophys. J.* **2000**, *79*, 328-339.

120. Mayer, L. D.; Hope, M. J.; Cullis, P. R. Vesicles of Variable Sizes Produced by a Rapid Extrusion Procedure. *Biochim. Biophys. Acta* **1986**, *858*, 161-168.

121. Hunter, D. G.; Frisken, B. J. Effect of Extrusion Pressure and Lipid Properties on the Size and Polydispersity of Lipid Vesicles. *Biophys. J.* **1998**, *74*, 2996-3002.

122. Thompson, M.; Lennox, R. B.; McClelland, R. A. Structure and Electrochemical Properties of Microfiltration Filter-Lipid Membrane Systems. *Anal. Chem.* **1982**, *54*, 76-81.

123. Nikolels, D. P.; Siontorou, C.; Andreou, V.; Krull, U. J. Stabilized Bilayer Lipid Membranes for Flow-through Experiments. *Electroanalysis* **1994**, *7*, 531-536.

124. Dhoke, M. A.; Ladha, P. J.; Boerio, F. J.; Lessard, L. B.; Malinowska, D. H.; Cuppoletti, J.; Wieczorek, D. S. Porous Membranes for Reconstitution of Ion Channels. *Biochim. Biophys. Acta* **2005**, *1716*, 117-125.

125. Phung, T.; Zhang, Y.; Dunlop, J.; Dalziel, J. Bilayer Lipid Membranes Supported on Teflon Filters: A Functional Environment for Ion Channels. *Biosens. Bioelectron.* **2011**, *26*, 3127-3135.

126. Amjad, O. A.; Mognetti, B. M.; Cicuta, P.; Michele, L. D. Membrane Adhesion through Bridging by Multimeric Ligands. *Langmuir* **2017**, *33*, 1139-1146.

127. Sarmento, M. J.; Prieto, M.; Fernandes, F. Reorganization of Lipid Domain Distribution in Giant Unilamellar Vesicles Upon Immobilization with Different Membrane Tethers. *Biochimica et Biophysica Acta* **2012**, *1818*, 2605-2615.

128. Manley, S.; Horton M. R.; Lecszynski, S.; Gast, A. P. Sorting of Streptavidin Protein Coats on Phase-Separating Model Membranes. *Biophys. J.* **2008**, *95*, 2301-2307.

129. Kisak, E. T.; Kennedy, M. T.; Trommeshauser, D.; Zasadzinski, J. A. Self-Limiting Aggregation by Controlled Ligant-Receptor Stoichiometry. *Langmuir* **2000**, *16*, 2825-2831.

130. Baumgart, T.; Hess, S. T.; Webb, W. W. Imagine Coexisting Fluid Domains in Biomembrane Models Coupling Curvature and Line Tension. *Nature* **2003**, *425*, 821-824.

131. Jülicher, F.; Lipowsky, R. Domain-Induced Budding of Vesicles. *Phys. Rev. Lett.* **1993**, *70*, 2964-2967.

132. Seifert, U. Configurations of Fluid Membranes and Vesicles. *Adv. Phys.* **1997**, *46*, 13-137.

133. Baumgart, T.; Das, S.; Web, W. W.; Jenkins, J. T. Membrane Elasticity in Giant Vesicles with Fluid Phase Coexistence. *Biophys. J.* **2005**, *89*, 1067-1080.

134. Blosser, M. C.; Starr, J. B.; Turtle, C. W.; Ashcraft, J.; Keller, S. L. Minimal Effect of Lipid Charge on Membrane Miscibility Phase Behavior in Three Ternary Systems. *Biophys. J.* **2013**, *104*, 2629-2638.

135. Vequi-Suplicy, C. C.; Riske, K. A.; Knorr, R. L.; Dimova, R. Vesicles with Charged Domains. *Biochim. Biophys. Acta* **2010**, *1798*, 1338-1347.

136. Imam, Z. I.; Kenyon, L. E.; Ashby, G.; Nagib, F.; Mendicino, M.; Zhao, C.; Gadok, A. K.; Stachowiak, J. C. Phase-Separation Liposomes Enhance the Efficiency of Macromolecular Delivery to the Cellular Cytoplasm. *Cell Mol Bioeng* **2017**, *10*, 387-403.

137. Okano, G.; Akino, T. Variations in the Molecular Species of Lung Phosphatidylglycerol. *Lipids* **1979**, *14*, 541-546.

138. Maltzeva, E.; Shapovalov, V. L.; Möhwald, H.; Brezesinski, G. Ionization State and Structure of L-1,2-Dipalmitoylphosphatidylglycerol Monolayers at the Liquid/Air Interface. *J. Phys. Chem. B* **2006**, *110*, 919-926.

139. Zhao, W.; Gurtovenko, A. A.; Vattulainen, I.; Karttunen, M. Cationic Dimyristoylphosphatidylcholine and Dioleoyloxytrimethylammonium Propane Lipid Bilayers: Atomistic Insight for Structure and Dynamics. *J. Phys. Chem. B* **2012**, *116*, 269-276.

140. Chiu, S. W.; Jakobsson, E.; Mashl, R. J.; Scott, H. L. Cholesterol-Induced Modifications in Lipid Bilayers: A Simulation Study. *Biophys. J.* **2002**, *83*, 1842-1853.

141. Róg, T.; Pasenkiewicz-Gierula, M.; Vattulaninen, L.; Karttunen, M. Ordering Effects of Cholesterol and Its Analogous. *Biochim. Biophys. Acta* **2009**, *1788*, 97-121.

142. Heftberger, P.; Kollmitzer, B.; Rieder, A. A.; Amenitsch, H.; Pabst, G. In Situ Determination of Structure and Fluctuations of Coexisting Fluid Membrane Domains. *Biophys. J.* **2015**, *108*, 854-862.

143. Ma, Y.; Ghosh, S. K.; DiLena, D. A.; Bera, S.; Lurio, L. B.; Parikh, A. N.; Sinha, S. K. Cholesterol Partition and Condensing Effect in Phase-Separated Ternary Mixture Lipid Multilayers. *Biophys. J.* **2016**, *110*, 1355-1366.

144. Chen, C.; Tripp, C. P. A Comparison of the Behavior of Cholesterol, 7-Dehydrocholesterol and Ergosterol in Phospholipid Membranes. *Biochim. Biophys. Acta* **2012**, *1818*, 1673-1681.

145. Bonechi, C.; Martini, S.; Ciani, L.; Lamponi, S.; Rebmann, H.; Rossi, C.; Ristori, S. Using Liposomes as Carriers for Polyphenolic Compounds: The Case of Trans-Resveratrol. *PLoS ONE* 2012, *7*: e41438.

146. Chibowski, E.; Szcześ, A. Zeta Potential and Surface Charge of DPPC and DOPC Liposomes in the Presence of PLC Enzyme. *Adsorption* **2016**, *22*, 755-765.

147. Gustafsson, O.; Mogensen, K. B.; Kutter, J. P. Underivatized Cyclic Olefin Copolymer as Substrate Material and Stationary Phase for Capillary and Microchip Electrochromatography. *Electrophoresis* **2008**, *29*, 3145-3152.

148. Burns, N. L.; Van Alstine, J. M.; Harris, J. M. Poly(Ethylene Glycol) Grafted to Quartz: Analysis In Terms of A Site-Dissociation Model of Electroosmotic Fluid Flow. *Langmuir* **1995**, *11*, 2768-2776.

149. Yanagisawa, M.; Imai, M.; Masui, T.; Komura, S.; Ohta, T. Growth Dynamics of Domains in Ternary Fluid Vesicles. *Biophys. J.* **2007**, *92*, 115-125.

150. Pantazatos, D. P.; MacDonald, R. C. Directly Observed Membrane Fusion Between Oppositely Charged Phospholipid Bilayers. *J. Membr. Biol.* **1999**, *170*, 27-38.

151. Südhof, T. C. The Synaptic Vesicle Cycle. *Annu. Rev. Neurosci.* **2004**, *27*, 509-547.

152. Wagle, S.; Georgiev, V. N.; Robinson, T.; Dimova, R.; Lipowsky, R.; Grafmüller, A. Interaction of SNARE Mimetic Peptides with Lipid Bilayers: Effects of Secondary Structure, Bilayer Composition and Lipid Anchoring. *Sci. Rep.* **2019**, *9*, 7708.

153. Edwards, K. A.; Baeumner, A. J. Liposomes in Analyses. *Talanta* **2006**, *68*, 1421-1431.

154. Bonifacino, J. S.; Glick, B. S. The Mechanisms of Vesicle Budding and Fusion. *Cell*, **2004**, *116*, 153-166.

155. Zimmerberg, J.; Kozlov, M. M. How Proteins Produce Cellular Membrane Curvature. *Nat. Rev. Mol. Cell Biol.* **2006**, *7*, 9-19.

156. Murtas, G. Artificial Assembly of A Minimal Cell. *Mol. BioSyst*. **2009**, *5*, 1292-1297.

157. Purnick, P. E. M.; Weiss, R. The Second Wave of Synthetic Biology: From Modules to Systems. *Nat. Review.* **2009**, *10*, 410-422.